(PRA-MS progress 12/05/05,12/20/05,
1/3/05, 1/9/06, 2/12/06, 4/13/06, 4/29/06, 5/12/06, submitted 5/15/06, 7/20/06 9/22.07.)

Optical space-time coordinates:
A phase-based spectral approach to relativistic mechanics

William G. Harter

Department of Physics
University of Arkansas
Fayetteville, AR 72701

Optical hetrodyne techniques developed by Evenson led to renaissance of time and frequency precision that resulted in an improved speed-of-light measurement of $c=299,792,458 m\ s^{-1}$ and a redefinition of the meter with applications to spectroscopy and global positioning systems. This success also begs for a renaissance in conceptual precision regarding electrodynamics, relativity and quantum theory that are so much a part of our metrology. Here we use some of Evenson's ideas to examine more closely the spectral and wave dynamical aspects of special relativity and quantum mechanics that help to simplify and bring the subjects closer together. This is done by allowing light and matter to serve as their own space-time coordinates so that the nature of momentum, mass, and energy is shown with an elegant simplicity that has heretofore been unnecessarily hidden.

By enhancing the precision of time, frequency, and speed of light measurement, Kenneth M. Evenson and co-workers[1] set the stage for the redefinition of the meter and construction of Global Positioning Systems (GPS) that are our worldwide electromagnetic space-time coordinate frames.

Using tiny optical versions of radio crystal sets called MIM diodes, Evenson made a chain of increasing frequency beat notes that gave a laser frequency count for the visible region (400-750 THz). Evenson's achievements were noted in many places including the Guinness Book of Records, which cited Evenson twice.[2] Unfortunately, Lou Gehrig's disease tragically cut his life short in 2002 before his contribution to laser physics and metrology could be fully recognized.

The practical value of high precision optical stabilization in both continuous wave (CW) and pulse wave (PW) lasers is cited in the 2005 Nobel Prize[3] for Physics to R. Glauber, T. Hensch and J. Hall[4] and includes high-resolution spectroscopy, time-keeping, and the GPS.[5] The third recipient, John Hall, was a long time colleague and collaborator of Evenson in CW experiments. Later PW techniques of Hall, Hensch, and others[6] have increased frequency precision to better than one part in 10^{15}.

Less has been said about the theoretical value of such high-precision achievements. Since before the time of Galileo, more precise precepts accompany more precise concepts. When we see more clearly we gain an opportunity to think more clearly and *vice-versa*. Now that we are seeing over 10^{12} times more clearly, should not our conceptual clarity increase by at least $ln(10^{12})$? Michelson's interferometric precision helped establish Einstein's leap of clarity, and so one wonders how the great optical precision of Evenson and coworkers can also sharpen current *conceptual* precision.

This article seeks to improve clarity of concepts in two pillars of modern physics, special relativity and quantum theory. The precision of optical chains used by Evenson suggests how Occam's razor[7] can sharpen axioms used by Einstein. The result is a clearer chain of logic between key works of Feynman, Planck, Einstein, Maxwell, Poincare, Fourier, Lagrange, Doppler, Newton, Galileo, and finally going back to Euclid's *Elements*. In light of this, physics becomes simpler and more powerful.

It will be shown how the developments of relativity and quantum theory in Einstein's 1905 *annus mirabilis*, as well as other work that followed, can be better understood both qualitatively and quantitatively using a *spectral* approach that exposes the *geometry* of wave interference. Such an approach has an elegant and powerful logic that is shown to develop 1905 results in a few ruler-and-compass steps or lines of algebra and relate them to earlier classical and later quantum mechanics. New insight into a unification of relativity and quantum mechanics begun by Dirac suggests practical results such as optical "Einstein-elevators" with ultra-precise coherent Compton micro-acceleration.

Unification of general relativity with quantum mechanics has been an elusive goal of string theories for many years[8]. Such large-scale unification presumes local unification since general relativity presumes special relativity to rule locally. A deep unification of special relativity and

quantum theory by clearer physical logic is an important conceptual result offered by the wave-based development described herein. This may serve as a precursor to unification with the general theory. If a quantum world is described by wave amplitudes $\langle a|b\rangle$ then a unification should account for them, too.

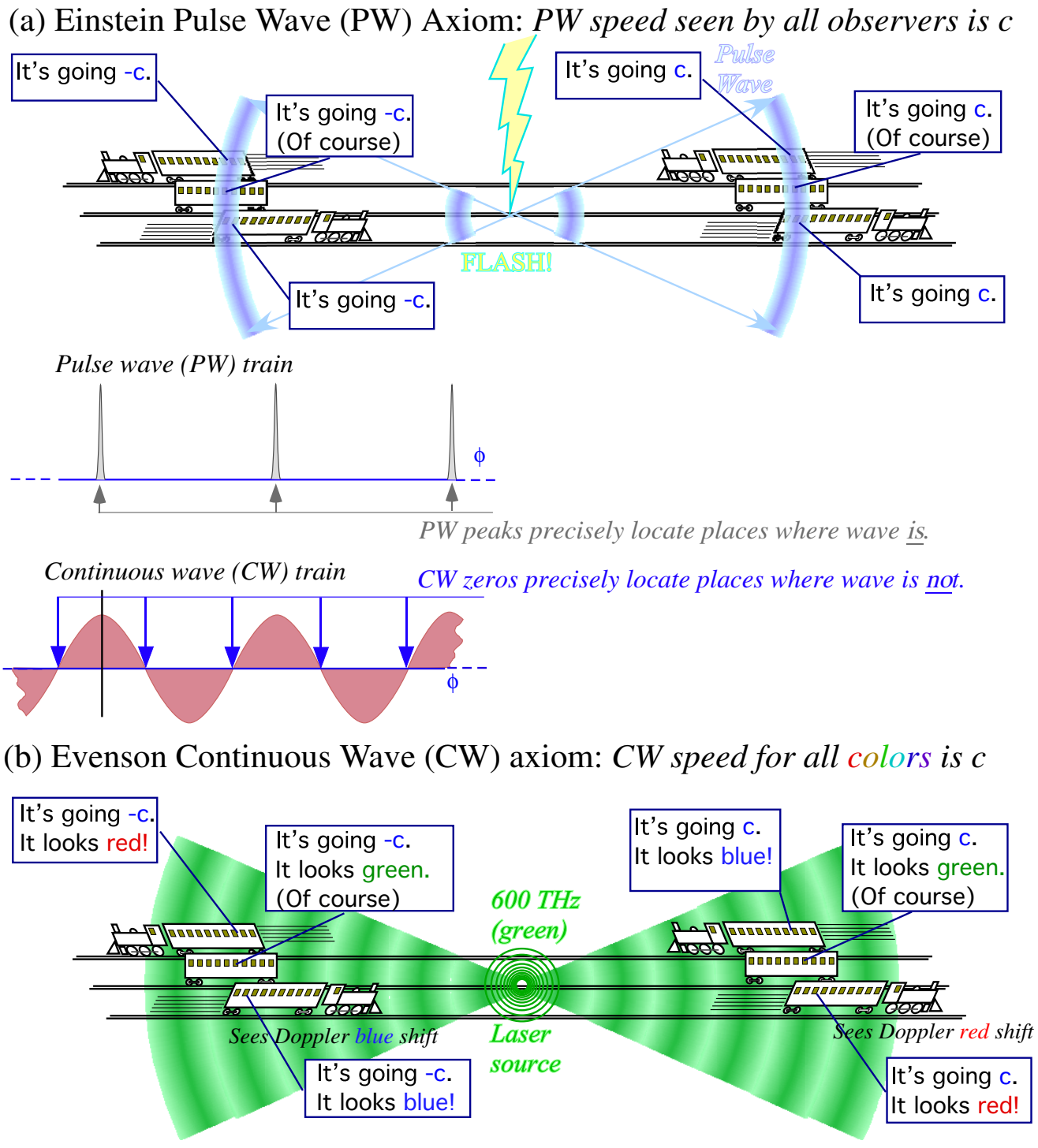

Fig. 1 Comparison of wave archetypes and related axioms of relativity.

(a) Pulse Wave (PW) peaks locate where a wave is. Their speed is c for all observers.

(b) Continuous Wave (CW) zeros locate where it is not. Their speed is c for all colors (or observers.)

1. Optical Axioms

Beginning relativity courses paraphrase Einstein's light speed axiom as in Fig. 1a, "Speed of a lightning flash is *c* according to passengers of any train," or simply, "Pulse wave (PW) speed *c* is invariant." For critically thinking students, that is a show-stopper. It boggles the mind that something of finite speed cannot *ever* be caught up to, indeed, cannot even *begin* to be caught.[9]

Occam's razor can dissect the *c*-axiom into a less mind-boggling form. As Evenson viewed a frequency chain of multiple "colors" of continuous wave (CW) laser beams, he assumed that, "All *colors* have speed *c*." Had Einstein imagined trains viewing a 600THz (green) laser as in Fig. 1b, his *c*-axiom might be, "CW speed is *c* according to passengers of any train, *but frequency and wavelength vary by a Doppler effect that depends on velocity of the train*," or more simply, "*All colors go c.*"

A CW spectral component Occam-sliced from a PW has a color variation with observer speed that "white" PW's do not show. A colored wave (CW) changes color by a blue-shift if approaching its source or a red-shift if departing. Doppler's theory of acoustical wave frequency shift was available to Einstein but laser technology came much later so he was unlikely to conceive of the ultra-precise 1st-order Doppler sensitivity of a coherent optical CW. Coherence and interference were problems left to Michelson and Morely fighting the *in*coherences of early interferometry in the privacy of their labs.

Also an optical Doppler shift depends on *one* relative velocity of source and observer while acoustical Doppler depends on *three* absolute (or three relative) velocities involving source, observer, and a "wind." The single-velocity simplicity of optical Doppler shifts is crucial for relativity.

Consider a 600THz green wave from a 600THz source. One may ask, "Is it distinguishable from another 600THz green wave sent by a 599THz source approaching or a 601THz source departing at just the right speed? Or, could 600THz light, seen as we approach a fixed 599THz source, differ in speed from 600THz light seen as we depart a fixed 601Thz source? How many kinds of 600 THz light exist?" (At first, we measure wave speed and frequency (color) but not polarization or amplitude.)

Evenson's axiom follows if one answers, "There is only one kind of each frequency (color) and only one speed independent of source or observer velocity." An undesirable alternative is to have many different kinds of each color, corresponding to many ways to make each color by tuning source up (or down) while moving out (or in). (In fact, one color illuminating a gas, liquid, or solid may involve two or many varieties of mode dispersion with wave speeds ranging above or below *c*.) Evenson's axiom demands that light in a vacuum be one speed for all frequency. In short, it is *dispersion-free*.

Then harmonic CW (Fourier) components form a pulse wave PW moving rigidly at the speed *c* shared by all its hidden colors. This derives Einstein's PW law as a *theorem* arising from Evenson's CW *axiom*. It also relates to appearance of distant nebulae and the night sky. If any colors were even a fraction of a percent slower than other frequencies, they would show up thousands or millions of years

later with less evolved images than neighboring colors. We might then enjoy a sky full of colorful streaks but would not have the clarity of modern astronomical images.

Spectroscopic view of CW axiom

Astronomy is just one dependent of Evenson's CW axiom. Spectroscopy is another. Laser atomic spectra are listed by frequency υ (s^{-1}) or period $\tau=1/\upsilon$ (s) while earlier tables list atomic lines from gratings by wavenumber κ (m^{-1}) or wavelength $\lambda=1/\kappa$ (m). The equivalence of temporal and spatial listings is a tacit assumption of Evenson's axiom and may be stated as follows.

$$c = \upsilon \cdot \lambda = \lambda/\tau = \upsilon/\kappa = 1/(\kappa \cdot \tau) = const. \qquad (1.1)$$

An atomic resonance is *temporal* and demands a precise *frequency*. Sub-nanometer atomic radii are thousands of times smaller than micron-sized wavelengths of optical transitions. Optical wavelength then seems irrelevant. (In dipole approximations, light has no spatial dependence.)

However, optical grating diffraction demands precise *spatial* fit of micron-sized wave*length* to micron grating slits. Optical frequency then seems irrelevant. (Bragg or Fraunhofer laws assume no time dependence.) Spatial geometry of a spectrometer grating, cavity, or lattice directly determines a wavelength λ. Frequency υ is determined indirectly from λ by (1.1). That is valid only to the extent that light speed $c = \upsilon \cdot \lambda$ is invariant throughout the spectrum (and throughout the universe.)

So spectroscopists expect an atomic laser cavity resonating at a certain atomic spectral line in one rest frame to do so in *all* rest frames. Each λ or υ value is a *proper quantity* to be stamped on the device and officially tabulated for its atoms. Passersby disagree that device output is υ but instead see a Doppler red shifted $r\upsilon$ or blue shifted $b\upsilon$. Yet, all can agree on whether the device is working!

Moreover, Evenson's CW axiom demands that υ and λ must Doppler shift *inversely* one to the other so that the product $\upsilon \cdot \lambda$ is always a constant $c=299,792,458\ m \cdot s^{-1}$. The same applies to τ and κ for which $\kappa \cdot \tau = 1/c$. Another inverse relation exists between Doppler blue and red shifts seen before and after passing a source. This is a CW property or axiom involving time reversal.

Time reversal axiom

Atoms behave like tiny radio transmitters, or just as well, like receivers. Unlike macroscopic radios, atoms are time-reversible in detail since they have no resistors or similarly irreversible parts. Suppose an atom A broadcasting frequency υ_A resonates an approaching atom B tuned to receive a blue shifted frequency $\upsilon_B = b\upsilon_A$. If time runs backwards all velocity values change sign. Atom B becomes a *transmitter* of its tuned frequency $\upsilon_B = b\upsilon_A$ that is *departing* from atom A who is a *receiver* tuned to its frequency $\upsilon_A = (1/b)\upsilon_B$. Atom A sees υ_A *red*-shifted from B's frequency υ_B by an *inverse* factor $r=1/b$.

$$b=1/r \qquad (1.2)$$

Phase invariance axioms

Optical CW axioms are based on deeper phase invariance principles. Elementary CW function $\Psi=A\ exp\ i(k\cdot x-\omega\cdot t)$ or its real part Re $\Psi=A\ cos(k\cdot x-\omega\cdot t)$ has a phase angle $\Phi=(k\cdot x-\omega\cdot t)$ that is regarded as an invariant or proper quantity. Our rationale is that each space-time point of the wave has a phase clock or *phasor* (Re Ψ, Im Ψ) turning at *angular* frequency $\omega=2\pi\cdot\upsilon$. Each phasor reading Φ could be stamped or officially tabulated. Any two observers agree on Φ even if Doppler shifts change frequency $\omega=2\pi\cdot\upsilon$ and *wavevector* $k=2\pi\kappa$ to new values (ω',k') or if space x and time t also transform to (x',t').

$$k\cdot x-\omega\cdot t=\Phi=k'\cdot x'-\omega'\cdot t' \tag{1.3}$$

The Lorentz-Einstein transformations for both space-time (x,t) to (x',t') and inverse space-time (ω,k) to (ω',k') are derived in Sec. 2 using CW axioms (1.1-2) and a few steps of algebra or ruler-and-compass.

Historically, invariance (1.3) relates to classical Legendre contact transforms of Lagrangian L to energy E or Hamiltonian H. Its differential with an $\hbar$ scale factor is Poincare's action invariant dS.

$$L=p\cdot\dot{x}-H \tag{1.4a}$$

$$\hbar d\Phi=dS=Ldt=p\cdot dx-Hdt \tag{1.4b}$$

Connecting (1.3) to (1.4b) requires quantum scaling relations $p=\hbar k$ of DeBroglie and $E=\hbar\omega$ of Planck. Sec. 3 derives these relations directly from CW axioms (1.1-2) that also give exact relativistic quantum and classical mechanical relations in a few algebraic[10] or ruler-and-compass steps that develop elegant and powerful wave-geometric[11] interpretations of mass and Poincare's invariant in Sec. 3 and Sec. 4.[12]

We surmise that Einstein might have liked geometric derivation since it was a compass that first caught his theoretical attention at an age of five.[13] Perhaps, it might also appeal to Poincare who also discovered relativity around the time of Einstein's *annus mirabilis*. Poincare phase invariance (1.3) underlies both CW lightspeed axiom (1.1) and time reversal axiom (1.2). Consider the $\Phi=0$ point.

$$k\cdot x-\omega\cdot t=0 \tag{1.5a}$$

Solving gives phase velocity x/t *(meters-per-second)* equal by (1.1) to υ/κ *(per second)-per-(per meter)*.

$$\frac{x}{t}=\frac{\omega}{k}=\frac{\upsilon}{\kappa}=c \tag{1.5b}$$

Doppler shift $(\omega\rightarrow b\omega$ and $k\rightarrow bk)$ leaves phase velocity invariant. Phase $\Phi=(k\cdot x-\omega\cdot t)$ itself is invariant to time reversal ($(\omega\rightarrow-\omega)$ and $(t\rightarrow-t)$) and that supports (1.2), the inverse-Doppler relation $b=1/r$.

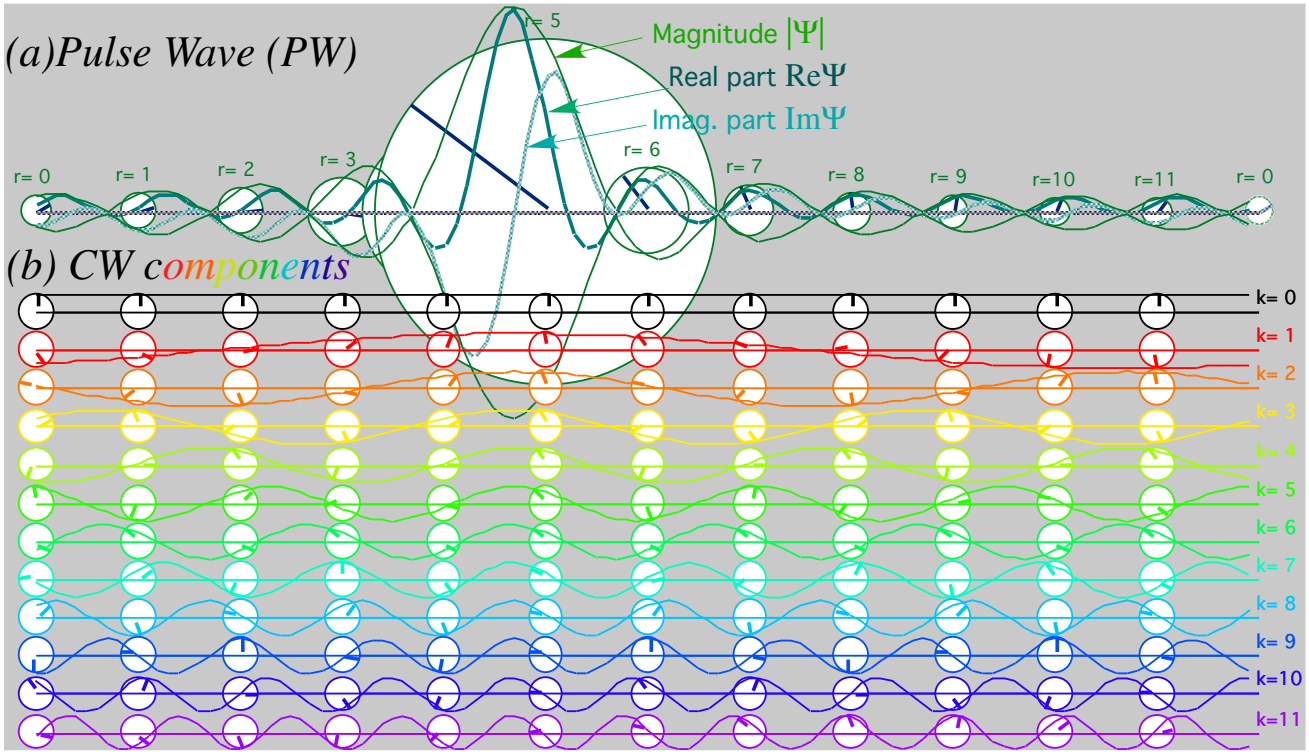

Fig. 2. Pulse Wave (PW) sum of 12 Fourier CW's *(a) PW parts: real Re Ψ, imaginary Im Ψ, and magnitude |Ψ|. (b) CW phasor clocks plot real vs. imaginary*

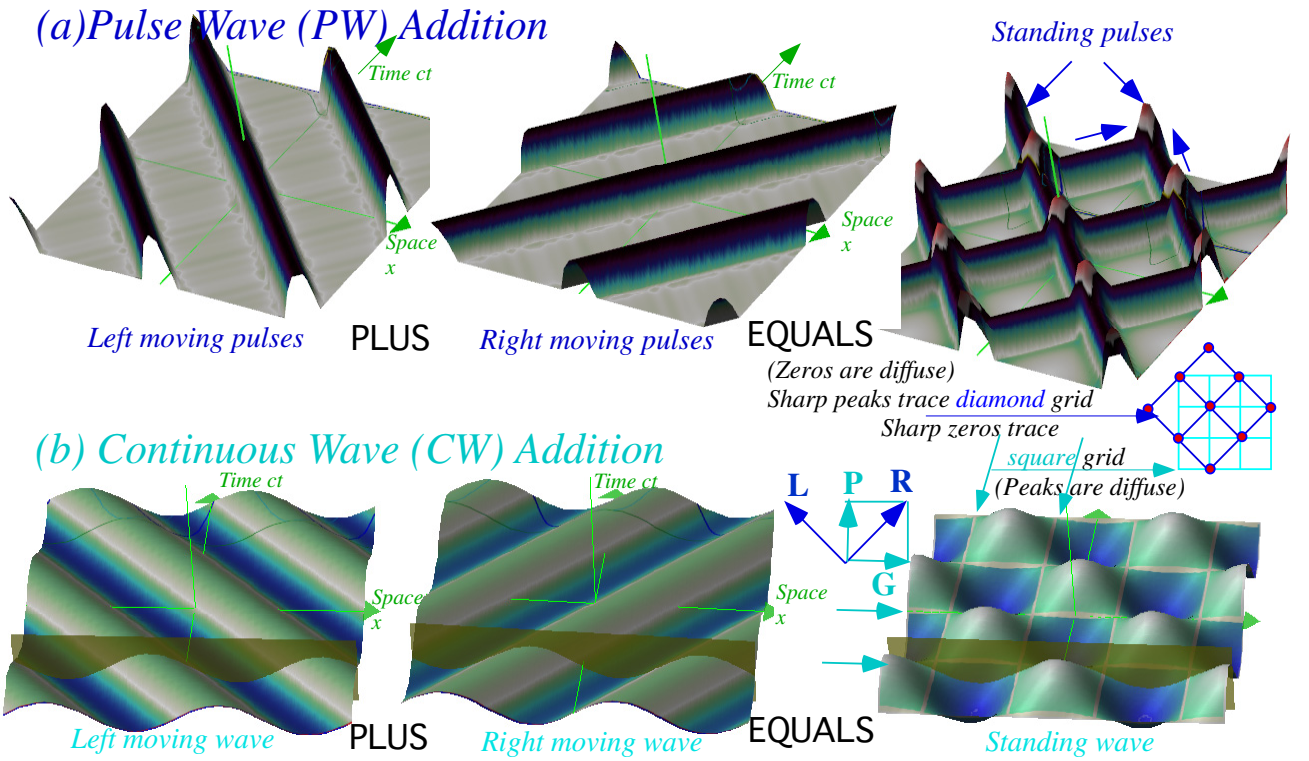

Fig. 3. Wave Addition *(a) 2-PW Boolean binary sum has 4 values (0,0),(0,1),(1,0),(1,1) and diamond grid of peak paths on a plane of zeros. (b) 2-CW interference sum has value continuum and square grid of zeros.*

Comparing pulsed and continuous wave trains

It is instructive to contrast two opposite wave archetypes, the *Pulse Wave* (PW) train sketched in Fig. 1a and the *Continuous Wave* (CW) train sketched in Fig. 1b. The claim is made that the CW is the more elementary theoretical entity, indeed the *most* elementary entity in classical optics since it has just one value of angular frequency $\omega=2\pi\cdot\upsilon$, one value of wavevector $k=2\pi\kappa$, and one amplitude A.

$$^{CW}\Psi_{k,\omega}(x,t) = Ae^{i(kx-\omega t)} = \langle k,\omega|x,t\rangle \tag{1.6}$$

The real part is the cosine wave $A\cos(kx-\omega t)$ shown in Fig. 1(b). Acronym CW fits cosine wave, as well. If frequency υ is in the visible 400-750THz range CW could also stand for colored wave.

In contrast, the PW is a *less* elementary wavefunction and contains N harmonic terms of CW functions where bandwidth N is as large as possible. Fig. 2 shows an example with $N=12$.

$$^{PW}\Psi_{N(k,\omega)}(x,t) = A\left(1+e^{i(kx-\omega t)}+e^{i2(kx-\omega t)}+e^{i3(kx-\omega t)}\cdots+e^{iN(kx-\omega t)}\right) \tag{1.7}$$

An infinite-N PW is a train of Dirac $\delta(x-a)$-functions each separated by fundamental wavelength $\lambda=2\pi/k$. The δ-spikes march in lockstep at light speed $c=\omega/k$ following Evenson's CW axiom.

$$^{PW}\Psi_{N(k,\omega)}(x,t) \xrightarrow[N\to\infty]{} A\sum_{n=-\infty}^{\infty}\delta(x-ct-n\lambda)$$

Delta functions have infinite frequency bandwidth and are thus impractical. Realistic PW trains apply cutoff or tapering amplitudes a_n to each harmonic to restrict frequency to a finite bandwidth Δ.

$$^{PW}\Psi_{\Delta}(x,t) = \sum_{n=0}^{\infty} a_n e^{in(kx-\omega t)} = \sum_{n=-\infty}^{\infty} G(x-ct-n\lambda) \quad \text{where: } a_n \ll 1 \text{ for } n>\Delta \tag{1.8}$$

A common choice is a Gaussian taper $a_n = e^{-(n/\Delta)^2}$ that gives Gaussian PW functions $G(\theta)=e^{-(\theta\cdot\Delta)^2}$.

PW functions (1.8) involve an unlimited number of amplitude parameters a_n in addition to fundamental frequency ω, while a CW function has a single amplitude parameter A. Thus, theory based on CW properties would seem to be closer to an Occam ideal of simplicity than one based on PW.

However, with regard to counter-propagating or colliding beams the PW *appear* in Fig. 3a to have simpler properties than CW in Fig. 3b. PW have a simple classical Boolean OFF (0) over most of space-time with an occasional ON (1) at a sharp pulse. On the other hand CW range gradually between +1 and –1 over most of space-time, but have a sharp zero (0) in between crest and trough. (A PW can be *designed* to show precisely where it *is*. A CW *naturally* shows precisely where it is *not*.)

Interference of colliding PW is *wysiwye (What you see is what you expect.)*, but the pattern of interference for the sum of colliding CW is subtler. PW paths in space-time *(x,ct)* resemble baseball *diamonds* like the baseline paths in the American sport, while the CW zeros are Cartesian space-time

squares made of horizontal spatial *x*-axial lines of equal times *(ct=...1,2...)* and vertical temporal *ct*-axial lines of fixed location *(x=...1,2...)*. PW diamonds, while deceptively simple, cover up a complicated network of zeros around each pulse. CW squares are a simple lattice of zeros for a standing wave that is just a factored sum of the following two equal-but-opposite colliding CW.

$$ {}^{CW}\Psi_{k,\omega} + {}^{CW}\Psi_{-k,\omega} = A\left(e^{i(kx-\omega t)} + e^{i(-kx-\omega t)}\right) = 2Ae^{-i\omega t}\left(\cos(kx)\right) \tag{1.9}$$

The *group envelope* factor $\left(\cos(kx)\right)$ is zero along *ct*-axial lines of position *(kx/π+1/2=...0,1,2...)*. The *phase* factor $(e^{-i\omega t})$ has zero real part along *x*-axial lines of simultaneous time *(ct/π+1/2=...0,1,2...)*.

Comparing wave-zero (WZ) and pulse-peak (PP) coordinates

It is now shown how general phase and group wave *zeros* of 2-CW interference define a space-time wave-zero (WZ) coordinate grid that complements a pulse peak or particle-path (PP) grid of 2-PW trains. This helps to visualize the wave-particle duality whose history goes back to Newton's corpuscular view of light before wave optics of Maxwell-Young or after Planck-Einstein physics of quanta. The visualization is done by superimposing a time-*vs*-space *(x,t)*-plot on top of its Fourier inverse *per-time-space* or *reciprocal space-time* plot of frequency-*vs*-wavevector *(ω,k)*.

The plots apply to general wave mechanics and not just optics. An example in Fig. 4 begins by picking four random numbers, say, *1*,*2*,*4*, and *4* to insert into frequency-wavevector $\mathbf{K}_2 = (\omega_2,k_2)=(1,2)$ of a mythical *source-2* and frequency-wavevector $\mathbf{K}_4 = (\omega_4,k_4)=(4,4)$ of another mythical *source-4*. (This is not light. Slope or velocity $c_2=\omega_2/k_2 = 1/2$ of *source-2* differs from $c_4=\omega_4/k_4 = 1$ of *source-4*.)

Let continuous waves (CW) from the two sources interfere in a 2-CW sum.

$$\Psi^{2-CW} = (e^{i(k_4x-\omega_4t)} + e^{i(k_2x-\omega_2t)})/2 \tag{1.10a}$$

To solve for zeros of this sum we first factor it into a phase-wave e^{ip} and a group-wave *cos g* factor.

$$\begin{aligned}\Psi^{2-CW} &= e^{i\left(\frac{k_4+k_2}{2}x-\frac{\omega_4+\omega_2}{2}t\right)}\left(e^{i\left(\frac{k_4-k_2}{2}x-\frac{\omega_4-\omega_2}{2}t\right)} + e^{-i\left(\frac{k_4-k_2}{2}x-\frac{\omega_4-\omega_2}{2}t\right)}\right)/2 \\ &= e^{i\left(\frac{k_4+k_2}{2}x-\frac{\omega_4+\omega_2}{2}t\right)}\cos\left(\frac{k_4-k_2}{2}x-\frac{\omega_4-\omega_2}{2}t\right) \\ &= e^{i(k_px-\omega_pt)}\cos\left(k_gx-\omega_gt\right) \equiv e^{ip}\cos g\end{aligned} \tag{1.10b}$$

Phase factor e^{ip} has a half-sum *(ω,k)*-vector $\mathbf{K}_{phase}=(\mathbf{K}_4+\mathbf{K}_2)/2$ in its argument $p = k_px-\omega_pt$. *Group factor cos g* has a half-difference *(ω,k)*-vector $\mathbf{K}_{group}=(\mathbf{K}_4-\mathbf{K}_2)/2$ in its argument $g = k_gx-\omega_gt$.

$$\mathbf{K}_{phase} = \frac{\mathbf{K}_4+\mathbf{K}_2}{2} = \frac{1}{2}\begin{pmatrix}\omega_4+\omega_2\\ k_4+k_2\end{pmatrix} = \begin{pmatrix}\omega_p\\ k_p\end{pmatrix} = \frac{1}{2}\begin{pmatrix}4+1\\ 4+2\end{pmatrix} = \begin{pmatrix}2.5\\ 3.0\end{pmatrix} \tag{1.10c}$$

$$\mathbf{K}_{group} = \frac{\mathbf{K}_4-\mathbf{K}_2}{2} = \frac{1}{2}\begin{pmatrix}\omega_4-\omega_2\\ k_4-k_2\end{pmatrix} = \begin{pmatrix}\omega_g\\ k_g\end{pmatrix} = \frac{1}{2}\begin{pmatrix}4-1\\ 4-2\end{pmatrix} = \begin{pmatrix}1.5\\ 1.0\end{pmatrix} \tag{1.10d}$$

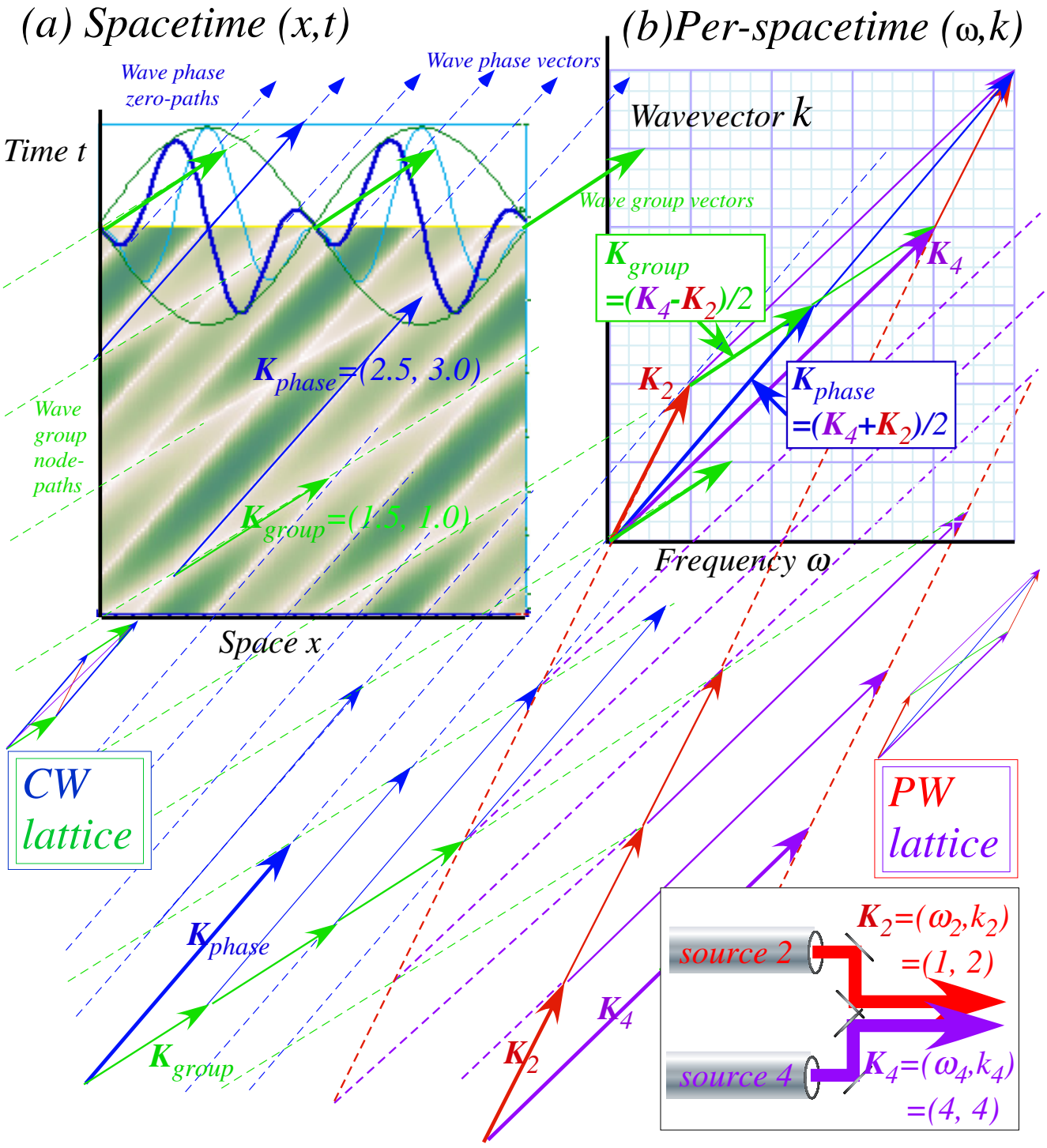

Fig. 4 "Mythical" sources and their wave coordinate lattices in (a) Spacetime and (b) Per-spacetime.

CW lattices of phase-zero and group-node paths intermesh with PW lattices of pulse, packet, or "particle" paths.

The *(ω,k)*-vectors $\mathbf{K}_n$ define paths and coordinate lattices for pulse peaks and wave zeros in Fig. 4a. Real zeros (ReΨ=*0*) have speed V_{phase} on $\mathbf{K}_{phase}$ paths. Group zeros (|Ψ|=*0*) move at V_{group} on $\mathbf{K}_{group}$.

$$V_{phase}=\frac{\omega_4+\omega_2}{k_4+k_2}=\frac{5}{6}=0.83 \qquad (1.11a) \qquad\qquad V_{group}=\frac{\omega_4-\omega_2}{k_4-k_2}=\frac{3}{2}=1.5 \qquad (1.11b)$$

Phase factor real part $\mathrm{Re}\,e^{ip}=\mathrm{Re}\,e^{i\left(k_p x-\omega_p t\right)}=\cos p$ zeros on *phase-zero paths* where angle *p* is *N(odd)·π/2*.

$$k_p x-\omega_p t=p=N_p\pi/2 \quad \left(N_p=\pm1,\pm3...\right).$$

Group factor $\cos g=\cos\left(k_g x-\omega_g t\right)$ zeros on *group-zero* or *nodal paths* where angle *g* is *N(odd)·π/2*.

$$k_g x-\omega_g t=g=N_g\pi/2 \quad \left(N_g=\pm1,\pm3...\right).$$

At *wave zero (WZ) lattice points (x,t) both* factors are zero. That defines the lattice vectors in Fig. 4a.

$$\begin{pmatrix} k_p & -\omega_p \\ k_g & -\omega_g \end{pmatrix}\begin{pmatrix} x \\ t \end{pmatrix}=\begin{pmatrix} p \\ g \end{pmatrix}=\begin{pmatrix} N_p \\ N_g \end{pmatrix}\frac{\pi}{2} \qquad (1.12a)$$

Solving gives *spacetime (x,t)* zero-path lattice shown by the white lines in Fig. 4a. Each intersecting lattice point is an odd-integer (N_p,N_g) combination of wave-vectors $\mathbf{P}=\pi\mathbf{K}_{phase}/2D$ and $\mathbf{G}=\pi\mathbf{K}_{group}/2D$.

$$\begin{pmatrix} x \\ t \end{pmatrix}=\frac{\begin{pmatrix} -\omega_g & \omega_p \\ -k_g & k_p \end{pmatrix}\begin{pmatrix} p \\ g \end{pmatrix}}{\omega_p k_g-\omega_g k_p}=\frac{-p\begin{pmatrix} \omega_g \\ k_g \end{pmatrix}+g\begin{pmatrix} \omega_p \\ k_p \end{pmatrix}}{\omega_p k_g-\omega_g k_p}=\frac{\pi}{2D}\left(-N_p\mathbf{K}_{group}+N_g\mathbf{K}_{phase}\right) \qquad (1.12b)$$

Scaling factor $2D/\pi=2(\omega_p k_g-\omega_g k_p)/\pi$ converts *(per-time, per-space)* vectors $\mathbf{K}_{group}$ or $\mathbf{K}_{phase}$ into *(space, time)* vectors $\mathbf{P}=\binom{x}{t}_p$ or $\mathbf{G}=\binom{x}{t}_g$. (Plot units are set so *2D/π =1* or *D=π/2 iff D* is *non*-zero.)

Fig. 4b is a lattice of source vectors $\mathbf{K}_2$ and $\mathbf{K}_4$ (the difference and sum of $\mathbf{K}_{group}$ and $\mathbf{K}_{phase}$).

$$\mathbf{K}_2=\mathbf{K}_{phase}-\mathbf{K}_{group}=\begin{pmatrix} \omega_2 \\ k_2 \end{pmatrix}=\begin{pmatrix} 1 \\ 2 \end{pmatrix} \quad (1.13a) \qquad\qquad \mathbf{K}_4=\mathbf{K}_{phase}+\mathbf{K}_{group}=\begin{pmatrix} \omega_4 \\ k_4 \end{pmatrix}=\begin{pmatrix} 4 \\ 4 \end{pmatrix} \quad (1.13b)$$

Phase of source-2 has speed V_2 on $\mathbf{K}_2$ paths. Phase of source-4 has speed V_4 on $\mathbf{K}_4$ paths.

$$V_2=\frac{\omega_2}{k_2}=\frac{1}{2}=0.5 \qquad (1.14a) \qquad\qquad V_4=\frac{\omega_4}{k_4}=\frac{1}{1}=1.0 \qquad (1.14b)$$

However, one can view the $\mathbf{K}_2$ and $\mathbf{K}_4$ paths in light of a classical or semi-classical viewpoint since pulse waves (PW) are wave packets (WP) that mimic particles. Newton took a hard-line view of nature and ascribed reality to mass particles but viewed waves as illusory. He misunderstood light when it exhibited interference effects and complained that its particles or "corpuscles" were having "fits."

Newtonian corpuscular views are parodied here by imagining that frequency $\upsilon_2=\omega_2/2\pi$ (or $\upsilon_4=\omega_4/2\pi$) is the rate at which source-2 (or 4) emits "corpuscles" of velocity V_2 (or V_4) so the wavelengths $\lambda_2=2\pi/k_2$ (or $\lambda_4=2\pi/k_4$) are just inter-particle spacing of $\mathbf{K}_2$ (or $\mathbf{K}_4$) lines in Fig. 4a.

Since wavelength λ_2 (λ_4) separates $\mathbf{K}_2$ ($\mathbf{K}_4$) lattice lines in Fig. 4b, one can imagine them as "corpuscle paths" on *diagonals* of the $\mathbf{K}_{group}$($\mathbf{K}_{phase}$) WZ-lattice in time *vs* space *(x,t)* of Fig. 4a.

Left and right baseline vectors **L** and **R** of diamonds in Fig. 3a are special cases of $\mathbf{K}_2$ and $\mathbf{K}_4$ vectors (1.13). Diamond paths in Fig. 3a are ±45° pulse wave (PW) paths due to a multi-term CW sum (1.17). Still, one might imagine pulses are "corpuscles" or particles, and the $\mathbf{L}_{(-45°)}$ and $\mathbf{R}_{(+45°)}$ paths, like the $\mathbf{K}_2$ and $\mathbf{K}_4$ "corpuscle" paths in Fig. 4b, are baselines for some kind of "optical base runners."

The square wave zero (WZ) grid in Fig. 3b is due to a two-term CW sum (1.9). It is a special case of the WZ lattice in Fig. 4a due to two-term sum (1.10). Half-sum phase vector $\mathbf{P} = (\mathbf{L} + \mathbf{R})/2$ and half-difference group vector $\mathbf{G} = (\mathbf{L} - \mathbf{R})/2$ define a square grid of nodal lines in Fig. 3a. Vectors **P** and **G** are a square example of the phase and group lattice vectors $\mathbf{K}_{phase}$ and $\mathbf{K}_{group}$ in (1.10) that define a non-square WZ path lattice of white lines (real zeros) in Fig. 4a. (Sec.2 analyzes Fig. 3 in detail.)

Primitive vectors **L** and **R** are optical pulse wave (PW) or particle paths (PP) in Fig. 3a while in Fig. 3b their half-sum $\mathbf{P} = (\mathbf{L} + \mathbf{R})/2$ and half-difference $\mathbf{G} = (\mathbf{L} - \mathbf{R})/2$ define optical phase and group wave zero (WZ) coordinate grid lines. Phase and group WZ lines are time and space axes, respectively, forming an optical coordinate basis for our subsequent development of relativistic quantum mechanics.

This development shows wave-particle, wave-pulse, and CW-PW duality in the cells of each CW-PW wave lattice. Each (**L**,**R**)-cell of a PW lattice has two CW vectors **P** or **G** on each diagonal, and each (**P**,**G**)-cell of the CW lattice has one PW vector **L** or **R** on each diagonal. This is due to sum and difference relations (1.10d) or (1.13b) between (**L**,**R**)= ($\mathbf{K}_2$, $\mathbf{K}_4$) and (**P**,**G**)=($\mathbf{K}_{phase}$, $\mathbf{K}_{group}$).

In order that space-time *(x,t)*-plots could be superimposed on frequency-wavevector *(ω,k)*-plots or *(υ,κ)*-plots, it is necessary to switch axes for one of them. The space-time *t(x)*-plots in Fig. 4a follow the convention adopted by most relativity literature for a vertical time ordinate *(t-axis)* and horizontal space abscissa *(x-axis)* that is quite the opposite of Newtonian calculus texts that plot *x(t)* horizontally. However, the frequency-wavevector *k(ω)*-plots in Fig. 4b switch axes from the usual *ω(k)* convention so that *t(x)* slope due to space-time velocity *x/t* or *Δx/Δt (meter/second)* in Fig. 4a matches that of equal per-time-per-space wave velocity *ω/k* or *Δω/Δk (per-second/per-meter)* in Fig.4b. (Recall (1.5))

Superimposing *t(x)*-plots onto *k(ω)*-plots also requires that the latter be rescaled by the scale factor $\pi/2D$ derived in (1.12b), but rescaling fails if cell-area determinant factor *D* is zero.

$$D = \omega_p k_g - \omega_g k_p = \left| \mathbf{K}_{phase} \times \mathbf{K}_{group} \right| \qquad (1.15)$$

Co-propagating light beams $\mathbf{K}_2 = (\omega_2,k_2)=(2c,2)$ and $\mathbf{K}_4 = (\omega_4,k_4)=(4c,4)$ plotted in Fig. 5b have *D=0* since all K-vectors including $\mathbf{K}_{phase}=(\omega_p,k_p)=(3c,3)$ and $\mathbf{K}_{group}= (\omega_g,k_g)=(c,1)$ lie on one *c*-baseline of speed *c* that has unit slope *(ω/ck=1)*. We rescale *(ω,k)*-plots to *(ω,ck)* and *(x,t)*-plots to *(x,ct)* in Fig. 5 and later.

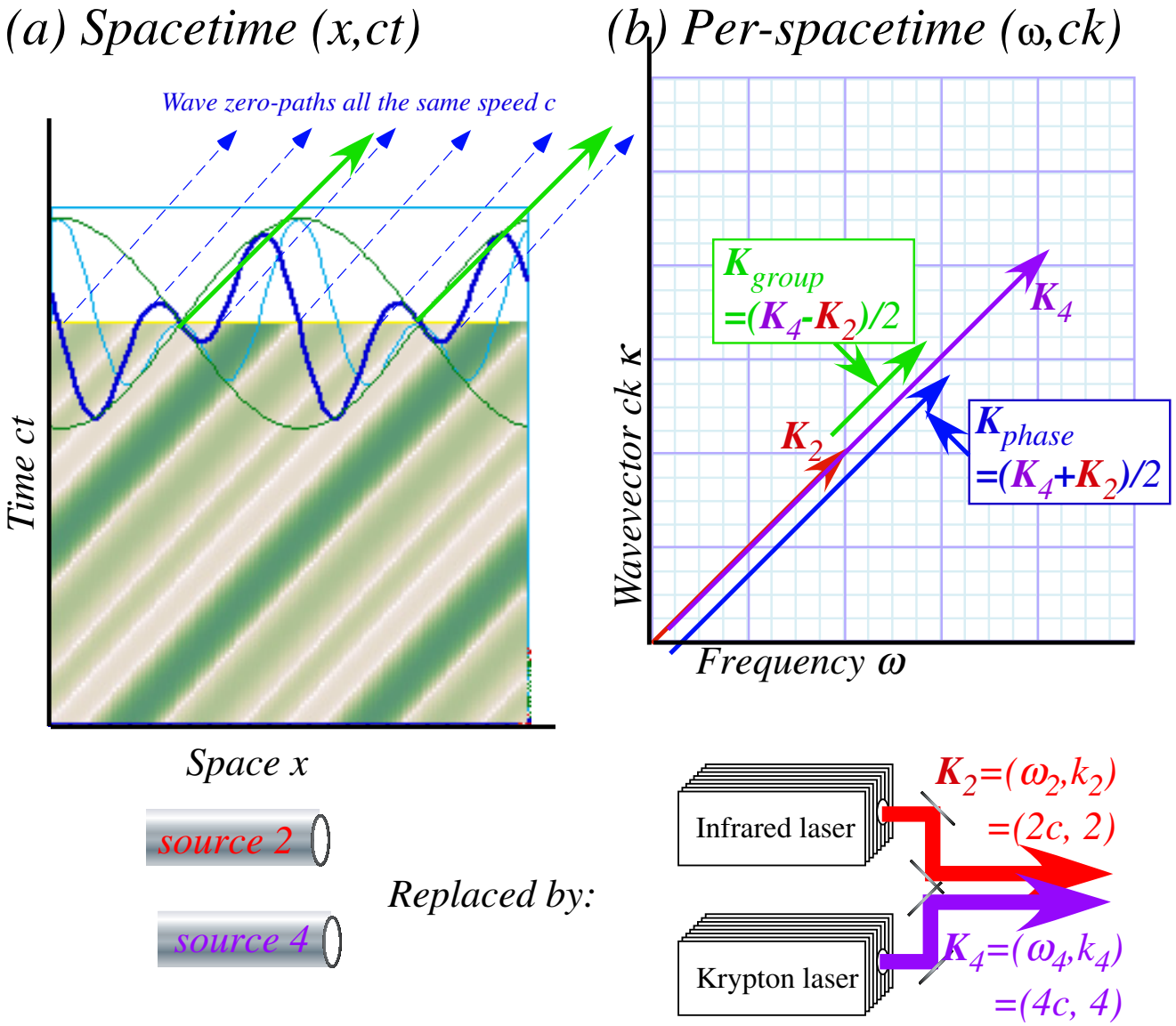

Fig. 5 Co-propagating laser beams produce a collapsed wave lattice since all parts have same speed c.

For *counter* propagating waves shown in Fig. 3 and Fig. 6-7 below, D is *not* zero because two opposite (right-left) baselines (**R**,**L**)= (**K**$_2$, **K**$_4$) are used to make CW square bases (**P**= **K**$_{phase}$, **G**= **K**$_{group}$) with a non-zero value for area D =|**GxP**|, an axis-switch of (1.15). PW base vectors (**R**,**L**) are sum and difference (**P+G**,**P-G**) of CW bases so a PW diamond area |**RxL**| is twice that of a CW square.

$$|\mathbf{RxL}| = |(\mathbf{P+G}) \times (\mathbf{P-G})| = 2|\mathbf{GxP}| \qquad (1.16)$$

It will be shown that these areas are key geometric invariants for relativity and quantum mechanics.

2.Wave coordinates for counter-propagating beams

Let us represent counter-propagating frequency-ω laser beams by a baseball diamond in Fig. 6a spanned by CW vectors for waves moving left-to-right (**R** on 1st base) and right-to-left (**L** on 3rd base).

$$\mathbf{R}=\mathbf{K}_1=(ck_1,\omega_1)=\omega(1,1) \quad (2.1a) \qquad \mathbf{L}=\mathbf{K}_3=(ck_3,\omega_3)=\omega(-1,1) \quad (2.1b)$$

Fig. 6 uses conventional *(ck,ω)*-plots for per-space-time and *(x,ct)*-plots for space-time. Both beams have frequency $\upsilon=\omega/2\pi=600THz$(green), the unit scale for ω and ck axes. For the **L**-beam, ck is $-\omega$.

Phase vector $\mathbf{P}=\mathbf{K}_{phase}$ and group vector $\mathbf{G}=\mathbf{K}_{group}$ are also plotted in *(ω,ck)*-space in Fig. 6b.

$$\mathbf{K}_{phase}=\frac{\mathbf{K}_1+\mathbf{K}_3}{2}=\frac{1}{2}\begin{pmatrix}ck_1+ck_3\\ \omega_1+\omega_3\end{pmatrix} =\mathbf{P}=\begin{pmatrix}ck_p\\ \omega_p\end{pmatrix}=\frac{\omega}{2}\begin{pmatrix}1-1\\ 1+1\end{pmatrix}=\omega\begin{pmatrix}0\\ 1\end{pmatrix} \quad (2.2a)$$

$$\mathbf{K}_{group}=\frac{\mathbf{K}_1-\mathbf{K}_3}{2}=\frac{1}{2}\begin{pmatrix}ck_1-ck_3\\ \omega_1-\omega_3\end{pmatrix} =\mathbf{G}=\begin{pmatrix}ck_g\\ \omega_g\end{pmatrix}=\frac{\omega}{2}\begin{pmatrix}1+1\\ 1-1\end{pmatrix}=\omega\begin{pmatrix}1\\ 0\end{pmatrix} \quad (2.2b)$$

Phase and group velocities of counter-propagating light waves may vary widely from c. These do!

$$\frac{V_{phase}}{c}=\frac{\omega_1+\omega_3}{ck_1+ck_3}=\frac{2}{0}=\infty \quad (2.3a) \qquad \frac{V_{group}}{c}=\frac{\omega_1-\omega_3}{ck_1-ck_3}=\frac{0}{2c}=0 \quad (2.3b)$$

The extreme speeds account for the square (Cartesian) wave-zero (WZ) coordinates plotted in Fig. 6c. As noted after Fig. 3, the group zeros or wave nodes are stationary and parallel to the time ct-axes, while the real-zeros of the phase wave are parallel to the space x-axes. The latter instantly appear and disappear periodically with infinite speed (2.3a) while standing wave nodes have zero speed (2.3b).

Fig. 6d shows 2-way pulse wave (2-PW) trains for comparison with the 2-CW WZ grid in Fig. 6c. As noted after Fig. 2, a PW function is an N-CW combination that suppresses its amplitude through *destructive* interference between pulse peaks that owe their enhancement to *constructive* interference.

Colliding PW's show no mutual interference in destroyed regions. Generally one PW is alone on its diamond path going $+c$ parallel to 1st baseline $\mathbf{R}=\mathbf{K}_1$ or going $-c$ parallel to 3rd baseline $\mathbf{L}=\mathbf{K}_3$.

$$\frac{V_1}{c}=\frac{\omega_1}{ck_1}=\frac{1}{1}=1 \quad (2.4a) \qquad \frac{V_3}{c}=\frac{\omega_3}{ck_3}=\frac{1}{-1}=-1 \quad (2.4b)$$

But wherever two PW peaks collide, each of the CW pairs will be seen trying to form a square coordinate grid that 2-CW zeros would make by themselves. This begins to explain the tiny square "bases" seen at the corners of the space-time "baseball diamonds" in Fig. 6d.

CW-Doppler derivation of relativity

Occam razors shorten derivations. How much does Evenson's CW razor-cut of Einstein's PW axiom shorten derivation of relativity? Quantifying length for Einstein's popular (and still common) derivation is difficult as is a step-by-step count for the CW derivation that follows. Let us just say that *several* steps are reduced to very *few* steps. More important is the wave-nature insight that is gained.

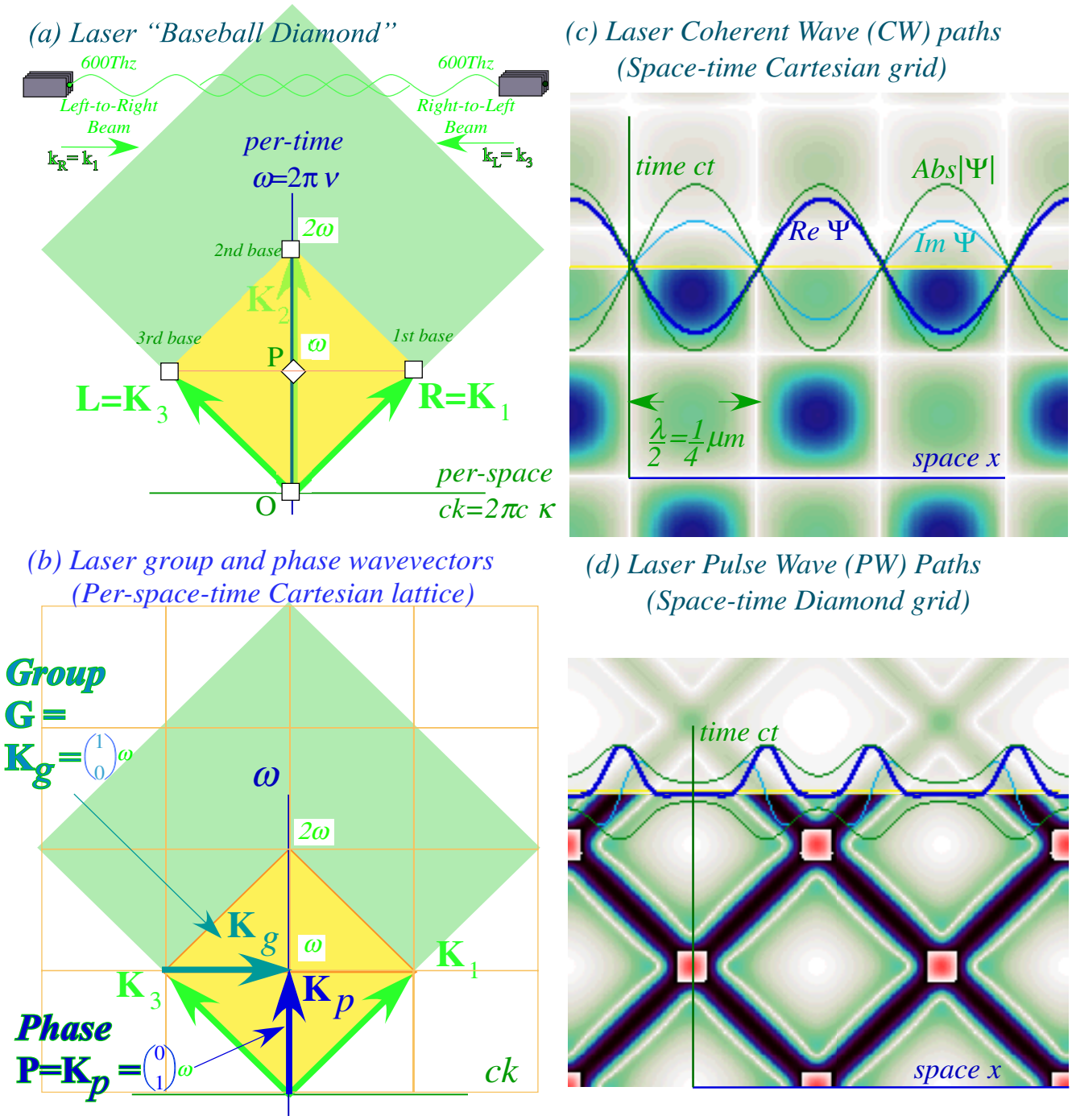

Fig. 6. Laser lab view of 600Thz CW and PW light waves in per-space-time (a-b) and space-time (c-d).

In fact, a case can be made that a CW derivation takes *zero* steps. The answer is already done by a 2-CW wave pattern in Fig. 7c that automatically produces an Einstein-Lorentz-Minkowski[14] grid of space-time coordinates. Still we need logical steps drawn in Fig. 7a-b that redo the Cartesian grid in Fig. 6 just by Doppler shifting each baseline one octave according to *c*-axiom (1.1) (*"Stay on baselines!"*) and *t*-reversal axiom (1.2) (*"If 1st base increases by one octave, 3rd base decreases by the same."*)

So Fig. 7 is just Fig. 6 seen by atoms going right-to-left fast enough to double *both* frequency $\upsilon=\omega/2\pi$ and wavevector ck of the vector **R** on 1st base (while halving vector **L** on 3rd base to obey (1.2).)

$$\mathbf{R}=\mathbf{K}_1=(ck'_1,\omega'_1)=\omega(2,2) \quad (2.5a) \qquad \mathbf{L}=\mathbf{K}_3=(ck'_3,\omega'_3)=\omega(-1/2,\,1/2) \quad (2.5b)$$

The atom sees head-on **R**-beam blue-shift to frequency $\upsilon_1'=2\upsilon=\omega_1'/2\pi=1200THz$(*UV*) by doubling green $\upsilon_1=\omega/2\pi=\upsilon_3=600THz$. It also sees the tail-on **L**-beam red-shift by half to $\upsilon_3'=\upsilon/2=\omega_3'/2\pi=300THz$(*IR*).

The phase vector $\mathbf{K}_{phase}$ and group vector $\mathbf{K}_{group}$ are plotted in (ck',ω')-space in Fig. 7b.

$$\mathbf{K}_{phase}=\frac{\mathbf{K}_1+\mathbf{K}_3}{2}=\frac{1}{2}\begin{pmatrix}ck'_1+ck'_3\\ \omega'_1+\omega'_3\end{pmatrix} \qquad \mathbf{K}_{group}=\frac{\mathbf{K}_1-\mathbf{K}_3}{2}=\frac{1}{2}\begin{pmatrix}ck'_1-ck'_3\\ \omega'_1-\omega'_3\end{pmatrix}$$
$$=\mathbf{P}'=\begin{pmatrix}ck'_p\\ \omega'_p\end{pmatrix}=\frac{\omega}{2}\begin{pmatrix}2-1/2\\ 2+1/2\end{pmatrix}=\omega\begin{pmatrix}3/4\\ 5/4\end{pmatrix} \quad (2.6a) \qquad =\mathbf{G}'=\begin{pmatrix}ck'_g\\ \omega'_g\end{pmatrix}=\frac{\omega}{2}\begin{pmatrix}2+1/2\\ 2-1/2\end{pmatrix}=\omega\begin{pmatrix}5/4\\ 3/4\end{pmatrix} \quad (2.6b)$$

Phase velocity is the inverse of group velocity in units of c, and V'_{group} is *minus the atoms' velocity!*

$$\frac{V'_{phase}}{c}=\frac{\omega'_1+\omega'_3}{ck'_1+ck'_3}=\frac{2+1/2}{2-1/2}=\frac{5}{3} \quad (2.7a) \qquad \frac{V'_{group}}{c}=\frac{\omega'_1-\omega'_3}{ck'_1-ck'_3}=\frac{2-1/2}{2+1/2}=\frac{3}{5} \quad (2.7b)$$

Velocity $u=V'_{group}=3c/5$ is the atoms' view for a lab speed of *zero* had by laser standing nodes. (It is the speed of the lasers' group nodes and their connecting lab bench relative to the atoms.) Phase velocity $V'_{phase}=5c/3$ is the atoms' view for a lab speed of *infinity* had by lasers' real wave zeros. (x-zero lines are simultaneous in the laser lab but not so in the atom-frame. x-lines tip *toward* ct-lines in Fig. 7c.)

Eqs. (2.5-7) use a Doppler blue-shift factor $b=2$. If each "2" is replaced by "b" then Eq. (2.7b) yields a relation for the laser velocity $u=V'_{group}$ relative to atoms in terms of their blue-shift b.

$$\frac{V'_{group}}{c}=\frac{u}{c}=\frac{b-1/b}{b+1/b}=\frac{b^2-1}{b^2+1} \quad (2.8a)$$

Inverting this gives standard relativistic Doppler b *vs.* u/c relations.

$$b^2=(1+u/c)/(1-u/c) \quad \text{or:} \quad b=\sqrt{(1+u/c)/(1-u/c)}=(1+u/c)/\sqrt{1-u^2/c^2} \quad (2.8b)$$

It is remarkable that most treatments of relativity first derive *second* order effects, time dilation and length contraction. Doppler and asimultaneity shifts are *first* order in u but treated second. Setting $2=b$ in (2.6) using (2.8) gives vectors $\mathbf{G}'=\mathbf{K}_g=\binom{d}{a}$ and $\mathbf{P}'=\mathbf{K}_p=\binom{a}{d}$ with dilation factor $d=1/\sqrt{1-u^2/c^2}$ and asimultaneity factor $a=u\cdot d/c$. (So d arrives early here, too, but with a wavelike finesse.)

$$\mathbf{K}_{phase}=\frac{\omega}{2}\begin{pmatrix}b-1/b\\ b+1/b\end{pmatrix}=\omega\begin{pmatrix}(u/c)/\sqrt{1-u^2/c^2}\\ 1/\sqrt{1-u^2/c^2}\end{pmatrix} \quad (2.9a) \qquad \mathbf{K}_{group}=\frac{\omega}{2}\begin{pmatrix}b+1/b\\ b-1/b\end{pmatrix}=\omega\begin{pmatrix}1/\sqrt{1-u^2/c^2}\\ (u/c)/\sqrt{1-u^2/c^2}\end{pmatrix} \quad (2.9b)$$

K-vector components d and a (in ω units) are Lorentz-Einstein (LE) matrix coefficients relating atom-values (ck',ω') or (x',t') to lab-values (ck,ω) or (x,t) based on lab unit vectors $\hat{\mathbf{G}}=\binom{1}{0}$ and $\hat{\mathbf{P}}=\binom{0}{1}$ in (2.2).

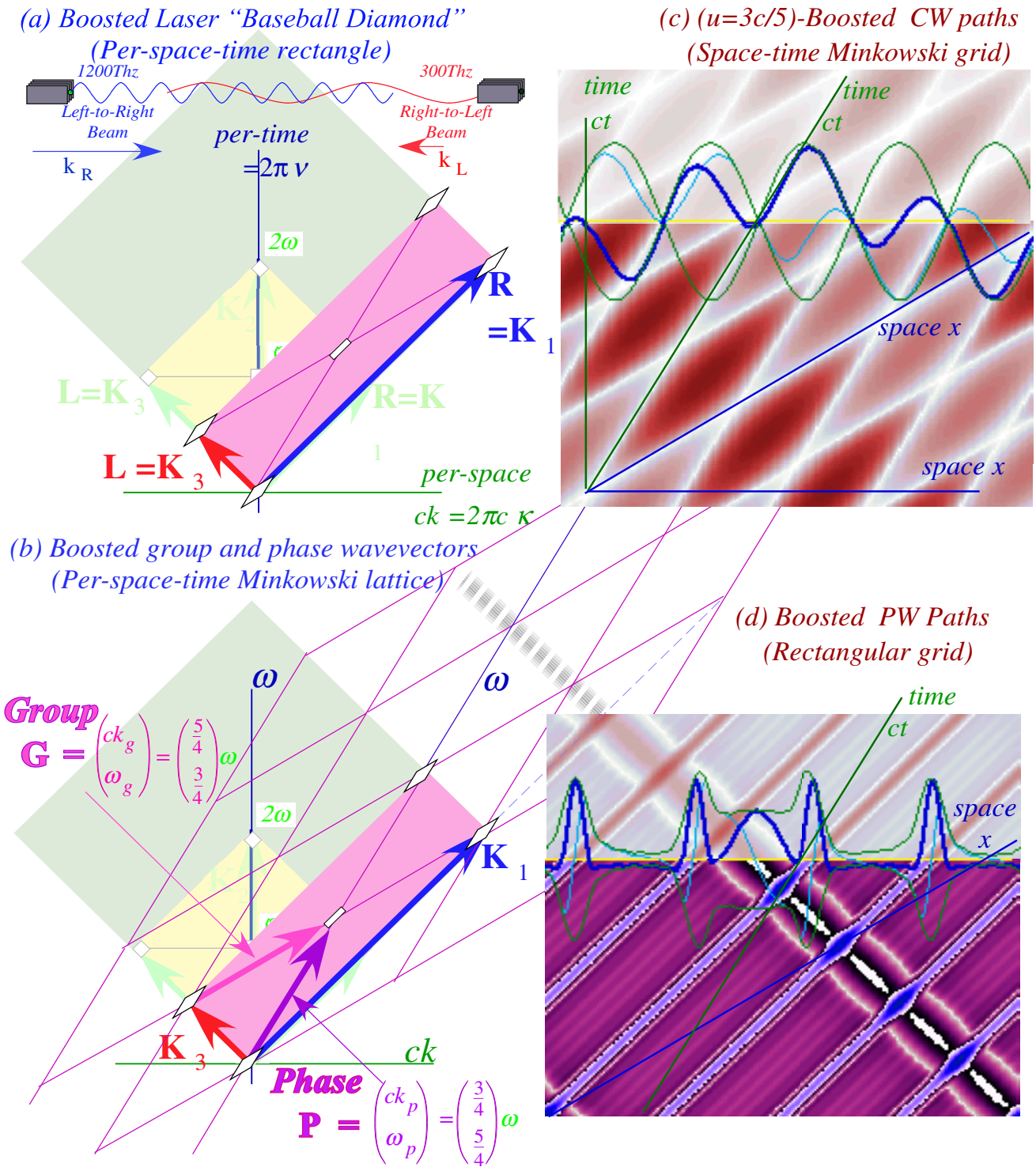

Fig.7 Atom view of 600Thz CW and PW light waves in per-spacetime (a-b) and space-time (c-d) boosted to u=3c/5.

The Lorentz[15]-Einstein[16] per-spacetime and spacetime transformations follow from **K**-vectors (2.9).

$$\begin{pmatrix} \omega' \\ ck' \end{pmatrix} = \begin{pmatrix} \frac{1}{\sqrt{1-u^2/c^2}} & \frac{u/c}{\sqrt{1-u^2/c^2}} \\ \frac{u/c}{\sqrt{1-u^2/c^2}} & \frac{1}{\sqrt{1-u^2/c^2}} \end{pmatrix} \begin{pmatrix} \omega \\ ck \end{pmatrix} \quad (2.10a) \qquad \begin{pmatrix} x' \\ ct' \end{pmatrix} = \begin{pmatrix} \frac{1}{\sqrt{1-u^2/c^2}} & \frac{u/c}{\sqrt{1-u^2/c^2}} \\ \frac{u/c}{\sqrt{1-u^2/c^2}} & \frac{1}{\sqrt{1-u^2/c^2}} \end{pmatrix} \begin{pmatrix} x \\ ct \end{pmatrix} \quad (2.10b)$$

Wave **K**-vectors are bases for space-time *and* per-space-time. One symmetric LE matrix, invariant to axis-switch *(ω,ck)* ⇄ *(ck,ω)*, applies to both. Conventional *ω*–ordinate *vs. ck*-abscissa per-space-time and *ct*-ordinate *vs. x*-abscissa space-time plots are used in Fig. 7 where $\widehat{\omega}$ =**P**=**K**$_{phase}$ and $\widehat{ck}$ =**G**=**K**$_{group}$ vectors serve as *ct*-time and *x*-space bases, respectively, and then also serve as *ω*–and-*ck*-bases.

The left and right pulse wave (PW) vectors **L** and **R** in per-space-time Fig. 7a also define left and right PW paths in space-time Fig. 7d. This holds in either convention because **L** and **R** lie on 45° reflection planes that are eigenvectors of an axis-switch *(ω,ck)* ⇄ *(ck,ω)* with eigenvalues *+1* and *–1* while half-sum-and-difference vectors $\mathbf{P} = (\mathbf{L} + \mathbf{R})/2$ and $\mathbf{G} = (\mathbf{L} - \mathbf{R})/2$ simply switch (**P** ⇄ **G**).

Einstein's PW axiom *"PW speed c is invariant,"* might give the impression that pulses themselves are invariant. This may hold for *δ*-pulses whose infinite bandwidth gives them enough energy to start a new universe! But, finite-*Δ* pulses in Fig. 7d clearly deform. Only their speed is invariant. Also, each PW intersection-interference square in Fig. 6d deforms into a Minkowski-like rhombus in Fig. 7d.

Geometry of relative phase

Einstein relativity shows Galilean relativity, based on simple velocity sums and differences, to be a 400 year-old approximation that fails utterly at high speeds. Einstein also dethrones *infinite* velocity, Galileo's one invariant velocity shared by his observers regardless of their (finite) velocity. In its place reigns a finite velocity limit *c* that is now the Einstein-Maxwell-Evenson invariant.

So it is remarkable that frequency sums and differences (1.10) simplify relativity by using Galilean-like rules for *angular* velocities $\omega_A = \dot{\phi}_A$ of light phases ϕ_A. Frequency sums or differences $\omega_A \pm \omega_B$ from interference terms like $\psi_A \psi_B{}^* = ABe^{-i(\omega_A - \omega_B)t}$ between wave pairs $\psi_A = Ae^{-i\omega_A t}$ and $\psi_B = Be^{-i\omega_B t}$ are *relative* frequencies (beat notes, overtones, etc.) subject only to simple addition and subtraction rules that are like Galileo's rules for linear velocity. Simple angular phase principles deeply underlie modern physics, and so far there appears to be no *c*-like speed limit for an angular velocity *ω*.

Phase principles have electromagnetic origins. Writing oscillatory wave functions using real and imaginary parts is common for studies of AC electrical phenomena or harmonic oscillators in general. The real part *q* of oscillator amplitude $q+ip= Ae^{-i\omega t}$ is position $q=A\cos\omega t$. The imaginary part $p=A\sin\omega t$ is velocity $v =-A\omega\sin\omega t$ in units of angular frequency *ω*. Positive *ω* gives a clockwise rotation like that of classical phase space or analog clocks, so a minus sign in conventional $Ae^{-i\omega t}$ phasors serves to remind us that wave frequency *ω defines* our clocks and wavevector *k=ω/c defines* our meter sticks.

A plane wave of wavevector *k* in Fig. 2 is drawn as a phasor array, one $A = |A|e^{ikx}$ for each location *x*. A plane wave advances in time according to $|A|e^{i(kx-\omega t)}$ at phase velocity $V=\omega/k$. Similar

convention and notation are used for light waves and for quantum matter waves, but only light waves have physical units, vector potential **A** and electric **E**-field, defining their real and imaginary parts. While classical laser wave phase is observable, only *relative* quantum wave phase appears to be so.

The concept of relative phase (and frequency) arises in classical or quantum interference where a sum of two waves $\psi_A = Ae^{i\phi_A}$ and $\psi_B = Be^{i\phi_B t}$ may be represented at each position *x* by a vector sum of a phasor-A with a phasor-B as in Fig. 8a. (Fig. 2 has a sum of 12 phasors at each *x*-point.) The result is a clockwise race around a track between the faster one, say A-phase $\phi_A = k_A x - \omega_A t$ of angular speed -ω_A, and the slower B-phase $\phi_B = k_B x - \omega_B t$ of angular speed -ω_B as sketched in Fig. 8b.

When A passes B the sum is a maximum or *beat* that then subsides to a minimum or *node* when A is on the opposite side of the track from B. If amplitude magnitudes |A| and |B| are equal as they are in Fig. 8, then the wave node is a wave *zero* that defines one of the group **G**-lines in WZ coordinates of Fig. 4 through Fig. 7. The *relative* angular velocity $\Delta = \omega_A - \omega_B$ (beat angular frequency) is the angular rate at which A passes B. A-B passings occur δ times *(per sec.)* where δ is Δ divided by track length 2π.

$$\delta_{beat} = \Delta / 2\pi = \upsilon_A - \upsilon_B \tag{2.11}$$

If one could ride in an angular Galilean frame of phasor-B, then A would be seen passing at angular speed Δ with frequency δ. Suppose instead, one could ride at their *average* angular speed $\bar{\Omega}$.

$$\bar{\Omega} = \frac{\omega_A + \omega_B}{2} \tag{2.12}$$

Then Galilean arithmetic (which lasers given no reason to doubt in these matters) implies that phasor A or B would each appear with a relative speed of plus-or-minus *half* their relative velocity.

$$\pm\frac{\Delta}{2} = \pm\frac{\omega_A - \omega_B}{2} \tag{2.13}$$

A point of view relative to phasor B is shown by the first of Fig. 8c. A dashed circle represents moving phasor A with ψ_A on one diagonal of an inscribed rectangle whose sides are the resultant sum $\psi_A + \psi_B$ and difference $\psi_A - \psi_B$. The other diagonal ψ_B appears fixed. A companion figure has ψ_A appear fixed instead. Resultants in either figure begin and end on a dashed circle traced by a phasor that is moving relative to the other. A rectangle-in-circle is a key Euclidian element of wave physics and is a key feature of a later figure (Fig. 10) that shows the essence of wave geometry.

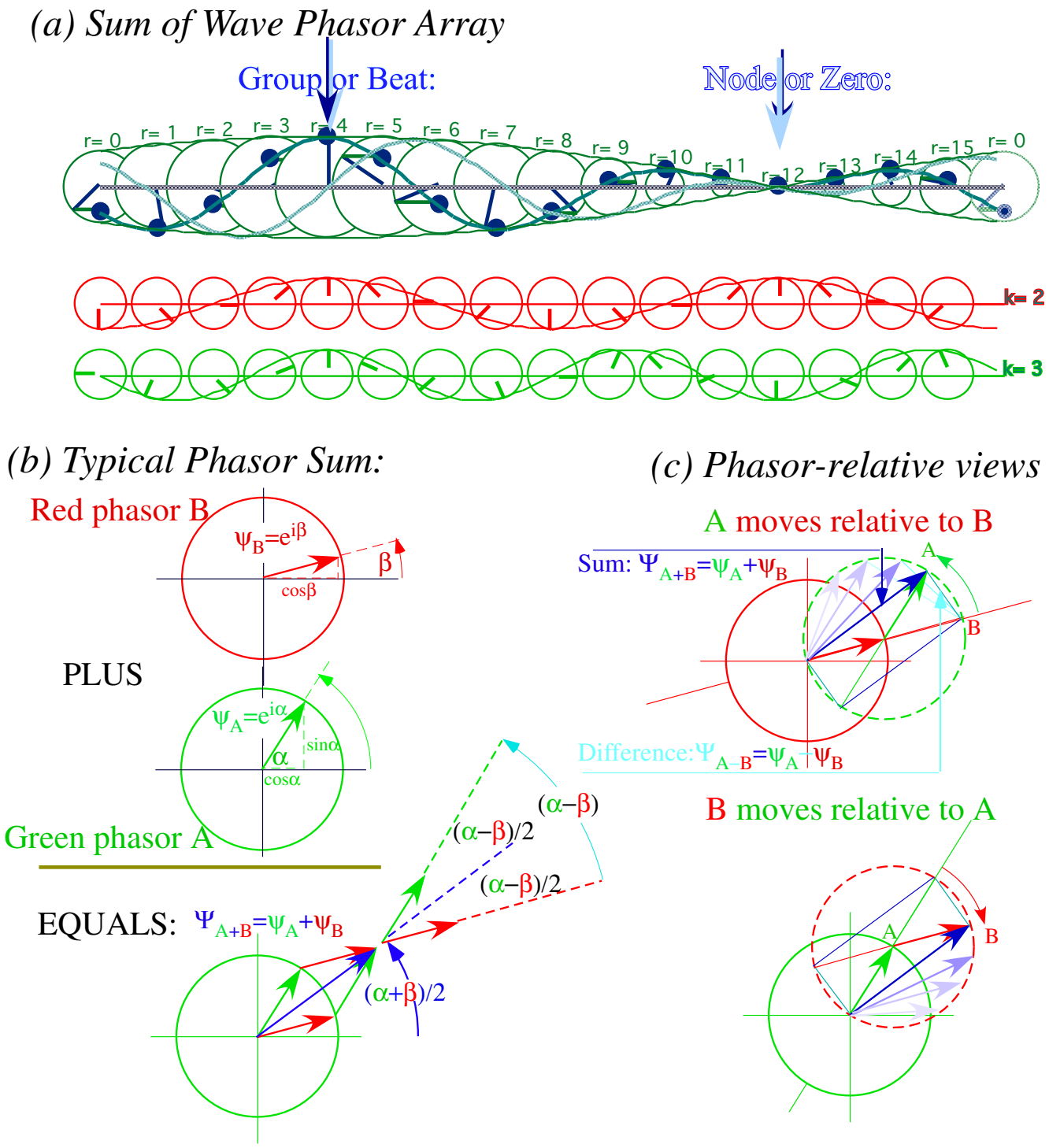

Fig. 8 Wave phasor addition. (a) Each phasor in a wave array is a sum (b) of two component phasors. (c) In phasor-relative views either A or else B is fixed. An evolving sum-and-difference rectangle is inscribed in the (dashed) circle of the phasor moving relative to the fixed one.

The half-sum and half-difference angles in Fig. 8b and frequencies (2.12) and (2.13) appear in the interference formulas (1.10) that lead to relativistic Lorentz-Einstein coordinate relations (2.10) and their WZ grid plots of Minkowski coordinates in Fig. 7c. One key is the *arithimetic mean* $(\alpha+\beta)/2$ of phases that gives the *geometric mean* $(\psi_A\psi_B)^{1/2} = Ae^{i(\alpha+\beta)/2}$ of wave phasor amplitudes. The other key is the *difference mean* $\left((\alpha-\beta)/2\right)$ and its *cross mean* $(\psi_A\psi_B{}^*)^{1/2} = Ae^{i(\alpha-\beta)/2}$. Euclidian means and rectangle-in-circle constructions underlie relativistic wave geometry and mechanics as is shown below.

Geometry of Doppler factors

Any number N of transmitter-receivers ("observers" or "atoms" previously introduced) may each be assigned a positive number b_{11}, b_{21}, b_{31}, …that is its Doppler shift of a standard frequency ω_1 broadcast by atom-1 and then received as frequency $\omega_{m1}= b_{m1}\,\omega_1$ by an atom- m. By definition the transmitter's own shift is unity. ($1= b_{11}$) Also, coefficient b_{m1} is independent of frequency since such *geometric* relations work as well on 1THz or 1Hz waves as both waves march in lockstep to the receiver by Evenson's CW axiom (1.1). The production times of a single wavelength of the 1Hz-wave and 10^{12} wavelengths of the 1THz wave must be the same *(1sec.)*, and so must be reception time for the two waves since they arrive in lock step, even if τ is shortened geometrically by $1/b_{m1}$.

If atoms travel at constant speeds on a straight superhighway, then b_{m1} in (2.8a) tells what is the relative velocity u_{m1} of the m^{th} atomic receiver relative to the number-*1* transmitter.

$$\frac{u_{m1}}{c} = \frac{{b_{m1}}^2 - 1}{{b_{m1}}^2 + 1} \qquad (2.14)$$

The velocity u_{m1} is positive if the m^{th} atom goes toward transmitter-*1* and sees a blue ($b_{m1}>1$) shift, but if it moves away u_{m1} is negative so it sees a red ($b_{m1}<1$) shift. Transmitter-*1* has no velocity relative to itself. ($u_{11}=0$) Infinite blue (or red) shift $b_{m1}=\infty$ (or $b_{m1}=0$) gives $u_{m1}=c$ (or $u_{m1}=-c$) and this defines the range of parameters. The b_{m1} are constant until atom-m passes atom-*1* so relative velocity changes sign ($u_{1m} \to -u_{1m}$). Doppler shift then inverts ($b_{1m} \to 1/b_{1m}$) as is consistent with axiom (1.2).

Suppose now b_{12}, b_{22}, b_{32}, …are Doppler shifts of frequency ω_2 transmitted by the *second* atom and received by the m^{th} atom as frequency $\omega_{m2}= b_{m2}\,\omega_2$. (Any atom (say the n^{th}) may transmit, too.)

$$\omega_{mn}= b_{mn}\,\omega_n \qquad (2.15a)$$

Recipients do not notice if atom-n simply passes on whatever frequency ω_{nm} came from atom-m. If frequency ω_n in (2.15a) is $\omega_{n1}= b_{n1}\,\omega_1$ that atom-n got from atom-*1* then atom-m will not distinguish a direct ω_{m1} from a perfect copy $b_{mn}\,b_{n1}\,\omega_1$ made by atom-n from atom-*1* and then passed on to atom-m.

$$\omega_{m1} = b_{m1}\,\omega_1 = b_{mn}\,b_{n1}\,\omega_1 \qquad (2.15b)$$

A multiplication rule results for Doppler factors and applies to light from atom-*1* or any atom-*p*.

$$\omega_{mp}/\omega_p = b_{mp} = b_{mn}\, b_{np} \qquad (2.15c)$$

An inverse relation results from atom-*p* comparing its own light to that copied by atom-*n*.

$$1 = b_{pp} = b_{pn}\, b_{np} \text{ or: } b_{pn} = 1/b_{np} \qquad (2.15d)$$

Notice that copying or passing light means just that and does not include reflection or changing $+k$ to $-k$ or any other direction. This presents a problem for a receiver not in its transmitter's $(+k)$-beam and certainly for atom-*p* receiving its own beam. The relations (2.15) depend only on relative velocities and not positions (apart from the problem that receivers might be on the wrong side of transmitters).

An obvious solution is to let the receiver overtake its transmitter or failing that delegate a slave transmitter or receiver on its right side. A more elegant solution is to conduct experiments in a large circular coaxial (dispersion-free) waveguide or ring laser so the $(+k)$-beam illuminates the backside as well as forward. Fig. 9 shows one arrangement with $N=5$ receivers of a $\omega_3=600THz$ source whose various speeds produce a matrix of $N(N-1)=20$ Doppler shifted frequencies ω_{mn} and factors b_{mn}.

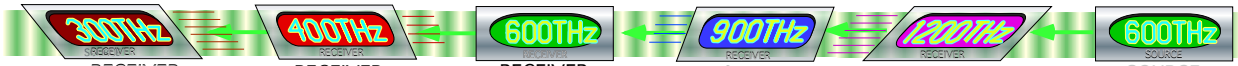

	300THz	400THz	600THz	900THz	1200THz
300THz	300/300 $b_{11}=1$	300/400 $b_{12}=0.75$	300/600 $b_{13}=0.5$	300/900 $b_{14}=0.333$	300/1200 $b_{15}=0.25$
400THz	400/300 $b_{21}=1.333$	400/400 $b_{22}=1$	400/600 $b_{23}=0.667$	400/900 $b_{24}=0.449$	400/1200 $b_{25}=0.333$
600THz	600/300 $b_{31}=2$	600/400 $b_{32}=1.5$	600/600 $b_{33}=1$	600/900 $b_{34}=0.667$	600/1200 $b_{35}=0.5$
900THz	900/300 $b_{41}=3$	900/400 $b_{42}=2.25$	900/600 $b_{43}=1.5$	900/900 $b_{44}=1$	900/1200 $b_{45}=0.75$
1200THz	1200/300 $b_{51}=4$	1200/400 $b_{52}=3$	1200/600 $b_{53}=2$	1200/900 $b_{54}=1.333$	1200/1200 $b_{55}=1$

10 Doppler red-shift ratios: $r_{l,h} = v_{lo}/v_{hi}$

10 Doppler blue-shift ratios: $b_{h,l} = v_{hi}/v_{lo}$

5 Doppler "no-shifts"

Fig. 9 Doppler shift b-matrix for a linear array of variously moving receiver-sources.

Doppler rapidity and mean values

Composition rules (2.15c) suggest defining Doppler factors $b=e^{\rho}$ in terms of *rapidity* $\rho=ln\ b$.

$$b_{mp}=b_{mn}b_{np} \quad \text{implies: } \rho_{mp}=\rho_{mn}+\rho_{np} \qquad \text{where: } b_{ab}=e^{\rho_{ab}} \tag{2.16}$$

Rapidity parameters ρ_{mn} mimic Galilean addition rules as do phase angles ϕ of wavefunctionss $e^{i\phi}$, and ρ and ϕ are the parameters that underlie relativity and quantum theory. In fact, by (2.14) rapidity ρ_{mn} approaches the relative velocity parameter u_{mn}/c between atom-*m* and atom-*n* for speeds much less than *c*. Rapidity is also convenient for astronomically large Doppler ratios b_{ab} since then the numerical value of $\rho_{ab}=\ln b_{ab}$ is much less than b_{ab} while the value of u_{mn}/c inconveniently approaches 1.

At intermediate relativistic speeds the geometric aspects of Doppler factors provide a simple but precise and revealing picture of the nature of wave-based mechanics. Any pair of counter moving continuous waves (CW) has mean values between a **K**-vector $\mathbf{R}=\mathbf{K}_1=(ck_1,\omega_1)$ going left-to-right and an $\mathbf{L}=\mathbf{K}_3=(ck_3,\omega_3)$ going right-to-left. A key quantity is the *geometric mean* ϖ of left and right frequencies.

$$\varpi=\sqrt{\omega_1\omega_3} \tag{2.17}$$

In Fig. 10a frequency $\omega_1=1$ or $\omega_3=4$ is a blue $(b=e^{+\rho}=2)$ or red $(r=e^{-\rho}=1/2)$ shift of mean $\varpi=\sqrt{1\cdot 4}=2$.

$$\omega_1=b\varpi=e^{\rho}\varpi \tag{2.18a}$$

$$\omega_3=r\varpi=e^{-\rho}\varpi \tag{2.18b}$$

In units of $2\pi\cdot 300THz$, frequency values $\omega_3=1$ and $\omega_1=4$ were used in Fig. 7. Their half-sum $5/2$ is their *arithmetic mean*. That is the radius of the circle in Fig. 10b located a *half-difference* (3/2) from origin.

$$\frac{\omega_1+\omega_3}{2}=\varpi\frac{e^{+\rho}+e^{-\rho}}{2}=\varpi\cosh\rho=\varpi\frac{5}{2} \tag{2.19a}$$

$$\frac{\omega_1-\omega_3}{2}=\varpi\frac{e^{+\rho}-e^{-\rho}}{2}=\varpi\sinh\rho=\varpi\frac{3}{2} \tag{2.19b}$$

By (2.8) the difference-to-sum ratio is the group or *mean frame* velocity-to-*c* ratio $u/c=3/5$ for $b=2$.

$$\frac{\omega_1-\omega_3}{\omega_1+\omega_3}=\frac{\sinh\rho}{\cosh\rho}=\tanh\rho=\frac{u}{c} \tag{2.19c}$$

The geometric mean ($\varpi=\sqrt{1\cdot 4}=2$) in units of $2\pi\cdot 300THz$ is the initial *600THz* green laser lab frequency used in Fig. 6. Diamond grid sections from Fig. 7b are redrawn in Fig. 10b to connect with the geometry of the Euclidian rectangle-in-circle elements of interfering-phasor addition in Fig. 8c.

Various observers see the single continuous wave frequencies ω_1 or ω_3 shifted to $\omega'_1=e^{+\rho}\omega_1$ and $\omega'_3=e^{-\rho}\omega_3$, that is, to values between zero and infinity. But, because factor $e^{-\rho}$ cancels $e^{+\rho}$, all will agree on the 2-CW mean value $\varpi=[\omega_1\omega_3]^{1/2}=[\omega'_1\omega'_3]^{1/2}$. A 2-CW function has an *invariant* ϖ of its *rest frame* (Recall Fig. 7c) seen at velocity $u=c(\omega_1-\omega_3)/(\omega_1+\omega_3)$. A single CW has no rest frame or frequency since all observers see it going *c* as in Fig. 5. To make a home frame, a single CW must marry another one!

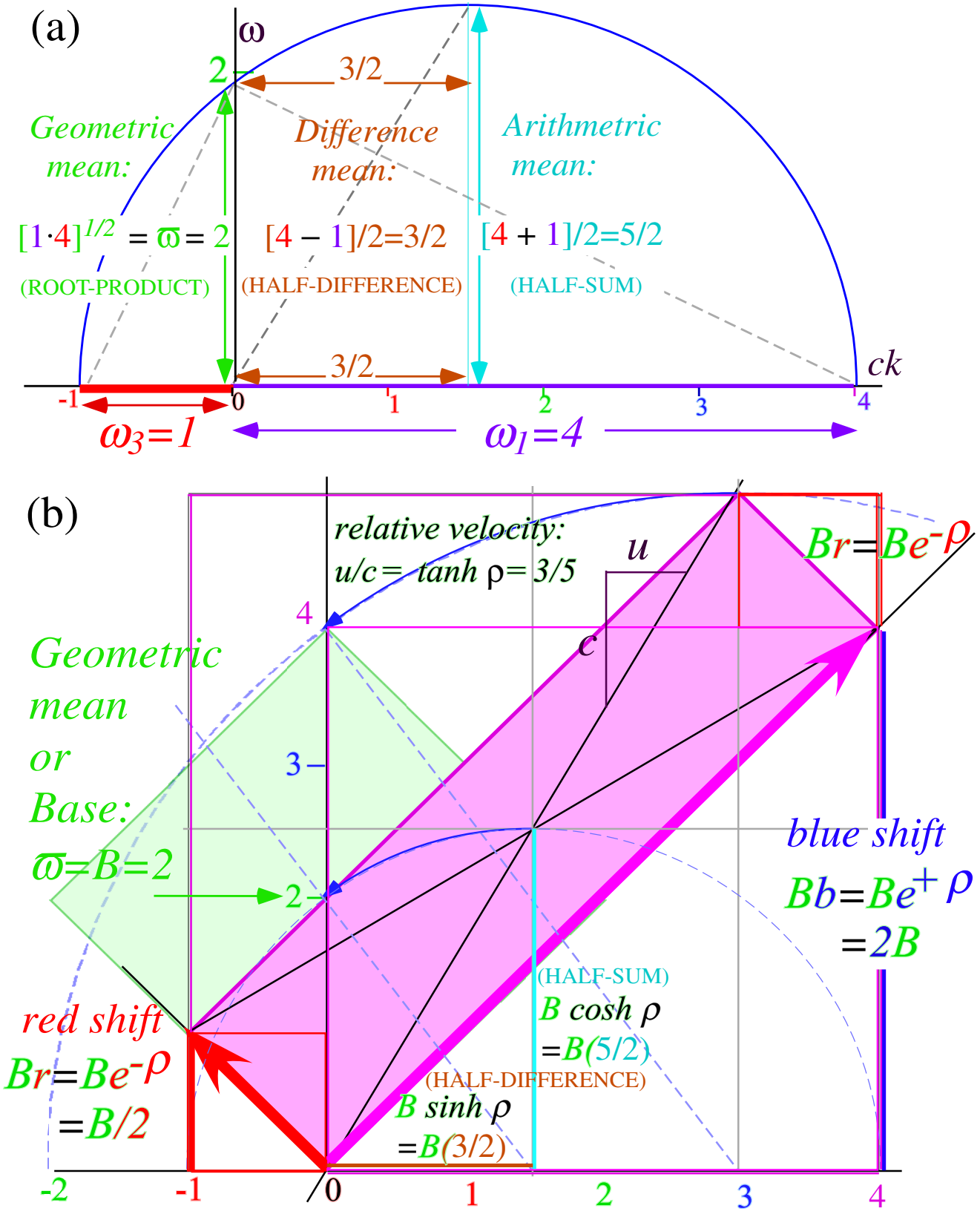

Fig. 10a Euclidian mean geometry for counter-moving waves of frequency 1 and 4. (300THz units).

Fig. 10b Geometry for the CW wave coordinate axes in Fig. 7.

Invariance of proper time and frequency

Space, time, and frequency may seem to have an out-of-control fluidity in a wavy world of relativism, so it is all the more important to focus on relativistic invariants. Such quantities make ethereal light billions of times more precise than any rusty old meter bar or clanking cuckoo clock.

It is because of the time-reversal (1.2) and Evenson axiom (1.1) that product $\omega_1\omega_3=\varpi^2$ is invariant to inverse blue-and-red Doppler shifts $b=e^{+\rho}$ and $r=e^{-\rho}$. It means the blue-red shifted diamond in Fig. 10b or Fig. 7 has the same area **R′xL′** as the original green "home field" baseball diamond area **RxL** drawn below it and in Fig. 6. Constant products $\omega_1\omega_3=const.$ give families of hyperbolas.

$$|\mathbf{RxL}|=2|\mathbf{GxP}|=2|\mathbf{K}_{group}\mathbf{xK}_{phase}|=2|\varpi^2\cosh^2\rho-\varpi^2\sinh^2\rho|=2\varpi^2$$

One hyperbola in Fig. 11a intersects bottom point $B=\varpi$ (*"pitchers' mound"*). The other hits *2B* (*2nd base*). Each horizontal **P** -hyperbola is defined by the phase vector $\mathbf{P}=\mathbf{K}_{phase}$ or some multiple of **P**.

$$\mathbf{K}_{phase}=\frac{\varpi}{2}\begin{pmatrix}e^{\rho}-e^{-\rho}\\ e^{\rho}+e^{-\rho}\end{pmatrix}=\varpi\begin{pmatrix}\sinh\rho\\ \cosh\rho\end{pmatrix}=\begin{pmatrix}ck_p\\ \omega_p\end{pmatrix}\quad\text{on P-hyperbola:}\quad \left(\omega_p\right)^2-\left(ck_p\right)^2=\varpi^2 \qquad (2.20a)$$

Each vertical **G** -hyperbola is defined by the wave group vector $\mathbf{G}=\mathbf{K}_{group}$ or some multiple of **G**.

$$\mathbf{K}_{group}=\frac{\varpi}{2}\begin{pmatrix}e^{\rho}+e^{-\rho}\\ e^{\rho}-e^{-\rho}\end{pmatrix}=\varpi\begin{pmatrix}\cosh\rho\\ \sinh\rho\end{pmatrix}=\begin{pmatrix}ck_g\\ \omega_g\end{pmatrix}\quad\text{on G-hyperbola:}\quad \left(ck_g\right)^2-\left(\omega_g\right)^2=\varpi^2 \qquad (2.20b)$$

The **G**-vectors serve as tangents to **P**-hyperbolas and vice-versa. The tangent slope $\frac{d\omega}{dk}$ to any $\omega(k)$ curve is a well known definition of group velocity. Fig. 11b shows how $\frac{d\omega}{dk}$ of a P-hyperbola is equal to secant slope $\frac{\Delta\omega}{\Delta k}$ in Fig. 11a as defined in the $u=V_{group}$ equation (2.7b) based on CW axioms. Phase velocity $\frac{\omega}{k}=V_{phase}$ and its **P**-vector is an axis-switch $(\omega,ck)\rightleftarrows(ck,\omega)$ of $\frac{\Delta\omega}{\Delta k}$ and its **G**-vector. In conventional *c*-units $V_{group}/c<1$ and $1<V_{phase}/c$ are inverses according to (2.7). ($V_{phase}\,V_{group}=c^2$)

Features on per-space-time (ck,ω) plots of Fig. 10-11 reappear on space-time (x,ct) plots as noted in Fig. 4, Fig. 6 and Fig. 7. A space-time invariant analogous to (2.20) is called *proper-time* τ.

$$\left(ct\right)^2-\left(x\right)^2=\left(c\tau\right)^2=\left(ct'\right)^2-\left(x'\right)^2 \qquad (2.21)$$

It conventional to locates oneself at $(0,ct)$ or presume one's origin $x=0$ is located on oneself. Then (2.21) reduces to time axis $ct=c\tau$. A colloquial definition of proper time is *age*, a digital readout of one's computer clock that all observers note. By analogy, ϖ is *proper-frequency*, a *rate of aging* or a digital readout on each of the spectrometers in Fig. 9. Each reading is available to all observers.

$$\left(\omega\right)^2-\left(ck\right)^2=\left(\varpi\right)^2=\left(\omega'\right)^2-\left(ck'\right)^2 \qquad (2.22)$$

The same hyperbolas (2.22) mark off the laser lab (ω,ck), the atom frame (ω',ck'), or any other frame.

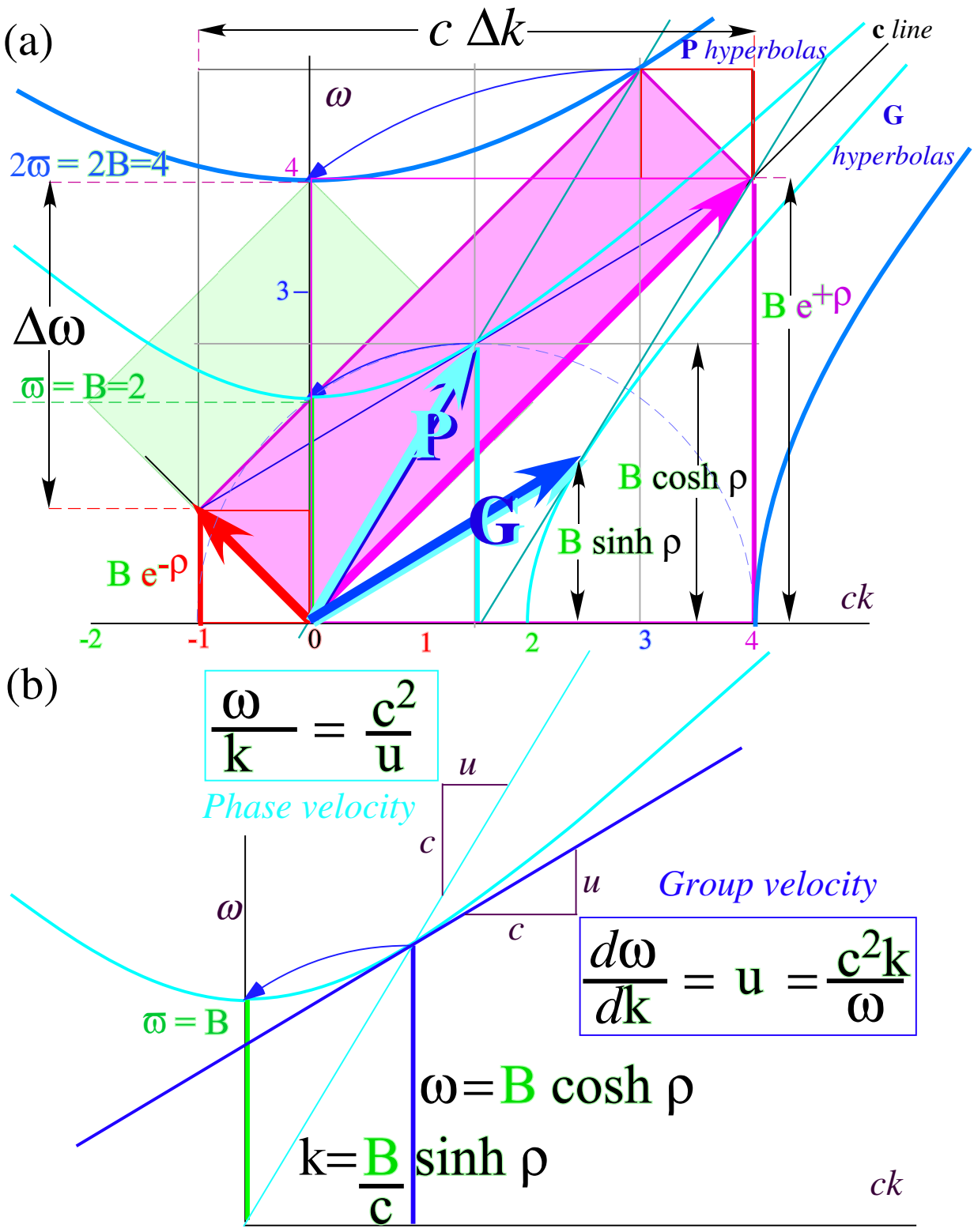

Fig. 11 (a) Horizontal G-hyperbolas for proper frequency B=ϖ and 2B and vertical P-hyperbolas for proper wavevector k. (b) Tangents for G-curves are loci for P-curves, and vice-versa.

The proper frequency of a wave is that frequency observed after one Doppler shifts the wave's kinks away, that is, the special frequency ϖ seen in the frame in which its wavevector is zero ($ck=0$) in

(2.22). Hence a single CW has a proper frequency that is identically zero ($\varpi=0$) by Evenson's axiom ($\omega=ck$), so single CW light cannot age. If we could go c to catch up to light's home frame then its phasor clocks would stop. (But, that would be an infinite Doppler shift that we can only approach.)

To produce a nonzero proper frequency $\varpi\neq0$ requires interference of at least two CW entities moving in different directions and this produces a standing wave frame like Fig. 6c moving at a speed less than c as shown in Fig. 7c. Matched CW-pairs of **L** and **R** baselines frame a "baseball diamond" for which the phase wavevector k_p in (2.2a) is zero. Then frame velocity $u=V_{group}$ in (2.3b) is zero, too.

Fig. 12 shows the plots of per-spacetime "baseball diamond" coordinates for comparison of lab and atom frame views. While Fig. 12a is a "blimp's-eye view" of the lab-frame diamond in Fig. 6, the atom frame view in Fig. 12b looks like the baseball field seen by a spectator sitting in the stands above the dugout. Nevertheless, identical hyperbolas are used to mark grids in both views.

Each point on the lower hyperbola is a bottom point $\omega'=B=2\ (600THZ)$ for the frame whose relative velocity u' makes it a ω'-axis ($k'=0$)-point, and every ($k'=0$)-point on the upper hyperbola is its bottom point $\omega'=2B=4\ (1200THZ)$, and so on for hyperbolas of any given proper frequency value ϖ. The same applies to space-time plots for which time ct' takes the place of per-time ω' and space x' takes the place of per-space ck'. Then bottom points are called proper time or τ-values from (2.21).

For single CW light the proper time must be constant since a single CW cannot age. It is a convention to make the baselines or *light cone* intersect at the origin in both time and space. This sets the baseline proper time constant τ to zero. Then invariants (2.21) reduce to baseline equations $x=\pm ct$ or $x'=\pm ct'$ for all frames. The space-time light cone relations are in direct correspondence with the per-space-time light cone relations $\omega=\pm ck$ or $\omega'=\pm ck'$ for zero proper frequency in all frames and are concise restatements of the Evenson CW axiom (1.1).

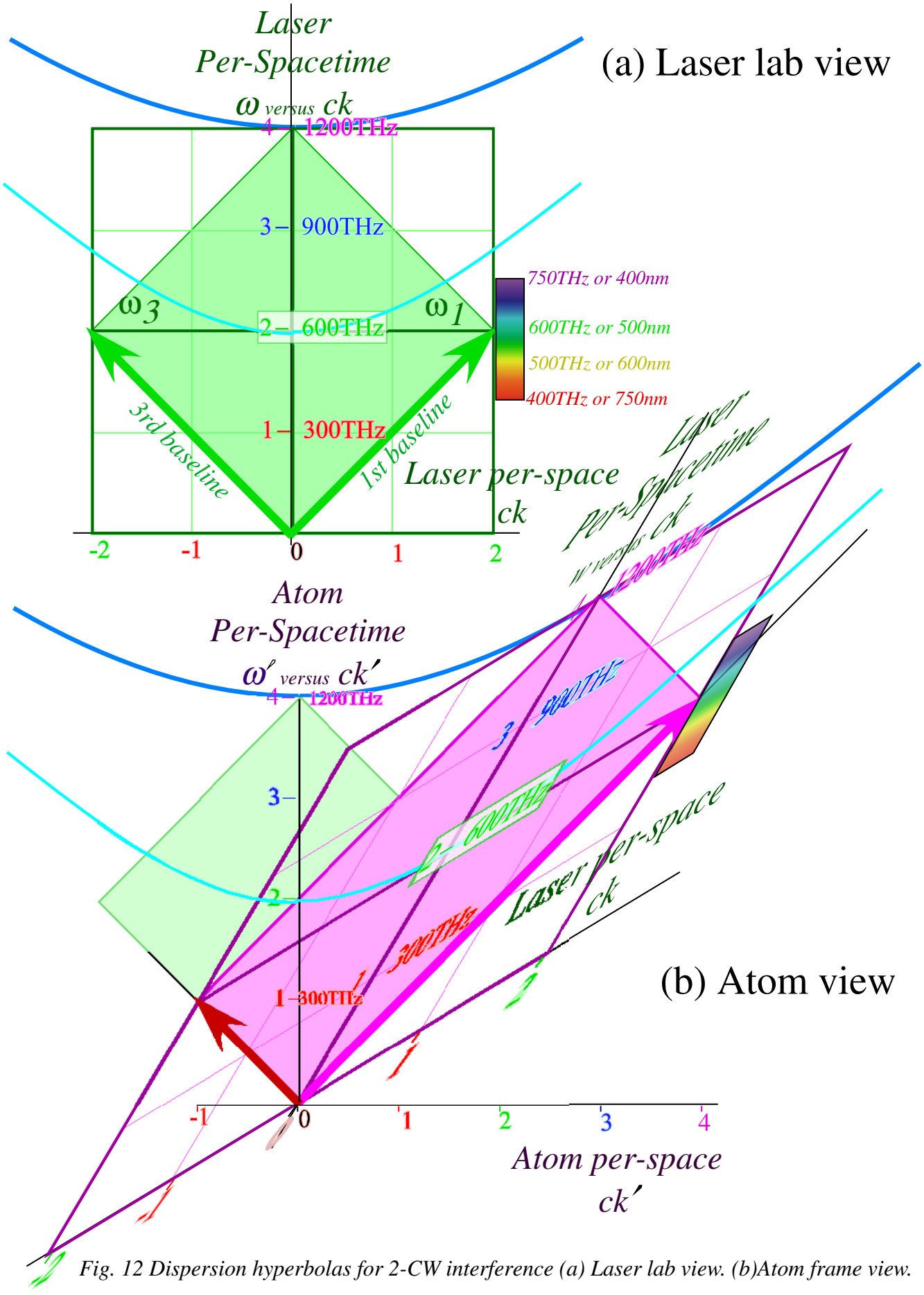

Fig. 12 Dispersion hyperbolas for 2-CW interference (a) Laser lab view. (b)Atom frame view.

3. Mechanics by CW axioms

Each of the 2-CW structures or properties discussed so far are due to relative interference effects between pairs of single CW entities that, by themselves, lack those properties. Single CW plane waves have no proper invariant frequency, no rest frame, and no velocity less than the unreachable c. To acquire such properties there must be an interference encounter or *pairing* with another CW.

Two-CW interference acquires other important properties including classical and relativistic mechanics of mass, energy, momentum that characterize a quantum matter wave. Such acquisition is from hyperbolic phase relations (2.19-20) that, in turn, follow from CW axioms (1.1) and (1.2).

$$\omega_p = B\cosh\rho \approx B + \frac{1}{2}B\rho^2 \ (\text{for } u \ll c) \quad (3.1a) \qquad ck_p = B\sinh\rho \approx B\rho \ (\text{for } u \ll c) \quad (3.1b) \qquad \frac{u}{c} = \tanh\rho \approx \rho \ \ (\text{for } u \ll c) \quad (3.1c)$$

Here $B=\varpi$. The first two are components (ω_p,ck_p) of the **P**-vector in Fig. 11, and u/c is the tangent slope at **P**. At low group velocity $(u\ll c)$ rapidity ρ approaches u/c, and ω_p and k_p are simple functions of u.

$$\omega_p \approx B + \frac{1}{2}\frac{B}{c^2}u^2\cdots \quad (3.2a) \qquad k_p \approx \frac{B}{c^2}u\cdots \quad (3.2b)$$

We note that these (ω_p,ck_p) functions fit classical Newtonian-energy E and Galilean-momentum p.

$$E = const. + \frac{1}{2}Mu^2 \quad (3.3a) \qquad p \approx Mu \quad (3.3b)$$

Multiplying wave *results* (3.2) by a single scale factor $s=Mc^2/B$ gives classical *definitions* (3.3).

$$E = s\omega_p \approx sB + \frac{1}{2}\frac{sB}{c^2}u^2\cdots \quad (3.4a) \qquad p = sk_p \approx \frac{sB}{c^2}u\cdots \quad (3.4b)$$

Newton's *const* in E (3.3a) is moot; only energy *difference* ΔE counts. But, in (3.4a) $const.=sB$ is the proper-frequency value $B=\varpi$ of Fig. 11b scaled to $sB=s\varpi$. It is also the famous Einstein rest energy.

$$const. = sB = Mc^2 = s\varpi \quad (3.4c)$$

Then exact relativistic Planck-DeBroglie quantum scaling laws follow from exact CW results (3.1).

$$E = s\omega_p = Mc^2\cosh\rho = \frac{Mc^2}{\sqrt{1-u^2/c^2}} \quad (3.5a) \qquad p = sk_p = Mc\sinh\rho = \frac{Mu}{\sqrt{1-u^2/c^2}} \quad (3.5b)$$

Scale factor s in Planck[17] $E=s\omega$ or DeBroglie[18] $p=sk$ laws is found by experiment. The lowest observed s-value is the Planck angular constant $\hbar=1.05\cdot10^{-34}J\cdot s$ in Planck's original law $E=\hbar\omega_N=\hbar N\omega$ for $N=1$. Integer N is a light-quantum-number or photon-count discussed in Sec. 6. (Occam's razor is used again to further slice classical CW's into N-photon waves belonging to *nets* of (ω_N,ck_N)-hyperbolas.)

Each photon of a 2-CW cavity adds a tiny mass $M_\gamma=\hbar\omega/c^2=\omega\,(1.2\cdot10^{-51})kg$ to the cavity but p is zero. A single free CW has no rest mass but its momentum $p_\gamma=\hbar k=\hbar\omega/c=\omega\,(3.5\cdot10^{-43})kg\cdot m\cdot s^{-1}$ from (3.5b) is $p_\gamma=M_\gamma c$. It is small, too, but M_γ times c is not as tiny as M_γ and it resembles Galileo's relation (3.3b).

Definitions of wave mass

If mass or rest energy is due to proper phase frequency ϖ, then a quantum matter wave has mass without invoking hidden Newtonian "stuff." There is a certain Occam-like economy in the fact that two CW's of light give exact classical mass-energy-momentum relations (3.5). However, a CW theory exposes multiple definitions of mass that a Newtonian theory would not distinguish.

First, the Einstein-Planck wave frequency-energy-mass equivalence relation (3.4c) ascribes *rest mass* M_{rest} to a scaled proper frequency $s\varpi/c^2$. The scale factor s is Planck's $s=\hbar N$ for cavity mode N.

$$M_{rest} = E/c^2 = \hbar N\varpi/c^2 \tag{3.6}$$

For rest electron mass $m_e = 9.1\cdot10^{-31}kg$ or $M_p = 1.67\cdot10^{-27}kg$ of a proton, the proper frequency times $N=2$ is called *zwitterbevegun* ("trembling motion") and is as mysterious as it is huge. (Electron rest frequency $\varpi_e = m_e c^2/\hbar = 7.76\cdot10^{+20}(rad)s^{-1}$ is the Dirac (e^+e^-)-pair production[19] threshold as discussed in Sec. 6.)

Second, define *momentum-mass* M_{mom} by ratio p/u of momentum (3.5b) to velocity u. (Galileo's $p=M_{mom}u$) Now M_{mom} varies as $\cosh\rho \to e^{\rho}/2$ at high rapidity ρ but approaches invariant M_{rest} as $\rho \to 0$.

$$\begin{aligned}\frac{p}{u} \equiv M_{mom} &= \frac{M_{rest}c}{u}\sinh\rho = M_{rest}\cosh\rho \xrightarrow[u\to c]{} M_{rest}e^{\rho}/2 \\ &= M_{rest}\Big/\sqrt{1-u^2/c^2} \xrightarrow[u\ll c]{} M_{rest}\end{aligned} \tag{3.7}$$

Frame velocity u is wave group velocity and the Euclid mean construction of Fig. 11a shows u is the slope of the tangent to dispersion function $\omega(k)$. A derivative of energy (3.5a) verifies this once again.

$$V_{group} = \frac{d\omega}{dk} = \frac{dE}{dp} = \frac{c^2 p}{E} = u \tag{3.8}$$

Third, define *effective-mass* M_{eff} as ratio $\dot{p}/\dot{u} = F/a$ of momentum-*change* to acceleration. (Newton's $F=M_{eff}a$) M_{eff} varies as $\cosh^3\rho \to e^{3\rho}/2$ at high rapidity ρ but is invariant M_{rest} as $\rho \to 0$.

$$\begin{aligned}\frac{F}{a} \equiv M_{eff} \equiv \frac{dp}{du} = \frac{\hbar dk}{dV_{group}} &= \hbar\Big/\frac{d}{dk}\frac{d\omega}{dk} = \hbar\Big/\frac{d^2\omega}{dk^2} \\ &= M_{rest}\Big/\left(1-u^2/c^2\right)^{3/2} \xrightarrow[u\ll c]{} M_{rest}\end{aligned} \tag{3.9}$$

Effective mass is $\hbar$ divided by the curvature of dispersion function, a general quantum wave mechanical result. Geometry of a dispersion hyperbola $\omega=B\cosh\rho$ is such that its bottom $(u=0)$ radius of curvature (RoC) is the rest frequency $B=M_{rest}c^2/\hbar$, and this grows exponentially toward ∞ as velocity u approaches c. The 1-CW dispersion $(\omega=\pm ck)$ is flat so its RoC is infinite everywhere and so is photon effective mass $(M_{eff}(\gamma)=\infty)$ consistent with the (*All colors go c*)-axiom (1.1). The other extreme is photon rest mass $(M_{rest}(\gamma)=0$. Between these extremes, photon momentum-mass depends on CW color ω.

$M_{rest}(\gamma)=0$ (3.10a) $M_{mom}(\gamma)=p/c=\hbar k/c=\hbar\omega/c^2$ (3.10b) $M_{eff}(\gamma)=\infty$ (3.10c)

For Newton this would confirm light's "fits" to be crazy to the point of unbounded schizophrenia.

Absolute vs. relative phases

Probably Newton would find a CW theory to be crazy. Claiming that heavy hard matter owes its properties to rapid hidden phase oscillations would not elicit a Newtonian invitation to the Royal Society but rather to a lunatic asylum. Even though CW results (3.2) give Newtonian axioms (3.3) at low speeds, the result would seem to fail at high speeds where exact results (3.5) sag below Newton's. Also, the enormous constant Mc^2 in the energy would, in 1670, seem meaningless.

Not until 1905[20] does Einstein's theory appear with energy sag and Mc^2. Yet Einstein's classical training left him leery of hidden quantum wave phases with dicey interpretations of intensity $\Psi^*\Psi$ as *probability*. Also, he may have asked why observable results depend on a square $\Psi^*\Psi=|\Psi|^2$ that kills the overall phase frequency, seemingly losing the one quantity that represents (or *is*) the total energy.

Square $|\Psi|^2$ of a 2-CW $\Psi=e^{ia}+e^{ib}$ loses phase factor $e^{i(a+b)/2}$ leaving only group functions $\cos^2(\frac{a-b}{2})$ of *differences* $\omega_1-\omega_3$ or k_1-k_3 of 1st and 3rd base frequencies or *k*-vectors. Group beat frequency $\Delta\omega=\omega_1-\omega_3$ is zero in the rest frame of Fig. 6c where it is a stationary wave. In Fig. 7c or any other frame, $|\Psi|^2$ is not stationary but is observed to have velocity $V_{group}\neq 0$. Fourier sums of $m=3$ or more terms $\Psi=a_1e^{i(k_1x-\omega_1t)}+a_2e^{i(k_2x-\omega_2t)}+a_3e^{i(k_3x-\omega_3t)}+...$ may have multiple beats in $\Psi*\Psi$ as in Fig. 7d.

$$P=|\Psi|^2=\Psi*\Psi=\sum a_i*a_je^{i(\Delta k_{ij}x-\Delta\omega_{ij}t)} \qquad (3.11)$$

With $m(m-1)/2$ observable *difference* $\Delta\omega_{ij}=\omega_1-\omega_j$ or *beat* notes, *P* cannot rest in any frame. Differences or derivatives are observable while absolute Ψ-frequency stays hidden *until two quantum objects interfere*. Then new beats arise from differences between the two absolute frequencies and old ones. A new absolute phase (not in $|\Psi|^2$) is the sum of them all. Limiting observation to beats or relative frequency may be a quantum version of Einstein's popularized saw, "It's *all* relative." (Phase velocity may escape with its Galilean arithmetic intact, but here it finally surrenders its absolutes to relativism.)

Total phase gives total energy *E* or momentum *p*, but *differential*s are what one feels through work ΔE or impulse Δp. Invariant quantities like ϖ and M_{rest} depend on *total* phase but intensity (3.11) has only differentials or *relative* beats. Among frame-dependent relative quantities are group velocity *u* (3.8), M_{mom} (3.7), and M_{eff} (3.9). But, rest mass M_{rest} (3.4c) is a frame-invariant absolute quantity. Recall however that M_{mom} and M_{eff} approach M_{rest} at zero velocity. (While $|\Psi|^2$ may register a ϖ beat with a DC *(static* $\omega_0=0$*)* wave, lack of resonance confines $(\omega_0=0)$-carrier waves to beat only locally.)

The phase frequency ω_p in a quantum wave $e^{ip}\cos g=e^{-i(k_px-\omega_pt)}\cos(k_gx-\omega_gt)$ is like a carrier frequency of a radio wave, fast and silent. The group frequency ω_g is like the audible signal, much slower and heard in resonant beats $\omega_a-\omega_b$ involving carrier and receiver. Atomic "carrier" frequencies $\omega_p=M_pc^2/\hbar$ due to rest mass are enormous as are those of atomic measuring devices that play the role of "receivers" in quantum experiments. Measurement involves resonant contact of an atom and devices that horse-trade beats much faster than even those achieved by Evenson or any laser technology so far.

One way to avoid huge $Mc^2/\hbar$-related phase frequencies is to ignore them and approximate the relativistic equation $E=Mc^2\cosh\rho$ of (3.5a) by the Newtonian approximation (3.4a) that deletes the big rest-energy constant $sB=Mc^2$. The exact energy (3.5a) that obeys CW axioms (1.1) is rewritten in terms of momentum (3.5b) in (3.12). Then (3.13) gives the Newtonian approximation with Mc^2 deleted.

$$E=\frac{Mc^2}{\sqrt{1-u^2/c^2}}=Mc^2\cosh\rho=Mc^2\sqrt{1+\sinh^2\rho}=\sqrt{\left(Mc^2\right)^2+\left(cp\right)^2} \tag{3.12}$$

$$E=\left[\left(Mc^2\right)^2+\left(cp\right)^2\right]^{1/2}\approx Mc^2+\frac{1}{2M}p^2\xrightarrow{S-approx}\frac{1}{2M}p^2 \tag{3.13}$$

Since only frequency differences affect an observation based on $|\Psi|^2$ (3.11), the energy origin may be dropped from $(E=Mc^2,\ cp=0)$ to $(E=0,\ cp=0)$. (*Frequency is relative!*) Hyperbola (3.12) is then Newton's parabola (3.13) for momentum $p=Mu$ much less than Mc, or u much less than c.

Group velocity $u=V_{group}=\frac{d\omega}{dk}$ of (3.8) is a relative or differential quantity so origin shifting does not affect it. However, phase velocity $\frac{\omega}{k}=V_{phase}$ is greatly reduced by deleting Mc^2 from $E=\hbar\omega$. It slows from $V_{phase}=c^2/u$ that is always faster than light to a sedate sub-luminal speed of $V_{group}/2$. Having V_{phase} go slower than V_{group} is an unusual situation but one that has achieved tacit approval for Bohr-Schrodinger matter waves.[21] The example used in Fig. 4 is a 2-CW matter wave exhibiting this.

Standard Schrodinger quantum mechanics, so named in spite of Schrodinger's protests[22], uses Newtonian kinetic energy (3.13) (or (3.3) with potential φ (as the *const.*-term) to give a Hamiltonian.

$$H=p^2/2M+\varphi \quad \text{or:} \quad \hbar\omega=\hbar^2k^2/2M+\langle\varphi\rangle_k \tag{3.14}$$

The CW approach to relativity and quantum exposes some problems with such approximations.

First, a non-constant potential φ must have a vector potential $\mathbf{A}$ so that $(\varphi,c\mathbf{A})$ transform like $(\omega,c\mathbf{k})$ in (2.10a) or $(ct,\mathbf{x})$ in (2.10b) or as $(E,c\mathbf{p})$ with scaling laws $\mathbf{p}=\hbar\mathbf{k}$ and $E=\hbar\omega$. Transformation demands equal powers for frequency (energy) and wavevector (momentum) such as the following.

$$(E-\varphi)^2=(\mathbf{p}-c\mathbf{A})^2/2M+Mc^2 \quad \text{or:} \quad (\hbar\omega-\langle\varphi\rangle_k)^2=(\hbar\mathbf{k}-c\mathbf{A})^2/2M+Mc^2 \tag{3.15}$$

Also, varying potentials perturb the vacuum so single-CW's may no longer obey axioms (1.1-2).

Diracs's elegant solution obtains ±pairs of hyperbolas (3.12) or (3.15) from avoided-crossing eigenvalues of *4x4* Hamiltonian matrix equations. These ideas require three-dimensional wavevectors and momenta as will be introduced later. First, the more fundamental Lagrangian geometry of quantum phase will be used to relate relativistic classical and quantum mechanics.

4. Classical vs. quantum mechanics

The CW-spectral view of relativity and quantum theory demonstrates that wave phase and in particular, optical phase, is an essential part of quantum theory. If so, classical derivation of quantum mechanics might seem about as viable as Aristotelian derivation of Newtonian mechanics.

However, the 19th century mechanics of Hamilton, Jacobi, and Poincare developed the concept of *action S* defined variously by area $\oint pdq$ in phase-space or a Lagrangian time integral $\int Ldt$. Action definition begins with the Legendre transformation of Lagrangian *L* and Hamiltonian *H* functions.

$$L = p \cdot \dot{x} - H \qquad (4.1a)$$

L is an explicit function of *x* and velocity $u = \dot{x}$ while the *H* is explicit only in *x* and momentum *p*.

$$0 = \frac{\partial L}{\partial p} \quad (4.1b) \qquad p = \frac{\partial L}{\partial \dot{x}} \quad (4.1c) \qquad 0 = \frac{\partial H}{\partial \dot{x}} \quad (4.1d) \qquad \dot{x} = \frac{\partial H}{\partial p} \quad (4.1e)$$

Multiplying by *dt* gives the differential Poincare invariant *dS* and its action integral $S = \int L dt$.

$$dS = L\,dt = p \cdot dx - H\,dt \qquad (4.2a) \qquad S = \int L\,dt = \int p \cdot dx - \int H\,dt \qquad (4.2b)$$

Planck and DeBroglie scaling laws $p=\hbar k$ and $E=\hbar\omega$ identify action *S* as scaled quantum phase $\hbar\Phi$.

$$\hbar\, d\Phi = L\,dt = \hbar k \cdot dx - \hbar\omega\, dt \quad (4.3a) \qquad \Phi = \int k \cdot dx - \int \omega\, dt \qquad (4.3b)$$

If action d*S* or phase dΦ is integrable, then Hamilton-Jacobi equations or *(k,ω)* equivalents hold.

$$\frac{\partial S}{\partial x} = p \quad (4.4a) \qquad \frac{\partial S}{\partial t} = -H \quad (4.4b) \qquad \frac{\partial \Phi}{\partial x} = k \quad (4.4c) \qquad \frac{\partial \Phi}{\partial t} = -\omega \quad (4.4d)$$

Phase-based relations (4.4c-d) define angular frequency ω and wave number *k*. The definition (3.8) of wave group velocity is a wave version of Hamilton's velocity equation (4.1e).

$$\dot{x} = \frac{\partial H}{\partial p} \quad \textit{equivalent to:} \quad u = V_{group} = \frac{\partial \omega}{\partial k}$$

The coordinate Hamilton derivative equation relates to wave diffraction by dispersion anisotropy.

$$\dot{p} = -\frac{\partial H}{\partial x} \quad \textit{equivalent to:} \qquad \dot{k} = -\frac{\partial \omega}{\partial x}$$

Classical HJ-action theory was intended to analyze families of trajectories (PW or particle paths), but Dirac and Feynman showed its relevance to matter-wave mechanics (CW phase paths) by defining an approximate semi-clasical wavefunction based on the Lagrangian action as phase.

$$\Psi \approx e^{i\Phi} = e^{iS/\hbar} = e^{i\int L\,dt/\hbar} \qquad (4.5)$$

The approximation symbol ($\approx$) indicates that only phase but not amplitude is assumed to vary here. An *x*-derivative (4.4a) of semi-classical wave (4.5) has the **p**-operator form in standard quantum theory.

$$\frac{\partial}{\partial x}\Psi \approx \frac{i}{\hbar}\frac{\partial S}{\partial x} e^{iS/\hbar} = \frac{i}{\hbar} p\Psi \quad (4.6a) \qquad \frac{\hbar}{i}\frac{\partial}{\partial x}\Psi = p\Psi \quad (4.6b)$$

The time derivative is similarly related to the Hamiltonian operator. The H-J-equation (4.4b) makes this appear to be a Schrodinger time equation.

$$\frac{\partial}{\partial t}\Psi \approx \frac{i}{\hbar}\frac{\partial S}{\partial t}e^{iS/\hbar} = -\frac{i}{\hbar}H\Psi \qquad (4.7a) \qquad\qquad i\hbar\frac{\partial}{\partial t}\Psi = H\Psi \qquad (4.7b)$$

However, this approximation like that of (3.14) ignores relativity and lacks the economy of logic shed by light waves. The Poincare phase invariant of a matter-wave needs re-examination.

Contact transformation geometry of a relativistic Lagrangian

A matter-wave has a rest frame where $x'=0=k'$ and its phase $\Phi = kx-\omega t$ reduces to $-\mu\tau$, a product of its proper frequency $\mu=N\varpi$ (or $Mc^2/\hbar$) with proper time $t'=\tau$. Invariant differential $d\Phi$ is reduced, as well, using the Einstein-Planck rest-mass energy-frequency equivalence relation (3.4c) to rewrite it.

$$d\Phi = kdx-\omega dt=-\mu\ d\tau = -(Mc^2/\hbar)\ d\tau. \qquad (4.8)$$

τ-Invariance (2.21) or time dilation in (2.10b) gives proper $d\tau$ in terms of velocity $u=\frac{dx}{dt}$ and lab dt.

$$d\tau = dt\ \sqrt{(1-u^2/c^2)}\ )=dt\ sech\ \rho \qquad (4.9)$$

Combining definitions for action $dS=Ldt$ (4.2) and phase $dS = \hbar d\Phi$ (4.3) gives the Lagrangian L.

$$L =-\hbar\mu\tau = -Mc^2\sqrt{(1-u^2/c^2)}= -Mc^2 sech\ \rho \qquad (4.10)$$

Fig. 13 plots this free-matter Lagranian L next to its Hamiltonian H using units for which $c=1=M$.

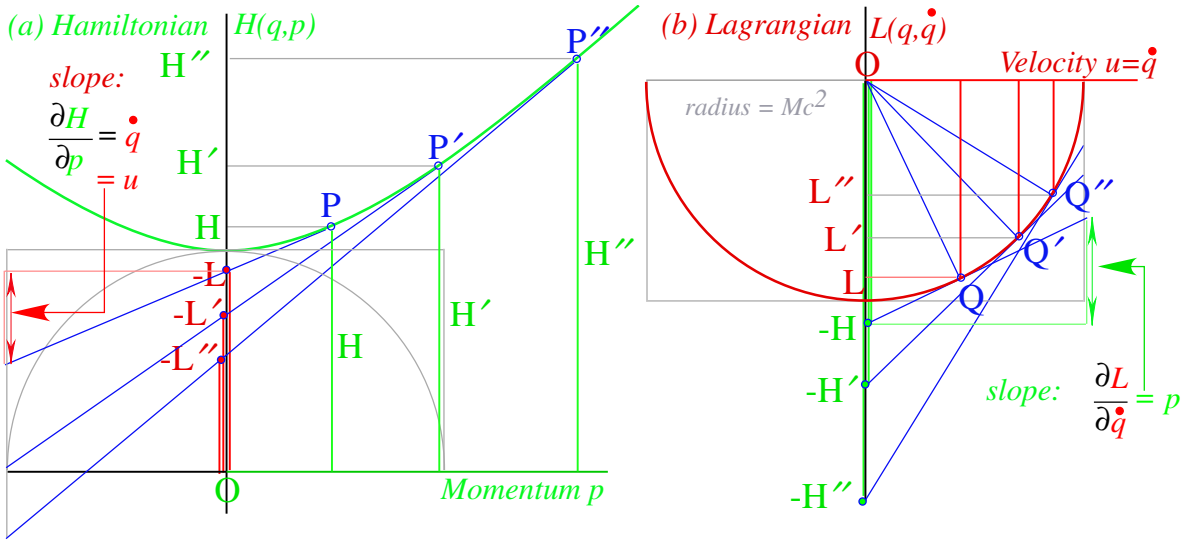

Fig. 13. Geometry of contact transformation between relativistic (a) Hamiltonian (b) Lagrangian

The *relativistic matter Lagrangian* in Fig. 13b is a circle. Three L-values L, L', and L'' in Fig. 13 are Legendre contact transforms of the three H-values H, H', and H'' on the Hamiltonian hyperbola in Fig. 13a. Abscissa p and ordinate H of a point P in plot (a) gives negative intercept $-H$ and slope p of the tangent contacting the transform point Q in plot (b) and *vice-versa*. Contact geometry shows a structure of wave-action-energy mechanics. Lagrange kinetic energy $L=\frac{1}{2}Mu^2$ equals $H = p^2/2M$ of

Hamilton with $p = Mu$ as hyperbola H and circle L both approximate a Newton parabola at low speed $u<<c$ in Fig. 13. But, as u nears c the L-circle rises and the H-hyperbola sags to meet its c-asymptote.

Action integral $S=\int Ldt$ is to be *minimized*. Feynman's interpretation of S minimization is depicted in Fig. 14. A mass flies so that its "clock" τ is *maximized*. (Proper frequency $\mu = Mc^2/\hbar$ is constant for fixed rest mass, and so minimizing $-\mu\tau$ means maximizing $+\tau$.) An interference of Huygen wavelets favors stationary and extreme phase and the fastest possible clock as is sketched in Fig. 15. Feynman imagines families of classical paths or rays fanning out from each space-time point on a wavefront of constant phase Φ or action S. Then, according to a matter wave application of Huygen's principle, new wavefronts are continuously built in Fig. 15 through interference from "the best" of all the little wavelets emanating from a multitude of source points on a preceding wavefront. The result is a classical momentum normal to each wavefront given by $\mathbf{p}=\nabla S$ or (4.4a) for the "best" ray.

The "best" are so-called *stationary-phase* rays that are extremes in phase and thereby satisfy *Hamilton's Least-Action Principle* requiring that $\int Ldt$ is minimum for "true" classical trajectories. This in turn enforces Poincare' invariance by eliminating, by de-phasing, any "false" or non-classical paths because they do not have an invariant (and thereby stationary) phase. "Bad rays" cancel each other in a cacophonous mish-mash of mismatched phases. Each Huygen wavelet is tangent to the next wavefront being produced. That contact point is precisely on the ray or true classical trajectory path of minimum action and on the resulting "best" wavefront. Time evolution from any wavefront to another is thus a contact transformation between them described by the geometry of Huygens Principle.

Thus a Newtonian clockwork-world appears to be the perennial cosmic gambling-house winner in a kind of wave dynamical lottery on an underlying wave fabric. Einstein's God may not play dice, but some persistently wavelike entities seem to be gaming at enormous $Mc^2/\hbar$-rates down in the cellar!

It is ironic that Evenson and other metrologists have made the greatest advances of precision in human history, not with metal bars or ironclad classical mechanics, but by using the most ethereal and dicey stuff in the universe, light waves. This motivates a view of classical matter or particle mechanics that is more simply and elegantly done by its relation to light and its built-in relativity, resonance, and quantization that occurs when waves are subject to boundary conditions or otherwise confined. While Newton was complaining about the seeming "fits" of light, it was just trying to tell him something.

Derivation of quantum phenomena using a classical particle paradigm appears a doomed effort. If particles are made by waves, optical or otherwise, rather than *vice versa* as Newton believed, the case is closed. Also, CW trumps PW as CW symmetry axioms (1.1-2) derive classical results (3.4) with exact relativity and quantum relations (3.5) tossed in the bargain. Such Occam economy is not found on a PW path from Newton to Einstein and Planck. This leaves the basic CW sum-and-difference phase relations that seem to underlie physics and Poincare contact geometry. They are clarified next.

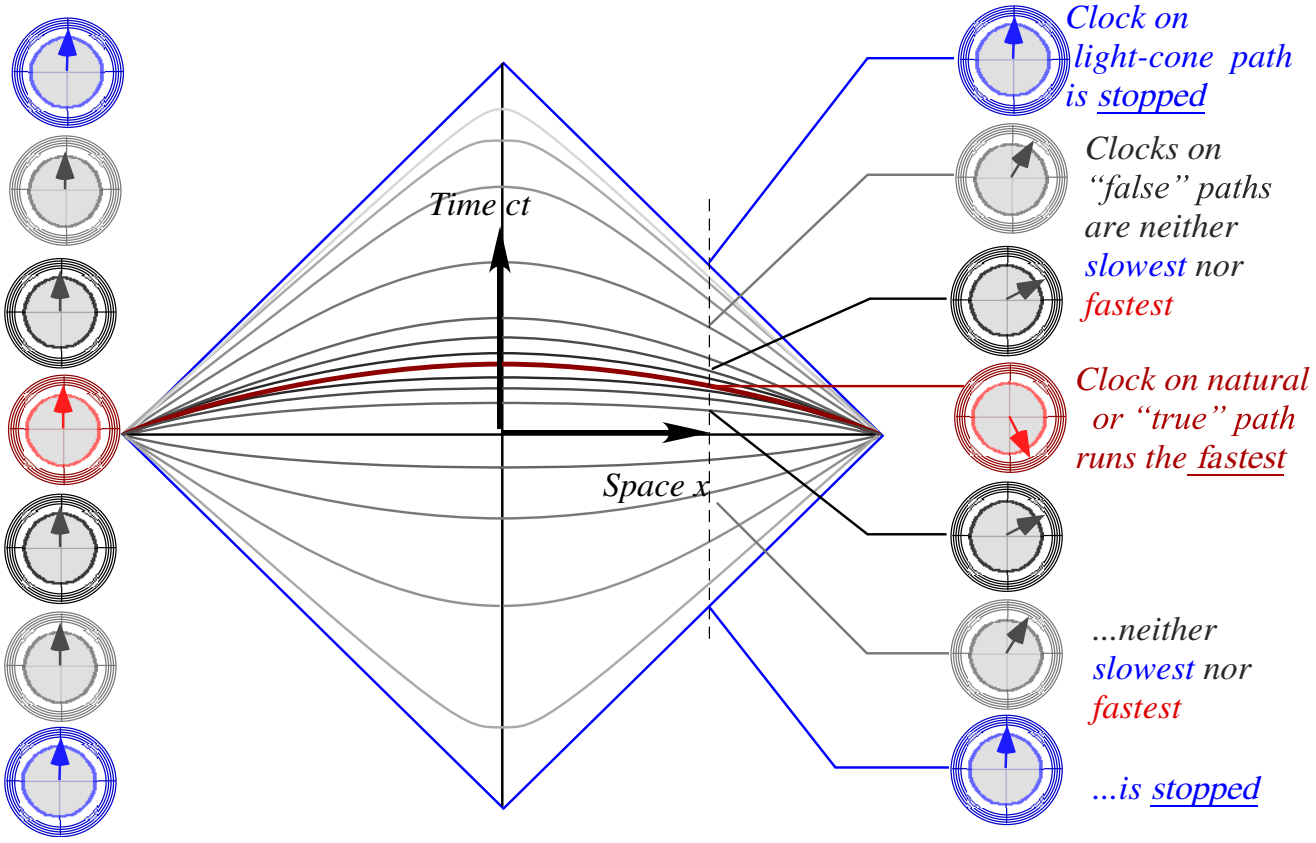

Fig. 14 "True" paths carry extreme phase and fastest clocks. Light-cone has only stopped clocks.

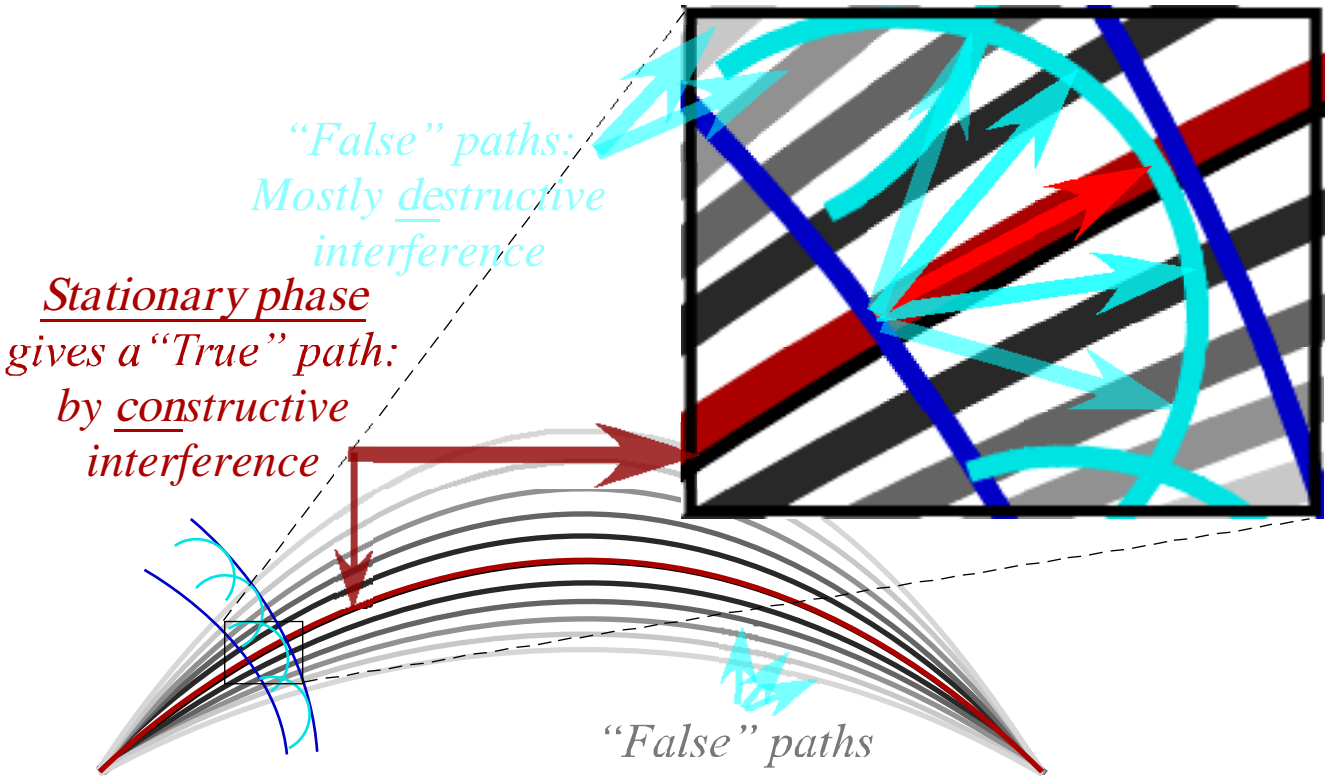

Fig. 15 Quantum waves interfere constructively on "True" path but mostly cancel elsewhere.

Geometry of circular and hyperbolic functions

Geometry of half-sum and half-difference phase **P**=(**R**+**L**)*/2* and group **G**=(**R**-**L**)*/2* vectors is based on trigonometric exponential identities that are crown jewels of 18th century mathematics and have Euclidian geometric origins shown in Fig. 16. Phase angle-ϕ identities apply to Fig. 16a.

$$e^{+i\phi} = \cos\phi + i\sin\phi \qquad e^{-i\phi} = \cos\phi - i\sin\phi \qquad (4.11a)$$

$$\cos\phi = (e^{+i\phi} + e^{-i\phi})/2 \qquad i\sin\phi = (e^{+i\phi} - e^{-i\phi})/2 \qquad (4.11b)$$

The circular function *tan*ϕ is named for a tangent to a unit circle shown in Fig. 16(a). Its incline (sine) elevation is *sin*ϕ. The complimentary tangent or cotangent *cot*ϕ completes the tangent distance between axes where ϕ is circle arc-length-ϕ or *subtended area*-ϕ. Hyperbolic functions use area ρ for "angle."

$$e^{+\rho} = \cosh\rho + \sinh\rho \qquad e^{-\rho} = \cosh\rho - \sinh\rho \qquad (4.11c)$$

$$\cosh\rho = (e^{+\rho} + e^{-\rho})/2 \qquad \sinh\rho = (e^{+\rho} - e^{-\rho})/2 \qquad (4.11d)$$

Fig. 16b shows how hyperbolic functions relate to circular ones in Fig. 16a. The circular sine equals the hyperbolic tangent (*sin*ϕ =*tanh*ρ) and *vice versa* (*tan*ϕ =*sinh*ρ). Each circular function has a segment that matches one for a hyperbolic function, for example (*cos*ϕ =*sech*ρ). These relations recap the CW view of the Legendre contact transformation in Fig. 13 that underlies classical and quantum theory that is the algebra and geometry for every bit of light-and-matter in and around us!

In Fig. 16, circular area ϕ and hyperbolic area ρ have been chosen so that *tan*ϕ *=1.15=sinh*ρ and *sin*ϕ *=0.75=tanh*ρ , that is for *u=3c/4*. The tangent to the circle in Fig. 16a-b is like the one that contacts the Lagrangian circle in Fig. 13b to contact-transform it to the Hamiltonian hyperbola in Fig. 13a, and *vice versa* the hyperbolic tangent in Fig. 16b is like the one that transforms the Hamiltonian hyperbola in Fig. 13a to the Lagrangian circle in Fig. 13b.

The hyperbolic tangent *u/c=tanh*ρ of (2.19) corresponds to frame rapidity ρ and group velocity $u=V_{group}=\frac{d\omega}{dk}$ in (2.8), (3.8) and in Fig. 11a-b. The circular tangent angle ϕ or inclination *sin*ϕ belongs to Lagrangian velocity function (4.10) in Fig. 13b. (The horizontal axis of the latter in the vertical axis of Fig.11. This geometry is symmetric to axis-switching.) As *u* and ρ approach *c* and ∞, respectively, the circular angle ϕ approaches $\pi/2$. This angle ϕ is the stellar velocity aberration angle, that is, the polar angle that vertical starlight is seen by a horizontally moving astronomer to tip into her direction of motion. Aberration angle ϕ, like rapidity ρ, is 1st-order in velocity *u* and equal *u/c* to low speeds.

Most of the twelve circular-hyperbolic trigonometric ratios in Fig. 13 belong to one or more physical or geometric effects shown in prior diagrams beginning with Euclid's rectangle-in-circle mean construction of Fig. 10. If prior ratio constructions are overlapped in the form of Fig. 13 there results in Fig. 17a what might be described as a global ratio riot. This riot is simplified and labeled in zoom-in views of Fig. 17b-d and they are the basis of the following discussion of the role of tangent-contact geometry in CW analysis of Poincare contact transformation and relativistic quantum waves.

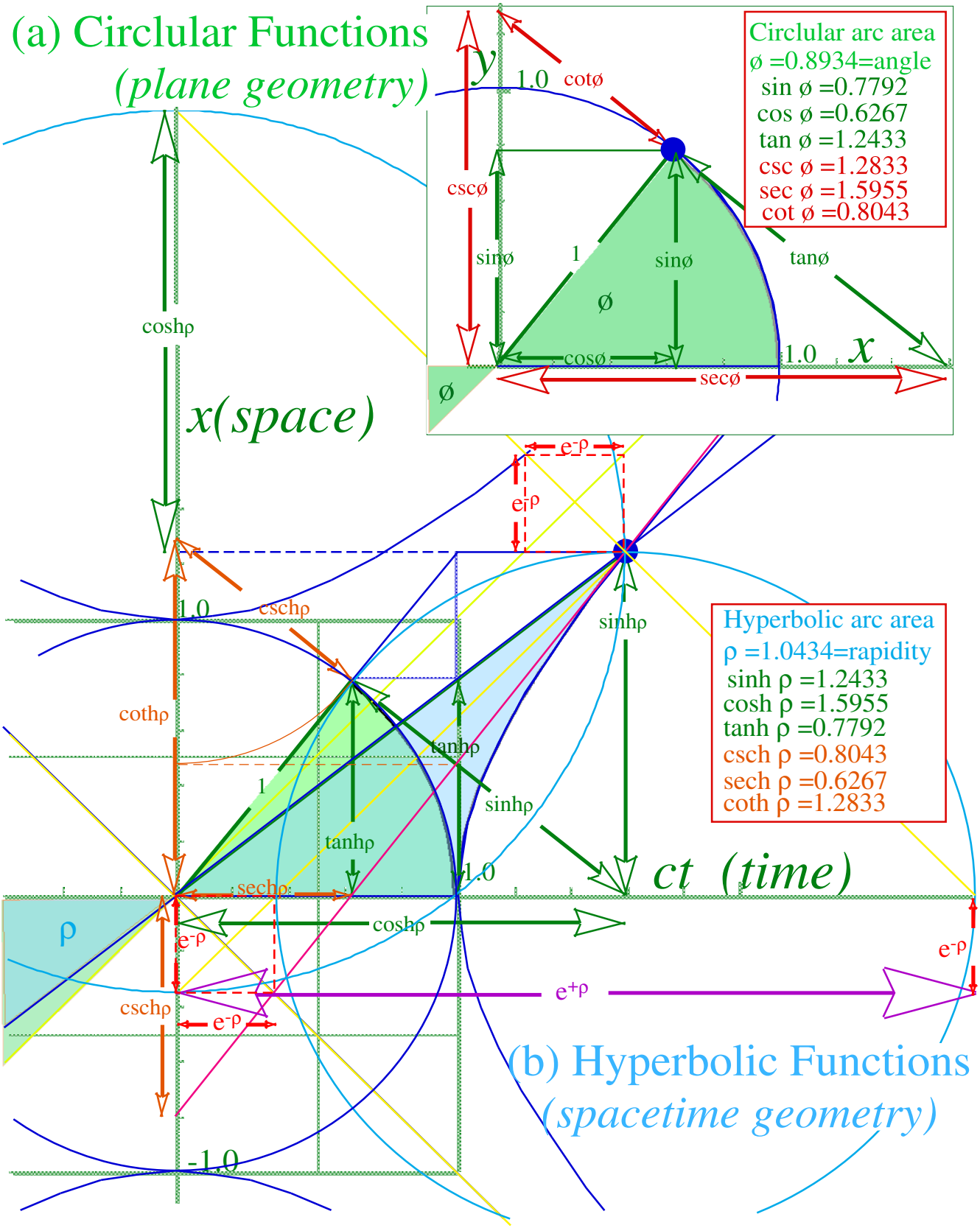

Fig. 16 Trigonometric geometry (a) Unit circular area ϕ=0.86 and (b) Unit hyperbolic area ρ=0.99.

Hyper-circular contacts

Beginning with the Euclidian mean diagram of Fig. 10, three mean frequencies arise from an interfering pair of left-moving "red" and right-moving "blue" beams of frequency ω_L and ω_R. First is a half-sum phase frequency $\omega_p=(\omega_R+\omega_L)/2$ (arithmetic mean) that defines the circle radius in Fig. 10. Second is a half-difference group beat frequency $\omega_g=(\omega_R-\omega_L)/2$ (difference mean) that is radial distance of circle center to origin. Third is a root-product proper frequency $\varpi=(\omega_R\cdot\omega_L)^{1/2}$ (geometric mean) that is the base radius or bottom of a $\omega(k)$ hyperbola of rest energy $B=\hbar\varpi=Mc^2$ above origin in Fig. 11.

Phase and group frequencies are defined as ratios or shifts of the geometric mean frequency ϖ, and this begins with the Doppler shift definition of the red $\omega_L=e^{-\rho}\varpi$ and blue $\omega_R=e^{+\rho}\varpi$ CW components. Ratio values $\omega_p=\varpi cosh\rho$ and $\omega_g=\varpi sinh\rho$ define each point on a ϖ-hyperbola dispersion curve in Fig. 17.

Fig. 17 is based on circles with three different radii, one for each mean frequency. The base circle-*b* drawn centered at origin has radius $B=\hbar\varpi=Mc^2$ of the Lagrangian circle in Fig. 13b. A smaller circle-*g* has group radius $\hbar\omega_g=Bsinh\rho$. A larger circle-*p* has phase radius $\hbar\omega_p=Bcosh\rho$ of the Euclidean circle in Fig. 10 and is drawn with dashed lines in Fig. 17. (Base value B is scaled for energy here.)

Circle-*p* of larger radius $\hbar\omega_p=Bcosh\rho$ is centered at $cp=\hbar\omega_g=Bsinh\rho$, a horizontal distance equal to the radius of the smaller circle-*g*, while the latter is centered at $E=\hbar\omega_p=Bcosh\rho$, a vertical distance equal to the radius of the larger circle-*p*. Tangents contacting the circles or the hyperbola define most of the physical quantities labeled in the zoom-in view of Fig. 17b. Intersections and chords shared by two of the circles also provide the key quantities as seen in Fig. 17a.

So far the CW development has emphasized the Doppler ratio as a starting point beginning with Fig. 7 and culminating with the Euclidean means of Fig. 10. However, most developments of relativity start with velocity *u*, and that geometric approach is excerpted in a simplified construction of Fig. 17c where *u/c=45/53* and Fig. 17d where *u/c=3/5*. (Fig. 17a-b and most other figures use *u/c=3/5*.) Once the velocity *u/c* line intersects the basic *b*-circle and its horizontal tangent of unit-energy ($B=1=Mc^2$), it only takes three more lines to derive Lagrangian $-L=Bsech\rho$, then momentum $cp=Bsinh\rho$, and finally the Hamiltonian $H=Bcosh\rho$. Then a compass is used to check accuracy with the phase *p*-circle by making sure it goes from *(cp,H)* to the *(0,B)*-point on top of the *b*-circle. The *p*-circle goes on to intersect the negative *cp*-axis at the Doppler red shift $rB=Be^{+\rho}$. Finally, the group *g*-circle in Fig. 17a-b has a chord intersection with the *p*-circle that is the hyperbolic contact tangent, and it grazes the ϕ-angle normal to the Lagrangian circle tangent in Fig. 17b. This helps to clarify geometry of *H-L* contact transformations introduced in Fig. 13. The construction also applies to the space-time domain.

If Fig. 17 is in space-time, the segment $-L=Bsech\rho$ is Lorentz contraction $\ell = B\sqrt{1-u^2/c^2}$. The $H=Bcosh\rho$ and $cp=Bsinh\rho$ segments are, respectively Einstien time dilation $d = B/\sqrt{1-u^2/c^2}$ and asimultaneity $a=ud/c$ coefficients. Node-to-node or peak-to-peak gaps contract by $\ell=4/5$ in Fig. 7d-e.

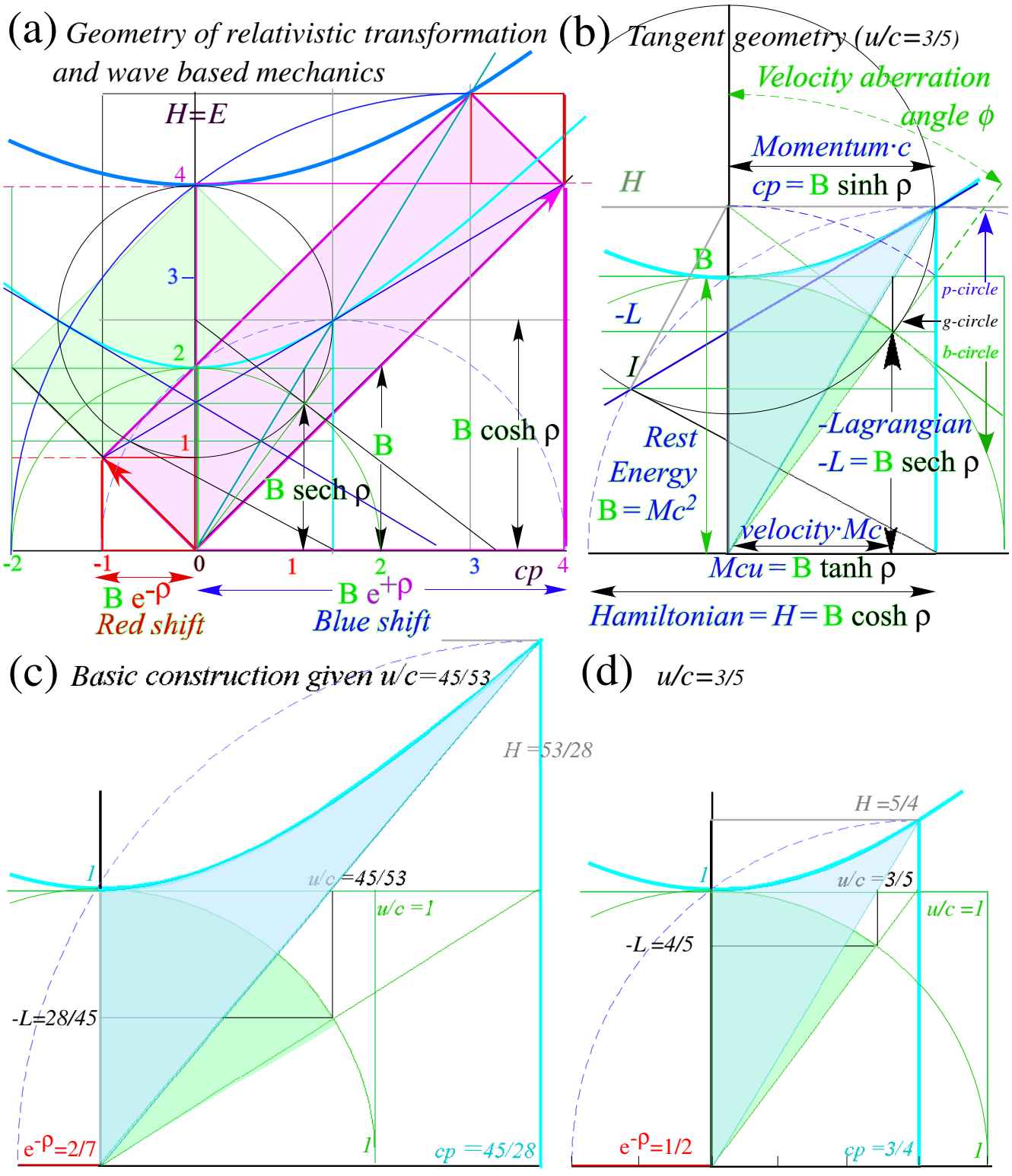

Fig. 17 Relativistic wave mechanics geometry. (a) Overview. (b-d) Details of contacting tangents.

As speed reduces in Fig. 17c-d from $u/c=45/53$ to $u/c=3/5$ or to lower values, the Lagrangian velocity angle ϕ and Hamiltonian rapidity ρ approach the velocity ratio u/c. Galilean velocity addition rules resume. In the opposite ultra-relativistic regime, ϕ approaches $\pi/2$, ρ approaches ∞, and u/c nears unit slope or $45°$ in Fig. 17c. But, Galilean-like rules (2.16) apply to rapidity ρ at all speeds (so far).

5. Symmetry and conservation principles

In Newtonian theory the first law or axiom is momentum conservation. Physical axioms, by definition, have only experimental proof. Logical proof is impossible unless a theory like Newton's becomes sub-summed by a more general theory with finer axioms. Proof of an axiom undermines it so it becomes a theorem or *result* of more basic axioms. (Or else an axiom might be *dis*proved or reduced to an approximate result subject to certain conditions.)

The logic of axioms yielding results or *theorems* in mathematical science probably goes back two thousand years to the time of Euclid's *Elements*. Also, axiomatic approaches to philosophy and natural science show up in writings as early as that of Occam or even Aristotle, but it is not until the European Renaissance that experiments are precise enough to support mathematical models. By the European Enlightenment period, mathematical logic of physical science had become more effective and productive than any preceding philosophy due in no small part to increasingly precise evidence.

As stated in the introduction, current time and frequency measurements have achieved almost unimaginable precision. Based on this, two continuous wave (CW) axioms (1.1-2) have been used to undermine Newtonian axioms concerning mass, energy, and momentum so they became approximate results (3.2) and give rise to exact equivalents of Newtonian concepts in Einstein and Planck relativity and quantum theory in (3.5). That is a modern example of an Occam razor-cut undermining axioms.

The undermining of Newton's first axiom (momentum conservation) by the shaved CW axioms is a good example to expose the logic involved. CW logic leads to the DeBroglie scaling law (3.5b) that equates momentum **p** to wavevector **k** scaled in $\hbar$ units. A rough statement of how CW axioms undermine or "prove" **p**-conservation axioms is that **k**-conservation is required by wave coherence and so $\mathbf{p}=\hbar\mathbf{k}$ must be conserved, as well. However, that oversimplifies a deeper nature of this logic.

The strength (and also, weakness) of CW axioms (1.1-2) is that they are *symmetry* principles due to the Lorentz-Poincare isotropy of space-time that invokes invariance to translation $\mathbf{T}(\delta,\tau)$ in the vacuum. Operator $\mathbf{T}$ has plane wave eigenfunctions $\psi_{k,\omega}=Ae^{i(kx-\omega t)}$ with eigenvalues $e^{i(k\cdot\delta-\omega\cdot\tau)}$.

$$\mathbf{T}\left|\psi_{k,\omega}\right\rangle=e^{i(k\cdot\delta-\omega\cdot\tau)}\left|\psi_{k,\omega}\right\rangle \qquad (5.1a) \qquad\qquad \left\langle\psi_{k,\omega}\right|\mathbf{T}^{\dagger}=\left\langle\psi_{k,\omega}\right|e^{-i(k\cdot\delta-\omega\cdot\tau)} \qquad (5.1b)$$

This also applies to 2-part or "2-particle" states $\Psi_{K,\Omega}=\psi_{k_1,\omega_1}\psi_{k_2,\omega_2}$ where exponents add *(k,ω)*-values of each constituent to $K=k_1+k_2$ and $\Omega=\omega_1+\omega_2$, and $\mathbf{T}(\delta,\tau)$-eigenvalues also have the form $e^{i(K\cdot\delta-\Omega\cdot\tau)}$ of (5.1). Matrix $\left\langle\Psi'_{K',\Omega'}\right|\mathbf{U}\left|\Psi_{K,\Omega}\right\rangle$ of **T**-symmetric evolution **U** is zero unless $K'=k'_1+k'_2=K$ and $\Omega'=\omega'_1+\omega'_2=\Omega$.

$$\begin{aligned}\left\langle\Psi'_{K',\Omega'}\right|\mathbf{U}\left|\Psi_{K,\Omega}\right\rangle&=\left\langle\Psi'_{K',\Omega'}\right|\mathbf{T}^{\dagger}(\delta,\tau)\mathbf{U}\mathbf{T}(\delta,\tau)\left|\Psi_{K,\Omega}\right\rangle \qquad (\text{if } \mathbf{UT}=\mathbf{TU} \text{ for all } \delta \text{ and } \tau)\\ &=e^{-i(K'\cdot\delta-\Omega'\cdot\tau)}e^{i(K\cdot\delta-\Omega\cdot\tau)}\left\langle\Psi'_{K',\Omega'}\right|\mathbf{U}\left|\Psi_{K,\Omega}\right\rangle=0 \text{ unless: } K'=K \text{ and: } \Omega'=\Omega\end{aligned} \qquad (5.2)$$

T-symmetry requires total energy $E=\hbar\Omega$ and total momentum $P=\hbar K$ be *conserved* for archetypical CW states, but laboratory CW have momentum uncertainty $\Delta\mathbf{k}=1/\Delta\mathbf{x}$ due to finite beam size $\Delta\mathbf{x}$ and energy uncertainty due to time limits. Newton's 1st law is verified but only as an ideal limit.

Symmetry is to physics what religion is to politics. Both are deep and grand in principle but roundly flaunted in practice. Both gain power quickly by overlooking details. In Sec. 3 relativistic and quantum kinetic properties of a massive "thing" arise from those of an optical 2-CW function in one space dimension. This means that mass shares *symmetry* with 2-CW light, not that mass *is* 2-CW light. Massive "things" do not vanish if the light is turned off as does a tiny optical mass $\hbar N\omega/c^2$ of a cavity.

Puzzling questions remain. Why do simple *wave* optics lead directly to general properties (3.5) of relativity and quantum mechanics of a massive *particle*? How does a cavity of counter-propagating green light *waves* act like it holds *particles* of mass $M=\hbar\omega/c^2$?

The short answer to one question is that particles are waves, too, and so forced by Lorentz symmetry to use available hyperbolic invariants $\omega^2-(ck)^2=(Mc^2/\hbar)^2$ for dispersion. To answer the second question entails further loss of classical innocence. In Sec. 6 Occam's razor is again applied to cut semi-classical CW laser fields down to single field quanta $\hbar\varpi$ or *photons*. So the second short answer is that waves are particles, too, even for optical dispersion $(\omega^2-(ck)^2=0)$.

By many accounts, quantum theory begins with Planck's axiom $E=\hbar N\omega$. This is distinguished from the scaling law $E=s\omega$ derived in (3.5) since its scale factor $s=\hbar N$ is not an obvious consequence of CW phase axioms (1.1-2) that lead to (3.5). CW logic seems to require additional axioms involving Maxwell energy E and field amplitude quantization by Planck. This is discussed shortly.

Quantization of phase variables

Waves were known to resonate at discrete wave numbers $k_m=m\frac{2\pi}{L}=mk_1$ in rings or boxes of fixed length L. The DeBroglie relations between k and momentum p force quantization $p_m=\hbar k_m=mp_1$ where momentum quantum numbers[23] $m=0,\pm1,\pm2,\ldots$ count waves on ring L as in Bohr models. Planck dispersion $E_m=\hbar\omega(k_m)$ (3.5) gives energy levels $E_m=m^2E_1$ for sub-relativistic cases with $E_1=p_1^2/2M$.

Heisenberg[24] showed quanta p_m or E_m arise from eigenvalues (literally "own-values") of matrix operators $\mathbf{p}$ or $\mathbf{H}$ whose eigenvectors ("own-vectors") $|p_m\rangle$ or $|E_m\rangle$ may be superimposed.

$$|\Psi\rangle=\psi_1|E_1\rangle+\psi_2|E_2\rangle+\psi_3|E_3\rangle+\ldots \qquad (5.3)$$

(Dirac's bra-ket[25] notation came later.) Allowing things to be at (or in) m places (or states) allows mean values $\bar{E}=\langle\Psi|\mathbf{H}|\Psi\rangle$ to range continuously from lowest quantum levels E_1 to the highest E_m.

$$\bar{E}=\langle\Psi|\mathbf{H}|\Psi\rangle=|\psi_1|^2E_1+|\psi_2|^2E_2+|\psi_2|^2E_2+\ldots \qquad (5.4)$$

For classicists, the notion that each multiple-personality-k has a probability $|\psi_k|^2$ seems, if not crazy, then at least dicey in the sense of Einstein's skeptical quote, "God does not play dice…" [26]

But, superposition is an idea borrowed from classical waves, and their interference makes them ultra-sensitive to relative position and velocity, a *first* order sensitivity that leads elegantly to relativity transformation (2.10) and kinematic relations (3.5) by geometry of optical phase kx-ωt. But, amplitude "A" of wave (1.9) or (1.10) is set arbitrarily. It is ignored in (4.5). Without Maxwell and Planck rules, CW amplitude or wave *quantity* is undefined and un-quantized. This must now be discussed.

6. Variation and quantization of optical amplitudes

What is deduced from wave phase alone? Wave *amplitude* has so far been skirted for Occam economy: *"Pluralitas non est ponenda sine neccesitate"* (Do not assume plurality without necessity.) CW phase axioms (1.1-2) give Lorentz-Doppler and Planck-DeBroglie symmetry relations yet 2-CW amplitudes (1.10) are not defined beyond assuming their 1-CW amplitudes match. Standing wave grid reference frames in Fig. 6 and Fig. 7 are just points where amplitude is *zero*, that is, loci of real wave function *roots*.

Discussion of non-zero amplitude variation begins with counter-propagating 2-CW dynamics involving two 1-CW amplitudes $A_{\rightarrow}$ and $A_{\leftarrow}$ that are *un*matched. $(A_{\rightarrow} \neq A_{\leftarrow})$

$$A_{\rightarrow}e^{i(k_{\rightarrow}x-\omega_{\rightarrow}t)} + A_{\leftarrow}e^{i(k_{\leftarrow}x-\omega_{\leftarrow}t)} = e^{i(k_{\Sigma}x-\omega_{\Sigma}t)}[A_{\rightarrow}e^{i(k_{\Delta}x-\omega_{\Delta}t)} + A_{\leftarrow}e^{-i(k_{\Delta}x-\omega_{\Delta}t)}] \quad (6.1a)$$

Half-sum mean phase rates $(k_{\Sigma},\omega_{\Sigma})$ and half-difference means $(k_{\Delta},\omega_{\Delta})$ appear here as in (1.10).

$$\begin{aligned} k_{\Sigma} &= (k_{\rightarrow} + k_{\leftarrow})/2 \\ \omega_{\Sigma} &= (\omega_{\rightarrow} + \omega_{\leftarrow})/2 \end{aligned} \quad (6.1b) \qquad \begin{aligned} k_{\Delta} &= (k_{\rightarrow} - k_{\leftarrow})/2 \\ \omega_{\Delta} &= (\omega_{\rightarrow} - \omega_{\leftarrow})/2 \end{aligned} \quad (6.1c)$$

Also important is amplitude mean $A_{\Sigma} = (A_{\rightarrow} + A_{\leftarrow})/2$ and half-difference $A_{\Delta} = (A_{\rightarrow} - A_{\leftarrow})/2$. Wave motion depends on standing-wave-ratio *SWR* or the inverse standing-wave-quotient *SWQ* affects.

$$SWR = \frac{(A_{\rightarrow} - A_{\leftarrow})}{(A_{\rightarrow} + A_{\leftarrow})} \quad (6.2a) \qquad SWQ = \frac{(A_{\rightarrow} + A_{\leftarrow})}{(A_{\rightarrow} - A_{\leftarrow})} \quad (6.2a)$$

Recall mean frequency ratios for group velocity (2.7b) or its inverse that is phase velocity (2.7a).

$$V_{group} = \frac{\omega_{\Delta}}{k_{\Delta}} = c\frac{(\omega_{\rightarrow} - \omega_{\leftarrow})}{(\omega_{\rightarrow} + \omega_{\leftarrow})} \quad (6.3a) \qquad V_{phase} = \frac{\omega_{\Sigma}}{k_{\Sigma}} = c\frac{(\omega_{\rightarrow} + \omega_{\leftarrow})}{(\omega_{\rightarrow} - \omega_{\leftarrow})} \quad (6.3b)$$

A 2-state amplitude continuum is bounded by $(A_{\rightarrow} = 1, A_{\leftarrow} = 0)$ a pure right-moving 1-CW of *SWR=1* and a pure left-moving 1-CW $(A_{\rightarrow} = 0, A_{\leftarrow} = 1)$ of *SWR=-1*. A 2-CW standing-wave $(A_{\rightarrow} = \frac{1}{\sqrt{2}} = A_{\leftarrow})$ has *SWR=0*.

Wave paths for various *SWR* values are drawn in Fig. 18 for *600THz* 2-CW pairs and in Fig. 19 for Doppler shifted *300THz* and *1200THz* 2-CW pairs at the same *SWR* values. The *SWQ* is the ratio of the envelope peak (interference maximum) to the envelope valley (interference minimum), and *vice versa* for *SWR=1/SWQ*. Single frequency 2-CW paths of nonzero-*SWR* in Fig. 18 do a galloping motion. Each wave speeds up to peak speed *c/SWR=c·SWQ* as it first shrinks to squeeze through its envelope minima and then slows to resting speed *c·SWR* as it expands to its maximum amplitude. Only at zero-*SWR* do 2-CW zero-paths appear to travel at a constant group speed (6.3a) and phase speed (6.3b) as in Fig. 18c or 19c. (For 1-CW paths or unit *SWR=±1* there is just one speed ±*c* by axiom (1.1).)

The real and imaginary parts take turns. One gallops while the other rests and *vice versa* and this occurs twice each optical period. If frequency ratio (6.3) and amplitude ratio (6.2) have opposite signs as in Fig. 18c (±0 or ±∞) and in Fig. 19e (±3/5 or ±5/3), wave zero paths will follow a right angle staircase. 1-frequency staircase ($V_{group}=0=SWR$) in Fig. 18c is a Cartesian grid like Fig. 6c. 2-frequency waves ($V_{group}\neq 0$) have Minkowski grids like Fig. 7c for *SWR=0* or quasi-Cartesian stair steps like Fig. 19e for $V_{group}=-cSWR$. To broadcast Cartesian grids to a *u*-frame one tunes both V_{group} and *cSWR* to *u*.

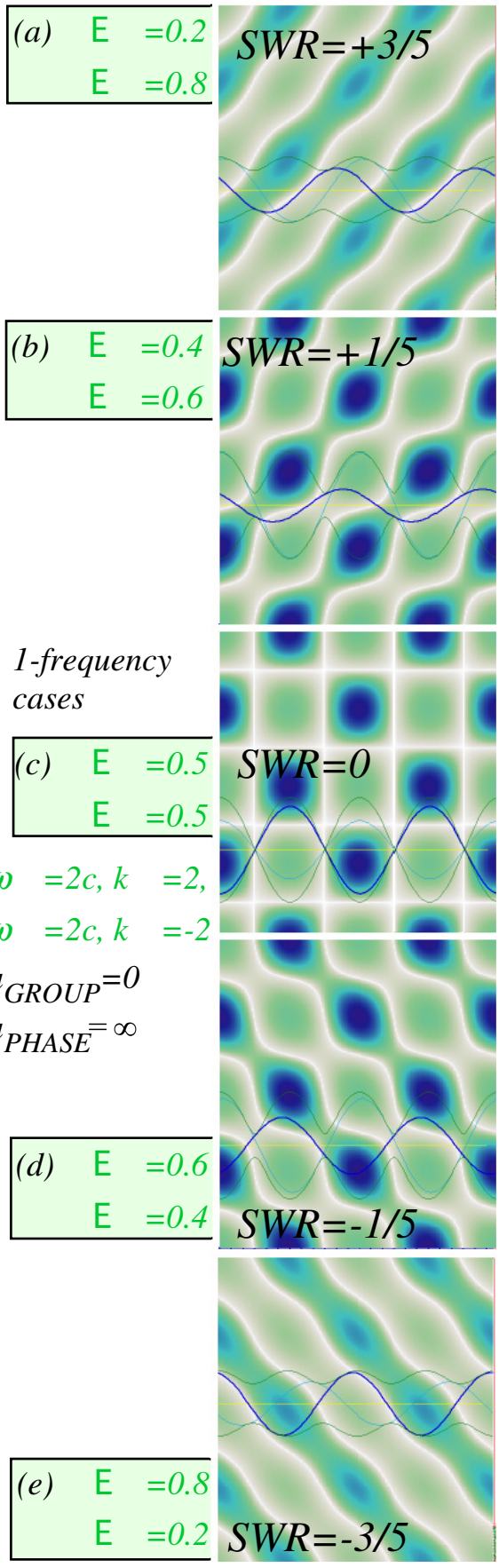

Fig. 18 Monochromatic (1-frequency) 2-CW wave space-time patterns.

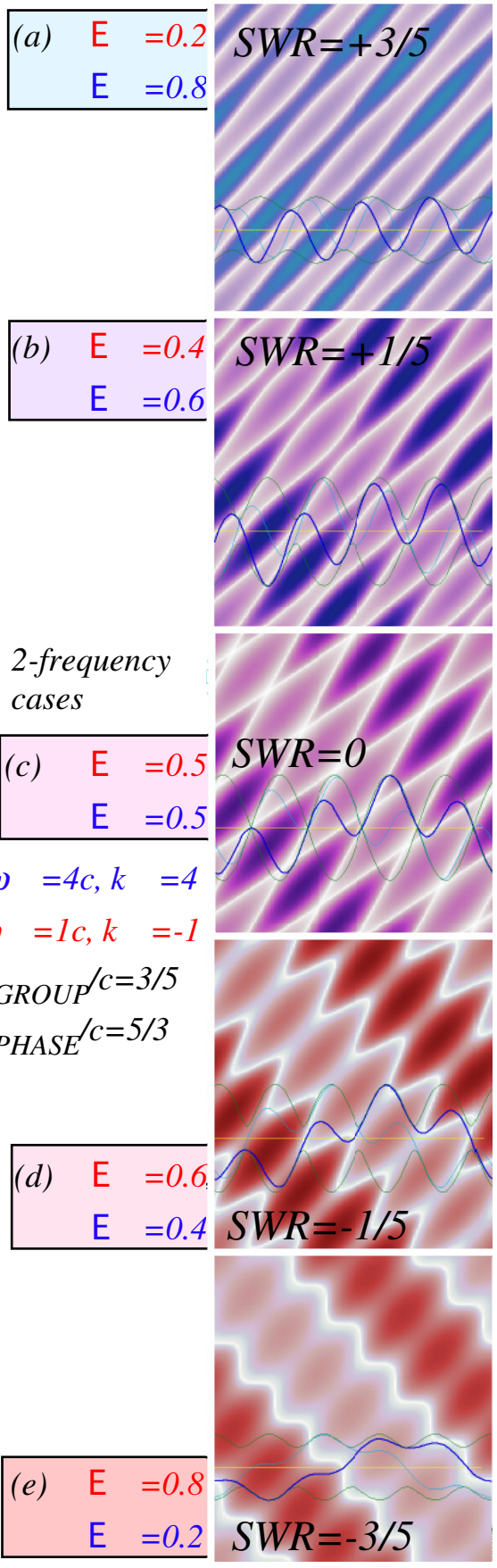

Fig. 19 Dichromatic (2-frequency) 2-CW wave space-time patterns.

Galloping is a fundamental interference property that may be clarified by analogy with elliptic orbits of isotropic 2D-harmonic oscillators and in particular with elliptic polarization of optical wave amplitudes. Fig. 20 relates polarization states and wave states of Fig. 18 beginning with left (right)-circular polarization that is analogous to a left (right)-moving wave in Fig. 20g (Fig. 20a). As sketched in Fig. 20(b-e), galloping waves are general cases analogous to general states of elliptic polarization or general 2DHO orbits obeying a Keplerian geometry shown in Fig. 20h. Standing waves correspond to plane-polarization. Polarization in the *x*-plane of Fig. 20d corresponds to a standing cosine wave and *y*-plane polarization (not shown) would correspond to a standing sine wave.

Isotropic oscillator orbits obey Kepler's law of constant orbital momentum. Orbit angular velocity slows down by a factor *b/a* at major axes or aphelions ±*a* and then speeds up by a factor *a/b* at minor axes or perihelions ±*b* just as a galloping wave, twice in each period, slows down to *SWR*·*c* and speeds up to *SWQ*·*c*. The galloping or eccentric motion of the eccentric anomaly angle $\phi(t)$ in Fig. 20h is a projection of a uniformly rotating mean anomaly (phase angle ωt) of the isotropic oscillator, and this gives a Keplarian relation of the two angles seen in the figure.

$$\tan\phi(t) = \frac{b}{a}\tan\omega\cdot t \tag{6.4a}$$

The eccentric anomaly time derivative of ϕ (angular velocity) gallops between $\omega\cdot b/a$ and $\omega\cdot a/b$.

$$\dot{\phi} = \frac{d\phi}{dt} = \omega\cdot\frac{b}{a}\frac{\sec^2\omega t}{\sec^2\phi} = \frac{\omega\cdot b/a}{\cos^2\omega t + (b/a)^2\cdot\sin^2\omega t} = \begin{cases}\omega\cdot b/a & \text{for: } \omega t = 0,\ \pi,\ 2\pi...\\ \omega\cdot a/b & \omega t = \pi/2,\ 3\pi/2,...\end{cases} \tag{6.4b}$$

The product of angular moment r^2 and $\dot{\phi}$ is orbital momentum, a constant proportional to ellipse area.

$$r^2\frac{d\phi}{dt} = constant = (a^2\cos^2\omega t + b^2\cdot\sin^2\omega t)\frac{d\phi}{dt} = \omega\cdot ab$$

Consider galloping wave zeros of a monochromatic wave (6.1a) having *SWQ* (6.2b).

$$0 = \mathrm{Re}\,\Psi(x,t) = \mathrm{Re}\left[A_{\rightarrow}e^{i(k_0x-\omega_0t)} + A_{\leftarrow}e^{i(-k_0x-\omega_0t)}\right] \text{ where: } \omega_{\rightarrow} = \omega_0 = \omega_{\leftarrow} = ck_0 = -ck_{\leftarrow}$$

$$0 = A_{\rightarrow}\left[\cos k_0x\ \cos\omega_0t + \sin k_0x\ \sin\omega_0t\right] + A_{\leftarrow}\left[\cos k_0x\ \cos\omega_0t - \sin k_0x\ \sin\omega_0t\right]$$

$$\left(A_{\rightarrow} + A_{\leftarrow}\right)\left[\cos k_0x\ \cos\omega_0t\right] = -\left(A_{\rightarrow} - A_{\leftarrow}\right)\left[\sin k_0x\ \sin\omega_0t\right]$$

Space k_0x varies with time ω_0t in the same way that eccentric anomaly varies in (6.4a).

$$\tan k_0x = -SWQ\cdot\cot\omega_0t = SWQ\cdot\tan\omega_0\bar{t} \text{ where: } \omega_0\bar{t} = \omega_0t - \pi/2 \tag{6.5a}$$

Speed of galloping wave zeros is the time derivative of root location *x* in units of light velocity *c*.

$$\frac{dx}{dt} = c\cdot SWQ\frac{\sec^2\omega_0\bar{t}}{\sec^2 k_0x} = \frac{c\cdot SWQ}{\cos^2\omega_0\bar{t} + SWQ^2\cdot\sin^2\omega_0\bar{t}} = \begin{cases}c\cdot SWQ & \text{for: } \bar{t} = 0,\ \pi,\ 2\pi...\\ c\cdot SWR & \bar{t} = \pi/2,\ 3\pi/2,...\end{cases} \tag{6.5b}$$

Single frequency 2-CW paths in Fig. 18 have a constant product of instantaneous wave velocity and wave amplitude analogous to the constant product of orbital velocity and radius. So vacuum optical amplitude and phase motion obey rules of Kepler and (Sec. 2) Galileo. That these 15th century geometric relations underlie basic wave physics has not been fully appreciated.

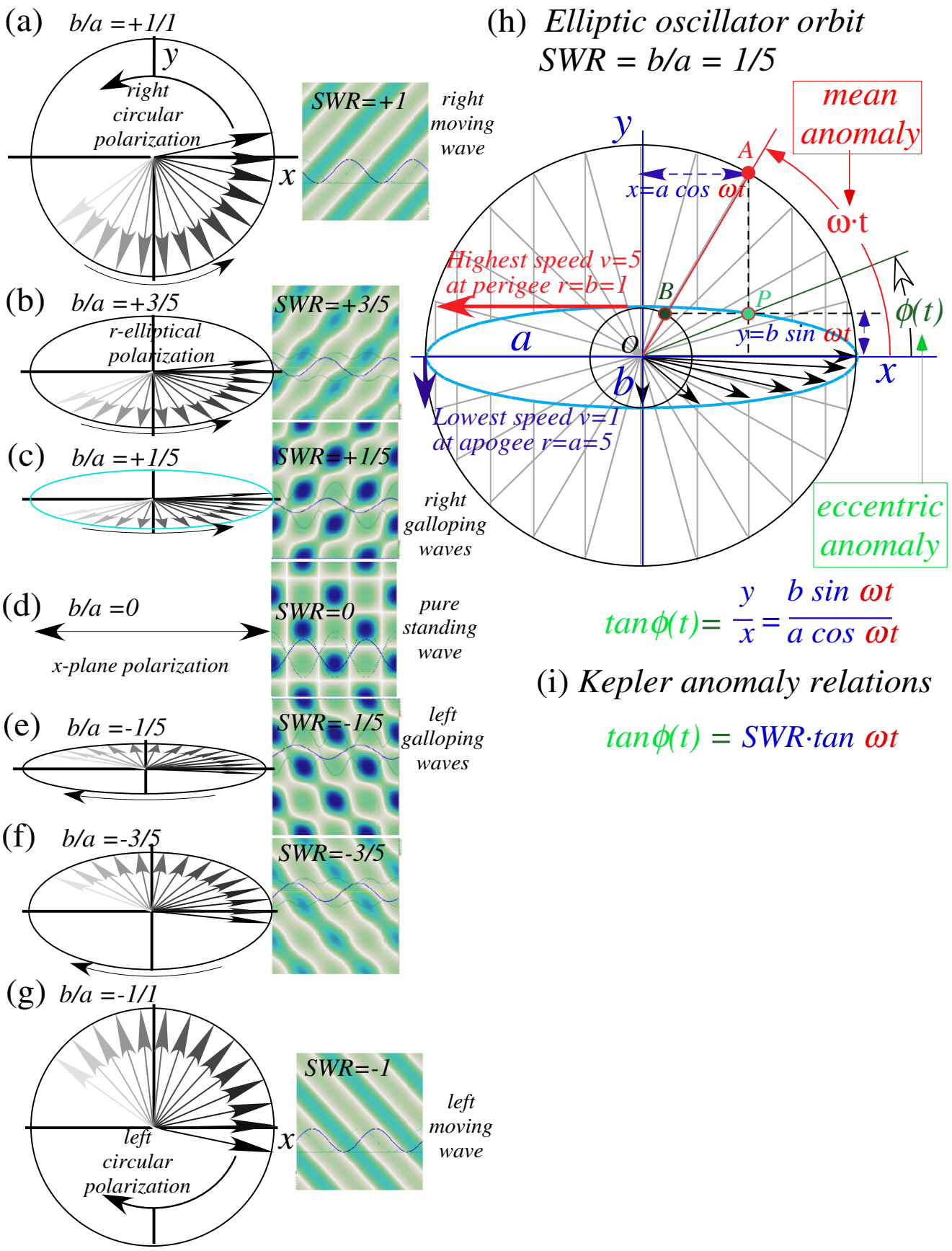

Fig. 20 (a-g) Elliptic polarization ellipses relate to galloping waves in Fig. 18. (h-i) Kepler anomalies.

Maxwell amplitudes and energy

Classical Maxwell field amplitudes $\mathbf{E} = -\dot{\mathbf{A}}$ and $\mathbf{B} = \nabla \times \mathbf{A}$ are derivatives of vector potential **A**. Maxwell energy U per volume V or total energy $U \cdot V$ is a sum of amplitude squares **E**•**E** and c^2**B**•**B**.

$$\langle U \rangle \cdot V = \left\langle \frac{\varepsilon_0}{2} \mathbf{E} \bullet \mathbf{E} + \frac{1}{2\mu_0} \mathbf{B} \bullet \mathbf{B} \right\rangle \cdot V \qquad \mu_0 \varepsilon_0 = \frac{1}{c^2} \tag{6.7}$$

Fourier analysis of **A** into amplitudes $\mathbf{a}_k$ and $\mathbf{a}_k^*$ leads to a harmonic oscillator sum over each plane CW mode frequency $\omega_k = \pm c\,|\,\mathbf{k}_m\,|$, $\boldsymbol{k}_m$-vector allowed by a large-cavity, and polarization α=*x,y* normal to $\boldsymbol{k}_m$.

$$\langle U \rangle \cdot V = 2\varepsilon_0 V \sum \omega_k^2 \mathbf{a}_k^* \mathbf{a}_k \tag{6.8}$$

Harmonic oscillator frequency is independent of amplitude. This is consistent with CW phase axiom (1.1) and dispersion relations (3.5) derived from 2-CW superposition, but such a simple axiom seems unable to derive the Maxwell vector amplitude structure of 2-dimensional polarization normal to $\boldsymbol{k}_m$ of each wave mode or even to establish that its wave variables **A**, **B**, **E**, or $\boldsymbol{k}_m$ are, in fact, 3D vectors.

The CW axiom (1.1) gives what is effectively a 2-dimensional harmonic oscillator (2DHO) with two complex amplitudes (a_L, a_R) for the two longitudinal propagation directions, but each comes with two transverse polarization amplitudes (a_x, a_y) that describe the second 2DHO in Maxwell light, namely polarization ellipsometry used in Fig. 20 as an analogy for propagation left-and-right along *z*.

Quantized optical fields

Mode amplitude $\mathbf{a}_k$ or $\mathbf{a}_k^*$ in classical electromagnetic energy $\sum \omega_k^2 \mathbf{a}_k^* \mathbf{a}_k$ are replaced by oscillator operators $\mathbf{a}_k$ or $\mathbf{a}_k^\dagger$ for a field Hamiltonian with explicit linear frequency dependence of Planck.

$$\mathbf{H} = \sum \hbar \omega_k (\mathbf{a}_k^\dagger \mathbf{a}_k) \Rightarrow \langle \mathbf{H} \rangle = \sum \hbar \omega_k N_k \tag{6.9}$$

The **H**-eigenstates $|N_1 N_2 \cdots N_k\rangle$ for exactly quantized photon numbers $\langle \mathbf{a}_k^\dagger \mathbf{a}_k \rangle = N_k$ fix a definite energy value $\hbar\omega_k N_k$ for each mode-k_m but has quite *un*certain field phase. Average energy of one mode is

$$\langle U_k \rangle \cdot V = 2\varepsilon_0 V \langle \mathbf{E}_k \bullet \mathbf{E}_k \rangle = \hbar \omega_k N_k \tag{6.10a}$$

where a 1-CW-1-photon E-field and vector potential *A*-amplitude is as follows.

$$\left\langle \left| \mathbf{E}_k \right| \right\rangle_{N_k = 1} = \sqrt{\frac{\hbar \omega_k}{2\varepsilon_0 V}} \tag{6.10b} \qquad \left\langle \left| \mathbf{A}_k \right| \right\rangle_{N_k = 1} = \sqrt{\frac{\hbar}{2\varepsilon_0 \omega_k V}} \tag{6.10c}$$

Field quantization is called 2nd-quantization to distinguish 1st-quantization k_m *mode* numbers *m*, used for classical light, from "purely quantum" *photon* numbers $n = N_{k_m}$ for wave amplitude. This may be a prejudice that waves (particles) are usual (unusual) for light but unusual (usual) for matter.

Amplitudes involve relations (6.7) to (6.10) that are more complex than axioms (1.1-2) for wave phase. While Maxwell-Planck relations lack the simplicity of the latter, they do derive the linear dispersion (1.1) by Fourier transform of the Maxwell wave equations, and they show optical wave amplitude has an internal symmetry analogous to that of wave frequency. The following discussion of this analogy involves a Doppler shift of wave *amplitude* with invariance or covariance of photon

number N_k and standing wave ratio *(SWR)* (6.5). Also, one begins to see how Born quantum probability formulas $\langle n \rangle = \psi^* \psi$ arise and are consistent with Dirac amplitude covariance.

Relativistic 1-CW covariance of Poynting flux

Maxwell-Planck energy density *U(Joule/m³)* in (6.10a) leads to a related Poynting flux **S***[Joule/(m²·s)]*.

$$\vec{\mathbf{S}} = \vec{\mathbf{E}} \times \vec{\mathbf{B}} = \left\langle U_k \right\rangle c\hat{\mathbf{k}} = 2\varepsilon_0 c \left\langle \mathbf{E}_k \bullet \mathbf{E}_k \right\rangle \hat{\mathbf{k}} = \hbar \omega_k \bar{n}_k \hat{\mathbf{k}} \quad \text{where: } n_k = cN_k / V\left[m^{-2}s^{-1}\right] \qquad (6.11)$$

Flux **S** contains two frequency factors, the fundamental laser frequency ω_k and the photon count rate n_k per*[(m²·s)]*. Frequency ω_k is quantum *quality* of a laser beam and rate n_k is its quantum *quantity*. The product $\hbar\omega_k \cdot n_k$ is Poynting *flux*. Rate n_k and frequency ω_k both Doppler shift by an exponential $e^{\pm\rho}$ of rapidity ρ in (2.16). So do 1-CW fields $E_{\pm k}$ as may be shown by Lorentz transforming them directly.

$$E'_{+k} = e^{+\rho} E_{+k} \quad (6.12a) \qquad\qquad E'_{-k} = e^{-\rho} E_{-k} \quad (6.12b)$$

Thus both electric field polarization **E**-amplitudes E_x an E_y of a 1-CW field undergo the same $e^{\pm\rho}$Doppler shift that the frequency ω_k or wavevector k experience. If **E** in (6.11) scaled by 1-photon factor (6.10) a probability wave ψ follows whose square ψ*ψ is a volume photon count *N/(m³)*.

$$\psi_k = \sqrt{\frac{2\varepsilon_0 V}{\hbar\omega_k}} E_k \Rightarrow \left\langle \quad \psi_k^* \psi_k \quad \right\rangle = \left\langle N_k \right\rangle = \bar{N}_k = \bar{n}_k \frac{V}{c} \qquad (6.13a)$$

Or, a flux probability wave ψ is defined so its square $\psi^*\psi$ is an expected flux photon count *n/(m²·s)*.

$$\psi_k = \sqrt{\frac{2\varepsilon_0 c}{\hbar\omega_k}} E_k \Rightarrow \left\langle \psi_k {}^* \psi_k \right\rangle = \left\langle n_k \right\rangle = \bar{n}_k = \frac{c}{V} \bar{N}_k \qquad (6.13b)$$

Due to the $1/\sqrt{\omega_k}$ scaling of (6.13) the Doppler factor of $\psi_{\pm k}$ drops an $e^{\pm\rho/2}$ factor from E_k in (6.12).

$$L_z(\rho)\left|\psi\right\rangle = \begin{pmatrix} \psi'_{+k} \\ \psi'_{-k} \end{pmatrix} = \begin{pmatrix} e^{+\rho/2} & 0 \\ 0 & e^{-\rho/2} \end{pmatrix} \begin{pmatrix} \psi_{+k} \\ \psi_{-k} \end{pmatrix} = e^{\sigma_z \rho/2} \left|\psi\right\rangle \qquad (6.14)$$

This is a starting point for the spinor form of Lorentz transformation for Dirac amplitudes.

Relativistic 2-CW invariance of cavity quanta

Mean photon number $\bar{N}_k$ of a 2-CW cavity mode, unlike a 1-CW flux quantum n_k, is invariant to cavity speed. By analogy, 2-CW modes have variant group-phase velocity (V_{group}, V_{phase}), energy-momentum *(ħck,ħω)*, but invariant mean velocity $c = \sqrt{V_{group} V_{phase}}$ and frequency $\varpi = \sqrt{\omega_{+k}\omega_{-k}} = \sqrt{\omega^2 - c^2 k^2}$.

$$\frac{V_{phase}}{c} = \frac{\omega_{+k} - \omega_{-k}}{\omega_{+k} + \omega_{-k}} \quad (6.15a) \qquad\qquad \frac{V_{group}}{c} = \frac{\omega_{+k} - \omega_{-k}}{\omega_{+k} + \omega_{-k}} \quad (6.15b)$$

Linear dispersion $\omega_{\pm k} = \pm ck$ and (1.11) or (2.7) are used. Note the analogy to *SWR* relations (6.2).

$$SWR = \frac{E_{+k} - E_{-k}}{E_{+k} + E_{-k}} \qquad (6.15c) \qquad\qquad SWQ = \frac{E_{+k} + E_{-k}}{E_{+k} - E_{-k}} \qquad (6.15d)$$

Each ratio (6.15) is a wave velocity that Doppler-transforms like relativistic (non-Galilean) velocity.

$$SWR' = \frac{SWR + u/c}{1 + SWR \cdot u/c} \quad (6.16a) \qquad\qquad \frac{V'_m}{c} = \frac{V_m/c + u/c}{1 + (V_m/c)\cdot(u/c)} \quad (6.16b)$$

Velocity $u_{AB}/c=\tanh\rho_{AB}$ is a hyperbolic sum since rapidity is a simple sum $\rho_{AB}=\rho_A+\rho_B$ by (2.16).

$$\frac{u_{AB}}{c}=\tanh\rho_{AB}=\tanh(\rho_A+\rho_B)=\frac{\tanh\rho_A+\tanh\rho_B}{1+\tanh\rho_A\tanh\rho_B}=\frac{u_A/c+u_B/c}{1+u_Au_B/c^2} \qquad (6.17)$$

The energy and momentum flux values are found for counter-k 2-CW beam functions $\Psi_{\rightleftarrows}$.

$$\Psi_{k\rightleftarrows}=\psi_{\rightarrow}e^{i(k_{\rightarrow}x-\omega_{\rightarrow}t)}+\psi_{\leftarrow}e^{i(k_{\leftarrow}x-\omega_{\leftarrow}t)}$$

Lab 1-CW flux number expectation values $|\psi_k|^2=\langle n_k\rangle$ give 2-CW flux expectations in lab.

$$\langle E\rangle=\langle\hbar\omega\rangle=\hbar\omega_{\rightarrow}\langle n_{\rightarrow}\rangle\ +\hbar\omega_{\leftarrow}\langle n_{\leftarrow}\rangle=\hbar\omega_{\rightarrow}|\psi_{\rightarrow}|^2+\hbar\omega_{\leftarrow}|\psi_{\leftarrow}|^2$$

$$\langle cp\rangle=\langle\hbar ck\rangle=\hbar ck_{\rightarrow}\langle n_{\rightarrow}\rangle+\hbar ck_{\leftarrow}\langle n_{\leftarrow}\rangle=\hbar\omega_{\rightarrow}|\psi_{\rightarrow}|^2-\hbar\omega_{\leftarrow}|\psi_{\leftarrow}|^2$$

The relation (6.13b) of quantum field ψ_k and classical Maxwell E_k -field expectation is used.

$$\langle E\rangle=\hbar\omega_{\rightarrow}|\psi_{\rightarrow}|^2+\hbar\omega_{\leftarrow}|\psi_{\leftarrow}|^2=2\varepsilon_0c\left(|E_{\rightarrow}|^2+|E_{\leftarrow}|^2\right) \qquad (6.18a)$$

$$\langle cp\rangle=\hbar\omega_{\rightarrow}|\psi_{\rightarrow}|^2-\hbar\omega_{\leftarrow}|\psi_{\leftarrow}|^2=2\varepsilon_0c\left(|E_{\rightarrow}|^2-|E_{\leftarrow}|^2\right) \qquad (6.18b)$$

Values $\langle cp\rangle$ and $\langle E\rangle$ lie on an invariant hyperbola of constant geometric means $\varpi\bar{N}$ or $|\bar{\mathbf{E}}|^2$.

$$\langle E\rangle^2-\langle cp\rangle^2=(2c\varepsilon_0)^2\left[\left(|E_{\rightarrow}|^2+|E_{\leftarrow}|^2\right)^2-\left(|E_{\rightarrow}|^2-|E_{\leftarrow}|^2\right)^2\right]=(2c\varepsilon_0)^2\left[4|E_{\rightarrow}|^2|E_{\leftarrow}|^2\right]$$

$$\langle E\rangle^2-\langle cp\rangle^2=4\left(2c\varepsilon_0|E_{\rightarrow}|^2\right)\left(2c\varepsilon_0|E_{\leftarrow}|^2\right)=4\left(\hbar\omega_{\rightarrow}\langle n_{\rightarrow}\rangle\right)\left(\hbar\omega_{\leftarrow}\langle n_{\leftarrow}\rangle\right) \qquad (6.19)$$

$$\sqrt{\langle E\rangle^2-\langle cp\rangle^2}\ =\ 2c\varepsilon_0|2\bar{\mathbf{E}}|^2\ =\ (\hbar\bar{\omega})(2\bar{n}) \qquad (6.20a)$$

The geometric mean frequency ϖ, mean quantum number $\bar{n}$, and mean field $|\bar{\mathbf{E}}|$ are defined.

$$\varpi=\sqrt{\omega_{\rightarrow}\omega_{\leftarrow}} \quad (6.20b) \qquad \bar{n}=\sqrt{n_{\rightarrow}n_{\leftarrow}} \quad (6.20c) \qquad |\bar{\mathbf{E}}|=\sqrt{E_{\rightarrow}E_{\leftarrow}} \quad (6.20d)$$

Doppler relations imply Lorentz invariance for the mean number $\bar{n}$ and for the mean frequency ϖ as well as their geometric mean $\sqrt{\bar{n}\varpi}$ that is $2c\varepsilon_0$ times the mean field $|\bar{\mathbf{E}}|$ and applies to a general 2-CW beam function Ψ. A factor 2 on $|2\bar{\mathbf{E}}|$ or $2\bar{n}$ in (6.20a) is consistent with 1-photon 2-CW states of balanced number $n_{\rightarrow}=\bar{n}=n_{\leftarrow}=\frac{1}{2}$ whose 1-photon Planck energy expectation is $E=\hbar\omega$.

Ideal cavities balance field $E_{\rightarrow}=\bar{\mathbf{E}}=E_{\leftarrow}$, frequency $\omega_{\rightarrow}=\varpi=\omega_{\leftarrow}$, and number. A general beam with $\omega_{\rightarrow}\neq\omega_{\leftarrow}$, $n_{\rightarrow}\neq n_{\leftarrow}$, and $E_{\rightarrow}\neq E_{\leftarrow}$ has a center-of-momentum *CoM*-frame of zero flux where $E_{\rightarrow}^{CoM}=E_{\leftarrow}^{CoM}$ by (6.18b), an isochromatic *IsoC*-frame with $\omega_{\rightarrow}^{IsoC}=\omega_{\leftarrow}^{IsoC}$, and an *IsoN*-frame with balanced photon count $N_{\rightarrow}^{IsoN}=N_{\leftarrow}^{IsoN}$. Frame speeds u^{α} may be distinct as sketched in Fig. 21.

$$\frac{u^{CoM}}{c}=\frac{E_{\rightarrow}-E_{\leftarrow}}{E_{\rightarrow}+E_{\leftarrow}}\ (6.21a) \qquad \frac{u^{IsoC}}{c}=\frac{\omega_{\rightarrow}-\omega_{\leftarrow}}{\omega_{\rightarrow}+\omega_{\leftarrow}}=\frac{V^{Group}}{c}\ (6.21b) \qquad \frac{u^{IsoN}}{c}=\frac{n_{\rightarrow}-n_{\leftarrow}}{n_{\rightarrow}+n_{\leftarrow}}\ (6.21c)$$

Flux invariant $|\bar{\mathbf{E}}|$ is maximized by balanced amplitude $E_{\rightarrow}=E_{\leftarrow}$ but is zero if $E_{\rightarrow}$ or $E_{\leftarrow}$ is zero.

Thus optical rest mass (6.20a) decreases continuously as a 2-CW beam is unbalanced toward 1-CW.

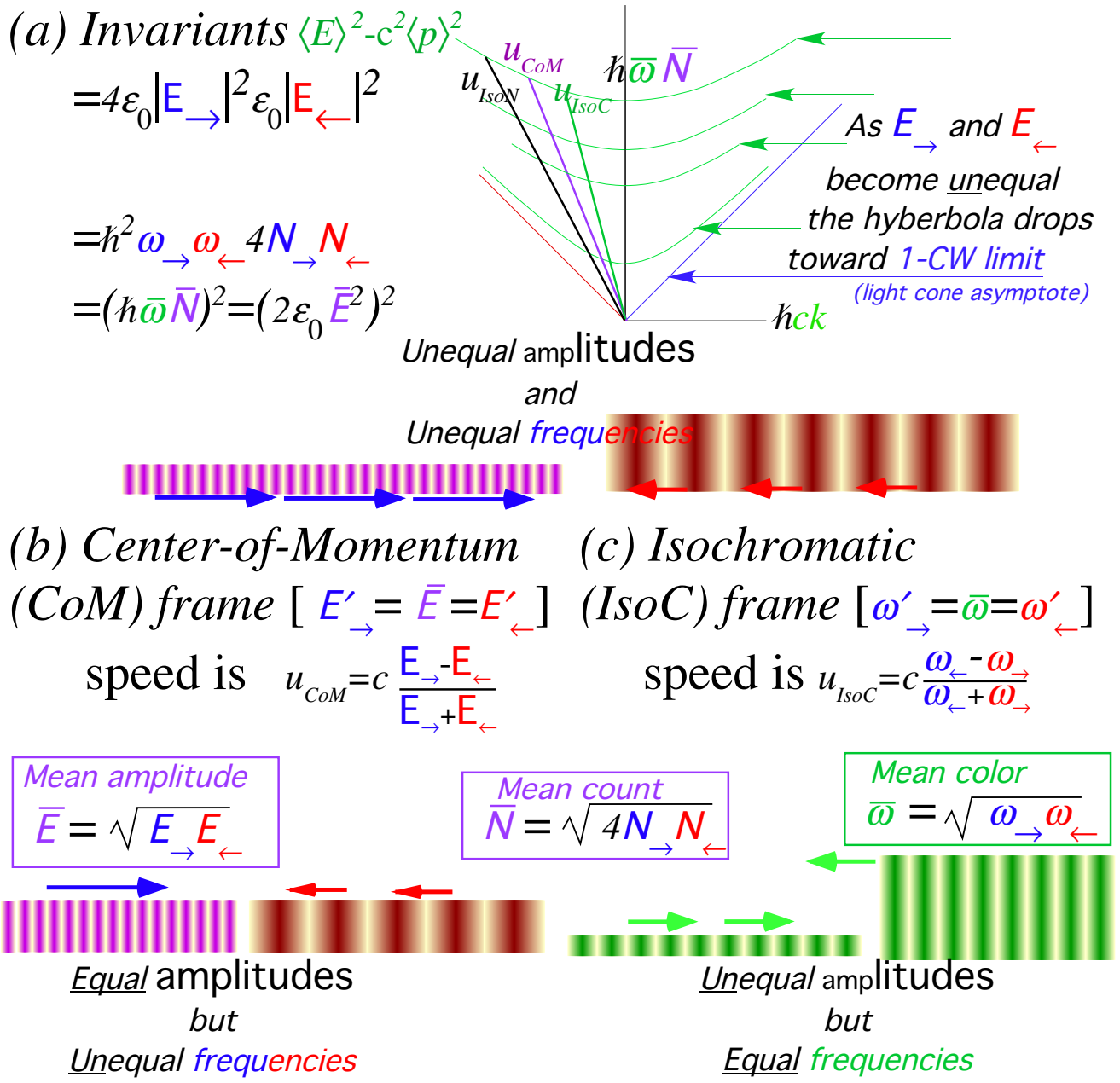

Fig. 21. Cavity 2-CW modes. (a) Invariant "mass" hyperbolas. (b) COM frame. (c) ISOC frame.

It is argued in Sec. 3 that mass is a coherent 2-CW interference effect that is not possible for a 1-CW beam. If we replace Planck energy relation $\varepsilon = Nh\upsilon$ by a Maslov form $\varepsilon = (N + \bar{\alpha})h\upsilon$ it has a tiny zero-point energy minimum $\bar{\alpha}h\upsilon$. Does a tiny mass $\bar{\alpha}h\upsilon / c^2$ exist for 1-CW and even 0-CW beams in all frames in spite of the incoherence of such zero-point fluctuations? Such a presence in (6.20) may be ruled out if the speed-of-light axiom (1.1) is exact. There is much yet to learn about zero-point effects in quantum electrodynamics and cosmology.

Photon-N vs Coherent-α-states

Optical fields **A** or **E** have quantum expectation values of field operators based on mode amplitudes $\mathbf{a}_k$ or $\mathbf{a}_k^*$ in classical energy $\sum \omega_k^2 \mathbf{a}_k^* \mathbf{a}_k$. Each $\mathbf{a}_k$ or $\mathbf{a}_k^*$ is replaced by oscillator boson operator $\mathbf{a}_k$ or $\mathbf{a}_k^\dagger$ in a quantum field Hamiltonian $\mathbf{H} = \Sigma \hbar\omega_k (\mathbf{a}_k^\dagger \mathbf{a}_k + \bar{\alpha})$ whose eigenstates $|N_1 N_2 \cdots N_k\rangle$ have exact quantized photon numbers $\langle \mathbf{a}_k^\dagger \mathbf{a}_k \rangle = N_k$ for each mode-k_m.

Each mode phase quanta m and amplitude quanta N_m are invariant constants that define another hyperbola with Einstein-Planck proper frequency $\varpi_{N,m} = \hbar N_m \omega_m$ as sketched in Fig. 21a and Fig. 22. The problem is that absolute certainty of photon number N_m implies totally *un*certain field phase just as absolutely certain k_m of 1-CW symmetry implies totally *un*certain position in space and time.

Space-time position coordinates were defined by taking 1-CW combinations to make 2-CW coordinates of Fig. 3b, Fig. 6c, or Fig. 7c. Ultimately an n-CW pulse-wave (PW) of Fig. 2, Fig. 3a, Fig. 6d, or Fig. 7d was localized with as low a space-time uncertainty $\Delta\tau$ as desired but it acquires per-space uncertainty or bandwidth $\Delta\upsilon$ according to Fourier-Heisenberg relation $\Delta\upsilon \cdot \Delta\tau > 1$.

So also must photon-number states be combined if amplitude and phase uncertainty are to be reduced to the point where wave space-time coordinates can emerge. Such combinations are known as coherent states or α-states of harmonic oscillation. Sharper wave zeros require fuzzier hyperbolas.

Fuzzy hyperbolas vs. fuzzy coordinates

Model micro-laser states are *coherent* states $|\alpha\rangle = \Sigma_N \psi_N |N\rangle$ made of single-mode eigenstates $|N\rangle = (\mathbf{a}_1^\dagger)^N |0\rangle$ with amplitudes $\psi_N = \alpha^N e^{-\alpha^2/2} / \sqrt{N!}$. Variable $\alpha = x + ip = |\alpha| e^{i\Phi}$ is average mode phase, and $(x = \mathrm{Re}\,\alpha, p = \mathrm{Im}\,\alpha)$, rescaled by a quantum field factor f, are field averages $(\langle A \rangle, \langle \dot{A} \rangle = -\langle E \rangle)$.

$$\langle \alpha | A | \alpha \rangle = \langle A \rangle = (\alpha + \alpha^*) f = (\alpha + \alpha^*) \sqrt{\frac{\hbar}{2\varepsilon_0 \omega V}} \qquad (6.22)$$

Amplitude factor f makes Planck's $\bar{E} = \hbar\omega\bar{N}$ equal Maxwell field energy $\bar{E} = \bar{U} \cdot V$.

$$\langle U \rangle V = 2\varepsilon_0 \omega^2 V \langle A^2 \rangle = \hbar\omega |\alpha|^2 = \hbar\omega\bar{N} \qquad (6.23)$$

A fundamental laser mode in a *0.25μm* cubic cavity (See E-wave sketched in one strip of Fig. 6c.) has green light with $\hbar\varpi = 4 \cdot 10^{-19} Joule$ or *2.5eV* per photon. The average photon number $\bar{N} = |\alpha|^2 = 10^{10}$ models a laser with mean energy $\bar{E} = \bar{U} \cdot V = \hbar\varpi\bar{N} = 4.0\, nanoJ$ in a volume $V = (\frac{1}{4}\mu m)^3$. Photon number uncertainty $\Delta N = |\alpha| = 10^5$ varies inversely to phase uncertainty $\Delta\Phi = \pi / \alpha \sim 3 \cdot 10^{-5}$.

Amplitude expectation value $\langle N | A | N \rangle$ is zero for $|N\rangle$ states due to *in*coherence of phase, but number value $\langle N | \mathbf{a}_k^\dagger \mathbf{a}_k | N \rangle = N$ is exact as is proper frequency ϖN due to the phase factor $(e^{-i\varpi t})^N$ of $(\mathbf{a}_1^\dagger)^N$. A volume V with $(N = 10^{10})$-photons has energy $E = \hbar\omega N$ or mass-equivalent $M = E / c^2 = 10^{-25} kg$ on a hyperbola 10^{10} quanta above the *N=1* hyperbola. A coherent-state $|\alpha = 10^5\rangle$ has a mass of about $M = 10^{-25} kg$ with uncertainty $\Delta M = 10^{-30} kg$ so its *phase* uncertainty $3 \cdot 10^{-5}$ is low enough to plot grids like Fig. 6c or Fig. 23a. A low-α state (Fig. 23c) has too few photon counts-per-grid to plot sharply. Photon eigenstate $|N\rangle$ is a wash even for high-N since $\Delta N = 0$ has total *(2π)* phase uncertainty. (Fig. 23d)

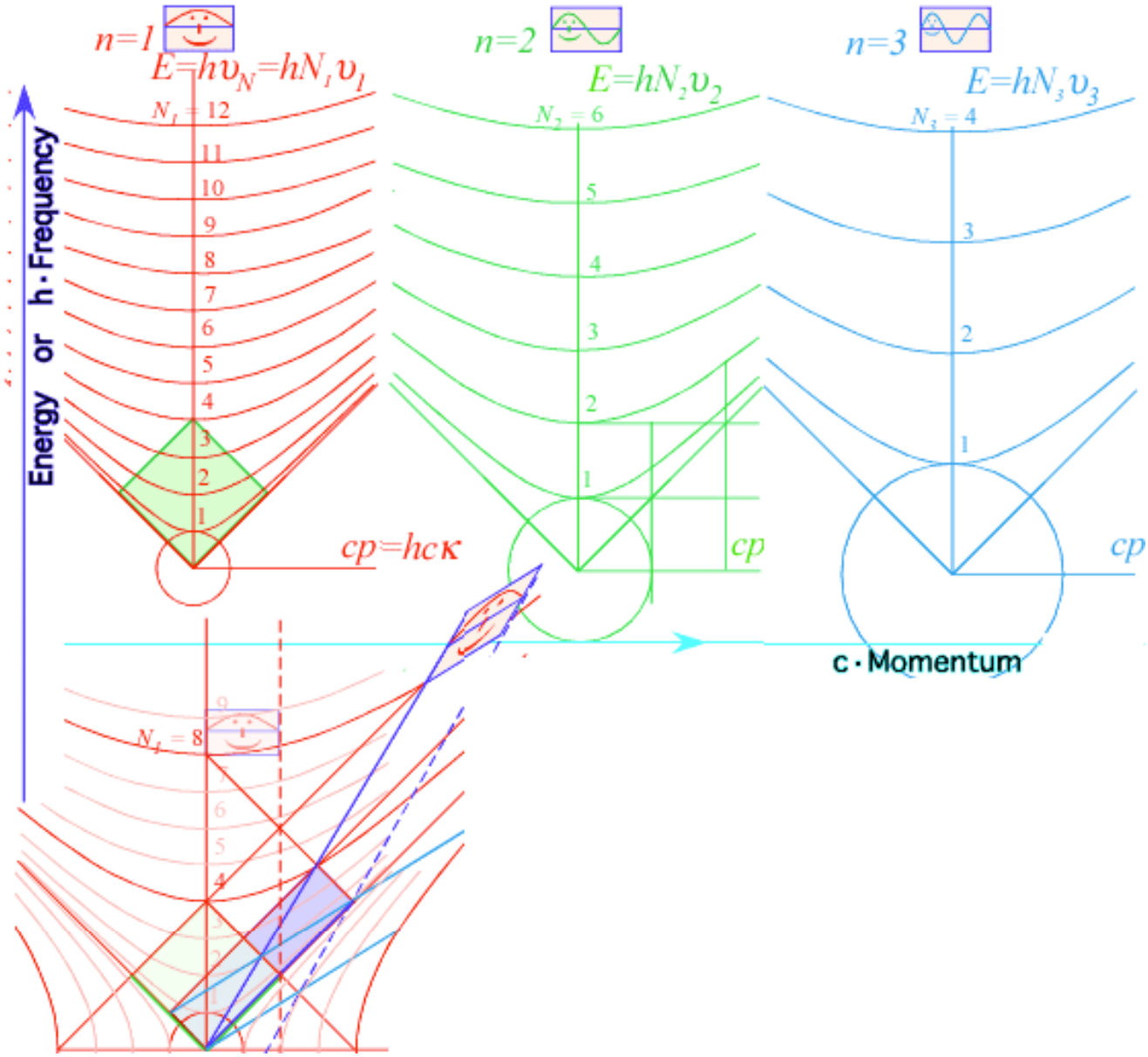

Fig. 22 Optical cavity energy hyperbolas for mode number n=1-3 and photon number N=0, 1, 2,....

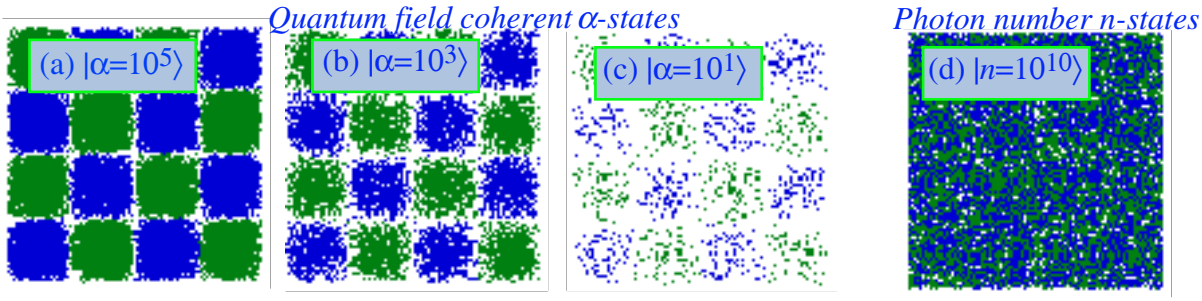

Fig. 23 Simulated spacetime photon counts for coherent (a-c) and photon-number states (d).

Deeper symmetry axioms

Discussion of relativity and quantum theory of wave amplitude requires further details. This includes Dirac's extraordinary theory that 2-CW light of certain frequencies in a vacuum may create "real" matter that does not vanish when the light is turned off. For example, we know that two *0.51MeV* γ-ray photons of frequency $\omega_e=m_ec^2/\hbar$ may create an electron and positron "hole" that form positronium $e+\bar{e}$ pairs. Also, *0.94GeV* γ-rays with $\omega_p=m_pc^2/\hbar$ may create proton-anti-proton $p+\bar{p}$ pairs, and so on.

Dirac creation processes raise questions, "What "cavity" traps *0.51MeV* γ-pairs into stable $e+\bar{e}$ pairs?" The discussion so far has only begun to define 2-CW symmetry properties by phase rates in per-spacetime *(K,Ω)*-quantum variables. Conservation (5.2) of these kinetic *(K,Ω)*-values means that the $e+\bar{e}$ or $p+\bar{p}$ pairs have the same *(K,Ω)*-values as the 2-CW light that "creates" them, yet some other less familiar internal lepton or baryon quantum variables may change as light becomes "trapped." This is beyond the scope of this discussion, and indeed, still largely beyond what is presently known.

7. Photo-emission

In the meantime it is fair to consider an electron, proton, or atom of mass *M* as having the same kinetic symmetry as a 2-CW light beam of frequency $\omega=Mc^2/\hbar$. This provides a simplified geometrical construction for recoil shifts in atomic or nuclear 1-photon-emission, 1-photon-absorption, or 2-photon Raman-Compton scattering processes by relating them to Doppler shifts on a *(k,ω)*-baseball diamond of a virtual 2-CW photon symmetry hidden in any atom or particle.

Feynman recalls trying to answer his father's question, "Where is a photon before an atom emits it?" A pricey MIT education seemed not up to this question.[27] Let us try to answer Feynman's father's query in a quantitative way using a 2-CW photon model of an atom that emits some of its "inner light" allowing a simpler Compton kinetics that uses the diamond geometry of Fig. 24.

Using the baseball diamonds of Fig. 6 or 7, we say atoms have the *symmetry* of 2-photon states represented by 2nd base $\mathbf{K}_2$. In the lower half of Fig. 24a, a 1st base $\mathbf{K}_1=(\varpi,\varpi)$ and 3rd base $\mathbf{K}_3=(-\varpi,\varpi)$ sum to an atom's 2nd base $\mathbf{K}_2=(0,2\varpi)$ on a hyperbola of mass M_Q at Q.

$$M_Q=2\hbar\varpi/c^2 \qquad (7.1)$$

The pitcher's mound P represents a 1-photon momentum-energy expectation value E_P at $\mathbf{K}_p=(1/2)\mathbf{K}_2$

$$E_P=\hbar\varpi/c^2 \qquad (7.2)$$

It is like Fig. 10 or Fig. 12, but Q is a 2-photon state of energy $M_Q=2E_P$.

In Fig. 24a an emitted photon $\omega_{QP'}$ is imagined being "cut" from 3rd base so $\omega_3=\varpi$ shrinks by what we will call[28] a *father-Feynman factor ff* as 3rd base alone loses the outgoing $\omega_{QP'}$ photon energy.

$$\omega_3'=ff\,\varpi=\omega_3-\omega_{QP'} \qquad (7.3)$$

If 1st base stays at its old value $(\omega_1'=\varpi=\omega_1)$ the 2nd base moves from Q on its initial 2ϖ-hyperbola to P′ on its final $2\varpi'$-hyperbola. Its new proper frequency ϖ' is a geometric mean of 3rd and 1st as in Fig. 10.

$2\varpi' = 2\sqrt{\omega_3'\omega_1'} = 2\sqrt{ff}\,\varpi$ (7.4a) $\omega_3' = f\varpi' = ff\varpi$ (7.4b) $\omega_1' = f^{-1}\varpi' = f^{-1}f\varpi = \omega_1$ (7.4c)

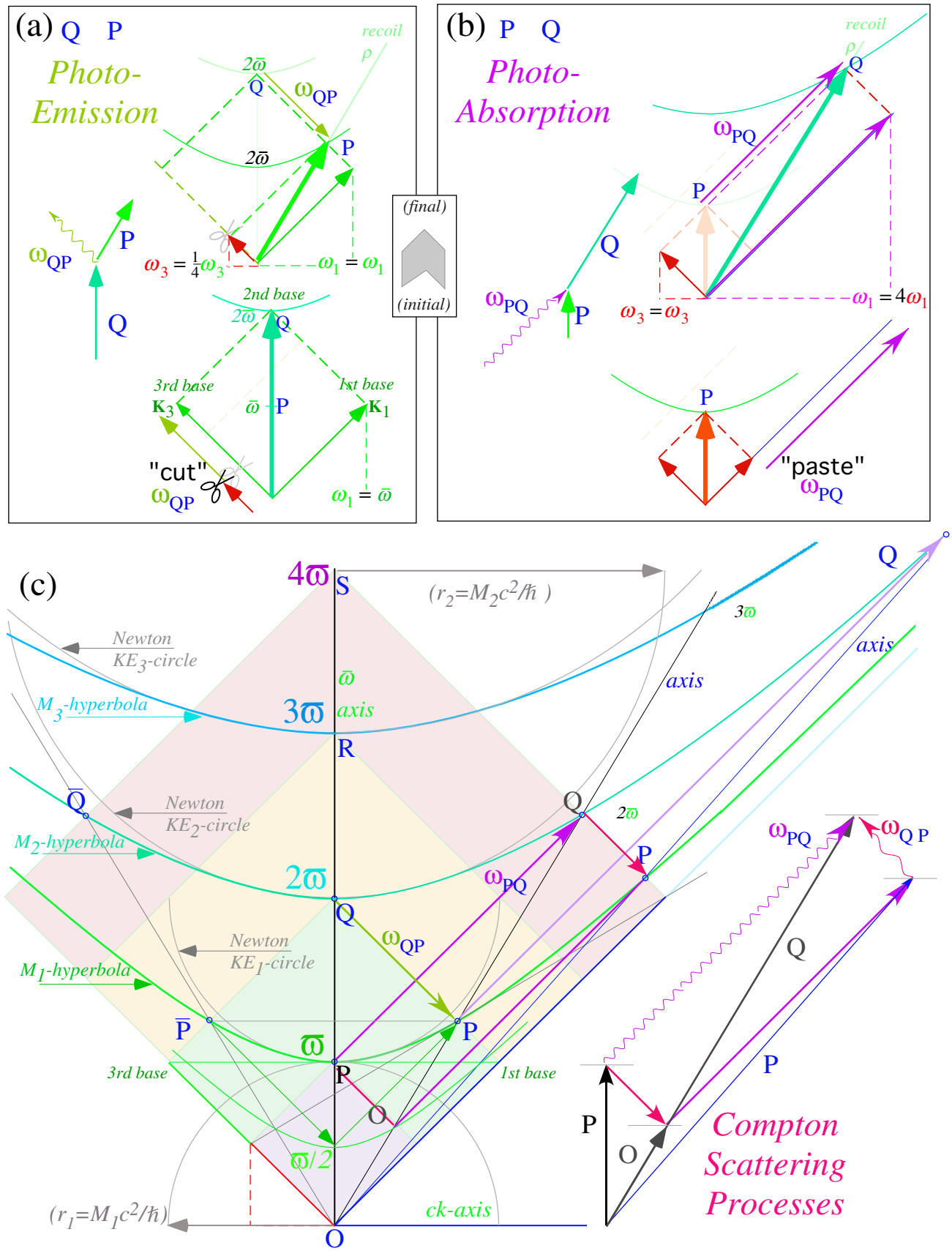

Fig. 24 Optical cavity model of (a) Emission, (b) Absorption, and (c) Compton scattering

The new 3rd base is a *Feynman*[29]*redshift* $f \equiv \sqrt{ff}$ of the new mean ϖ' and a father-Feynamn shift ff of the old bases values $\omega_3 = \varpi = \omega_1' = \omega_1$ that, in turn, are each an inverse-shift f^{-1} of the new mean ϖ'.

The ff-shift is a product of two f-shifts $ff=f^2$. This is more than just tricky notation. It is due to the group multiplication rule (2.16) of $f = b_{3'2'}$ and an equal $f = b_{2'1}$ to give composite $ff = b_{3'1} = b_{3'2'}b_{2'1} = f^2$.

In Fig. 24a old 1st base and new 3rd base span a diamond of rapidity ρ like the one in Fig. 10b where $e^{-\rho} = \frac{1}{2}$. That redshift $\varpi'/\varpi = f$ is the final-to-initial rest mass ratio $(f = \frac{1}{2})$ used in Fig. 24a-c.

$$e^{-\rho} = f \equiv \sqrt{ff} = \varpi'/\varpi = M_P / M_Q \qquad (7.5a)$$

We may relate (7.5a) to a "rocket science" relation $V_f = V_e \, ln \, (M_F/M_E)$ for final-velocity V_f *vs.* specific-impulse V_e (velocity of exhaust). This matches (7.5a) for non-relativistic speeds where $\rho \sim u/c$.

$$\rho = \ln(M_Q / M_P) \xrightarrow[u \ll c]{} u = c \ln(M_Q / M_P) \qquad (7.5b)$$

The excited rest mass M_Q is like a fully fueled rocket mass M_F, and the lower rest mass M_P is like an empty rocket mass M_E, and the velocity of exhaust V_e is the speed c of the ejected photon. It might surprise a rocket scientist that (7.5) results from two CW c-axioms (1.1-2) and that it also works for relativistic sub-atomic rockets! When they are assembled, this span of ideas from Euclid to Einstein to Evenson represent an elegant and powerful train of experiment and logic.

Photo-absorption and Compton effects

The factor $ff = \frac{1}{4}$, chosen in Fig. 24a, cuts a fraction $1 - ff = \frac{3}{4}$ off the 3rd base photon $\omega_3 = \varpi$ to emit $\omega_{QP'} = \frac{3}{4}\varpi$ and reduces mass M_2 by factor $f = \sqrt{ff} = \frac{1}{2}$ to M_1. Doppler factor $f^{-1}=2=e^{\rho}$ gives an atomic recoil boost of $u = \frac{3}{5}c$. (Recall a double Doppler gives frame velocity $u = \frac{3}{5}c$ in Fig. 7.)

Mass M_1 gets the same boost by absorbing $\omega_{PQ'} = \frac{3}{2}\varpi$ as it jumps from P up to Q′ in Fig. 24b, an inverse to the $\omega_{QP'}$ "cut" that falls from Q down to P′ in Fig. 24a. A "paste" of $\omega_{PQ'} = \frac{3}{2}\varpi$ onto the 1st baseline in Fig. 24b ups M_1 to M_2 on ω'-axis P′Q′ in Fig. 24c. Final ω'-frame shift is $b=e^{\rho}=2$ of rapidity $\rho = \ln 2$ for either process. Emission $\omega_{Q'P''}$ is the final "cut" in a Compton "paste-and-cut" $P \to Q' \to P''$ process with the Feynman diagram in Fig. 25c. Its segments form an OPQ′P″O "kite" in Fig. 24c that is bent from a symmetric kite $O\bar{P}'QP'O$ by the boost $\rho = \ln 2$ of the main kite OQ-axis relative to either of its wings $O\bar{P}'$ or OP′. Any mass jump $M_P \leftrightarrow M_Q$ causes a boost $\rho = \pm \ln \frac{M_Q}{M_P}$ as per (7.5).

Both "paste-and-cut" $(P \to Q' \to P'')$ and reverse "cut-and-paste" $(P \to O' \to P'')$ processes in Fig. 25 entail total recoil boost $2\rho = \ln 2^2$ from the lab ϖ axis to an ω'' axis of the Compton scattered atom in Fig. 24c. The latter first "cuts" down to point O′ on a $\frac{\varpi}{2}$-hyperbola by emitting photon $\omega_{PO'} = \frac{3}{8}\varpi$ before absorbing the $\omega_{O'P''} = \frac{3}{2}\varpi = \omega_{PQ'}$ photon that comes first in the former sequence.

An inverse Compton process $(Q \to P' \to Q'')$ emits photon $\omega_{QP'} = \frac{3}{4}\varpi$ (as in Fig.18a) then absorbs photon $\omega_{P'Q''} = 3\varpi$ that moves it from rapidity ρ on hyperbola-ϖ to rapidity 2ρ on hyperbola 2ϖ at point Q″ (upper right of Fig. 24c). Here a fixed mass $M_2 = 2\hbar\varpi$ emits $\frac{3}{4}\varpi$ to gain speed $(\frac{u}{c} = \frac{3}{5})$ by reducing its mass to $M_1 = \hbar\varpi$ then recovers it all by absorbing 3ϖ to go even faster $(\frac{u}{c} = \frac{15}{17})$.

Photon **K**-vectors for any Compton process between *2:1*-rest mass hyperbolas make a ρ-warped baseball diamond with $\rho=ln2$ according to (7.5) as shown in Fig. 24c and Fig. 25a. Like a *2:1*-Doppler diamond in Fig. 10b, it has an aspect ratio that is twice its blue-shift $b=e^{\rho}=2$, that is $2e^{\rho}=4$. Unlike the basic diamond in Fig. 10b, the one in Fig. 25a is suspended on **K**-vectors of initial, intermediate, and final atomic states that form the Feynman graphs in Fig. 25b-c. By drawing the vectors and graphs in the center of momentum (COM) frame Fig. 25d-f, an original diamond like Fig. 6a-b is made.

A *2:1*-rest mass drop shows geometry more clearly than a realistic ratio $10^{10}:10^{10}-1$ for an atomic transition that is about 10^{-10} of rest mass. Atomic rest-energy level ratios $E_m: E_h$ are close to unity and fortunately so for our health! Harmonic levels with integral $m:h$ ratios used in Fig. 24 apply to optical-cavity models but m and h are small integers only for special spectra like Rydberg or rotor transitions.

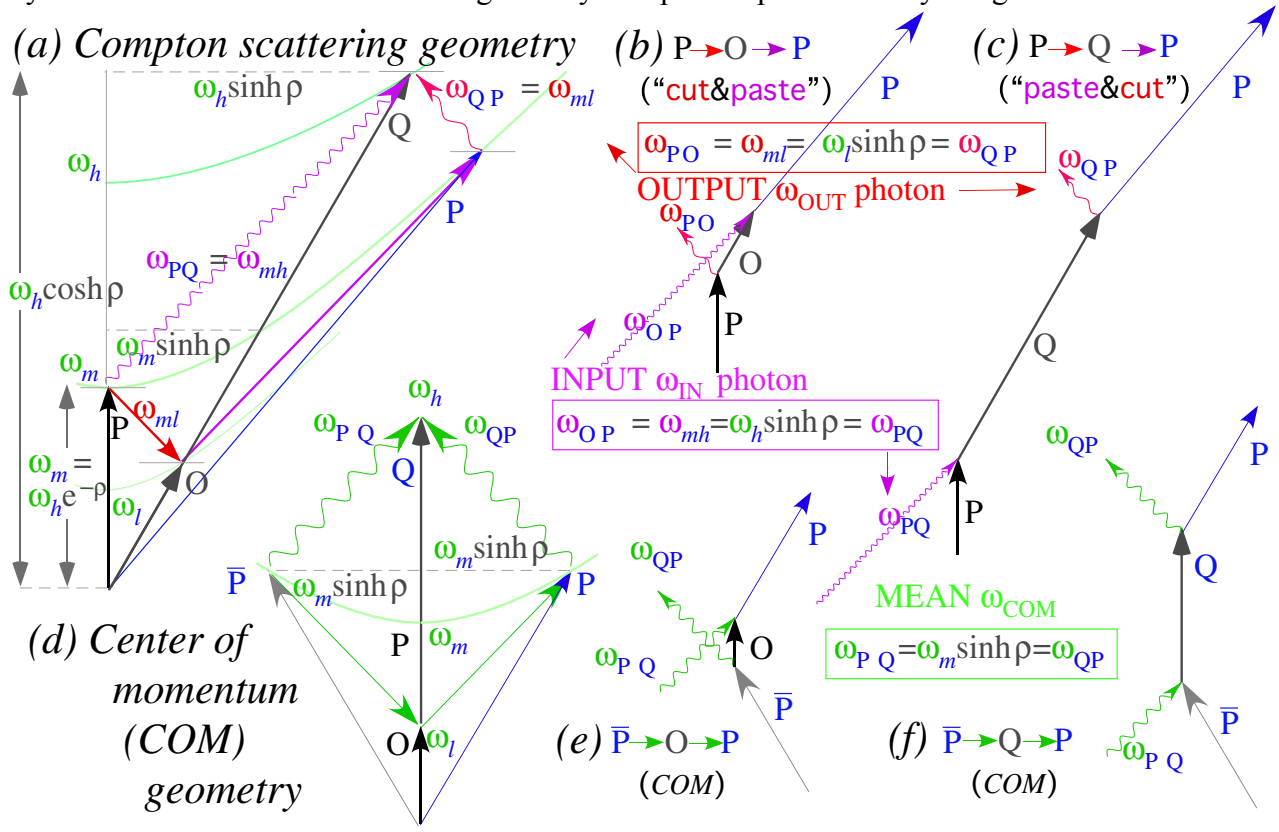

Fig. 25 Compton scattering. (a) Vector sums on mass hyperbolas of low ω_ℓ, medium ω_m, and high ω_h. (b-c) Feynman graphs. (d) Center of Momentum (COM) vector sums. (e-f) COM Feynman graphs.

Compton-Doppler staircase

In going from higher hyperbola $h\varpi$ to middle $m\varpi$ the lab recoil shift is $f_{hm}=e^{-\rho_{hm}}=\frac{m}{h}$ by (7.5), and its emitted frequency ω_{hm} is the altitude of a kite triangle, like $\bar{P}'QP'$ in Fig. 24c, given as follows.

$$\omega_{hm}=(1-f_{hm}{}^2)\frac{h\varpi}{2}=\frac{h^2-m^2}{2h}\varpi=m\varpi\sinh\rho_{hm} \qquad (7.6)$$

The example in Fig. 24a has $\omega_{QP'}=\frac{3}{4}\varpi=\omega_{2,1}$. Doppler shifts of $\omega_{2,1}$ by $f_{2,1}=\frac{1}{2}$ form a geometric series $(\cdots,\frac{3}{32},\frac{3}{16},\frac{3}{8},\frac{3}{4},\frac{3}{2},3,6,12,\cdots)\varpi$ of steps on a Compton staircase $PQ'P''Q''\ldots$ between *(2:1)*-levels 2ϖ and 1ϖ

in Fig. 24c. For any rational level ratio $e^{\rho_{hm}} = \frac{h}{m}$, each dilation factor γ_{hm}, recoil β_{hm}, or ratio ω_{hm} / ϖ is a rational ratio, too, and the Pythagorean sum $1 = \gamma_{hm}^{-2} + \beta_{hm}^2$ belongs to a rational triangle, *e.g.*, $1 = \frac{3^2}{5^2} + \frac{4^2}{5^2}$.

$$\beta_{hm} = \frac{u_{hm}}{c} = \tanh \rho_{hm} = \frac{h^2 - m^2}{h^2 + m^2} \qquad (7.7a)$$

$$\gamma_{hm} = \cosh \rho_{hm} = \frac{h^2 + m^2}{2mh} \qquad (7.7b) \qquad \sinh \rho_{hm} = \frac{h^2 - m^2}{2mh} \qquad (7.7c)$$

Recoil trims emitted ω_{hm} below $\Delta = |h-m| \varpi$ by a factor $(h+m)/2h$ while absorption ω_{mh} costs more than Δ by a factor $(h+m)/2m$. Newtonian recoil $KE_h \cong M_h u^2 / 2$ is a circle of radius $M_h c^2$ in Fig. 24, so even low-u recoil costs a little. Photons, like money-changing tourists, get nicked coming and going.

An absorption ($m<h$) frequency $\omega_{mh} = \omega^{IN}$ is greater than emission ω_{hm} by a factor $f_{mh} = \frac{h}{m}$. A Compton ω^{OUT} due to ω^{IN} is less than ω_{hm} by the inverse factor $f_{mh}^{-1} = f_{hm} = \frac{m}{h}$. Hence a Compton output ω^{OUT} is less than its input ω^{IN} by the Doppler ratio-square $ff = f_{hm}^2 = (\frac{m}{h})^2$ as shown before.

$$\omega^{IN} = \omega_{mh} = \tfrac{h}{m} \omega_{hm} \ , \qquad \omega^{OUT} = \tfrac{m}{h} \omega_{hm} = (\tfrac{m}{h})^2 \omega^{IN} \qquad (7.8)$$

Compton processes in Fig. 25 start on middle $\omega_m = m\varpi$ hyperbola to do a 2-photon bounce off a lower $\omega_\ell = \ell\varpi$ or a higher $\omega_h = h\varpi$ hyperbola. An intermediate "bouncer" is said to be a *virtual* level if its ω_ℓ or ω_h values are integration variables being summed. A process $(m \to h \to m)$ or $(m \to \ell \to m)$ is said to be a *resonant* Compton process if an h-state or ℓ-state exists. Whether numbers m, h, and ℓ are integers in a cavity model or real values for an atomic model, the results (7.6), (7.7), and (7.8) apply in any case.

Inverse frequencies $\omega^{-1} = (kc)^{-1} = \lambda (2\pi c)^{-1} \equiv \lambda\!\!\!^{-} / c$ give the famous Compton wavelength sum rule.

$(\omega^{OUT})^{-1} = (\omega^{IN})^{-1} + 2(m\varpi)^{-1}$, or: $\lambda\!\!\!^{-OUT} = \lambda\!\!\!^{-IN} + 2\lambda\!\!\!^{-}_C$ where: $\lambda\!\!\!^{-}_C = \frac{\hbar c}{m\varpi} = \frac{\hbar}{M_m c}$.

Compton radius $\lambda\!\!\!^{-}_C \equiv \lambda_C / 2\pi$ is a minimum cavity radius with a frequency equal to the "*zwitterbevegun*" of mass M_m. As input $\lambda\!\!\!^{-IN}$ reflects from an M_m-cavity it picks up diameter $2\lambda\!\!\!^{-}_C$ to become $\lambda\!\!\!^{-OUT}$. Size $\lambda\!\!\!^{-OUT}$ depends on mass M_m of level-m, *not* on M_h or M_ℓ of higher level-h or lower level-ℓ that bounces level-m. Compton radius is a curious measure of mass size. Larger mass M_m has a *smaller* $\lambda\!\!\!^{-}_C$ size that recoils less and reflects photons elastically as one expects in classical wave optics where light is "light."

A geometric ϖf^p-series $\varpi(\ldots f^{-2}, f^{-1}, 1, f^1, f^2 \ldots)$ of *levels* also has a geometric series $f^p \left| f^2 - 1 \right| \frac{\varpi}{2}$ of *transitions*. This gives Compton "nets" such as the $(f = 2)$-net in Fig. 26a or a finer $(f = \sqrt{2})$-net in Fig. 26b. Finer fractions ($f \to 1$) give smaller jumps and acceleration that is more continuous and constant.

An acceleration of space-time frames by geometric or exponential frequency chirping is described below. The space-time grids have a geometric spacing that is like the Compton nets in Fig. 26 below. The space-time grids are at right angles to the per-space-time nets to which they are equivalent. They provide an optical realization of Einstein's famous constant-g elevators.

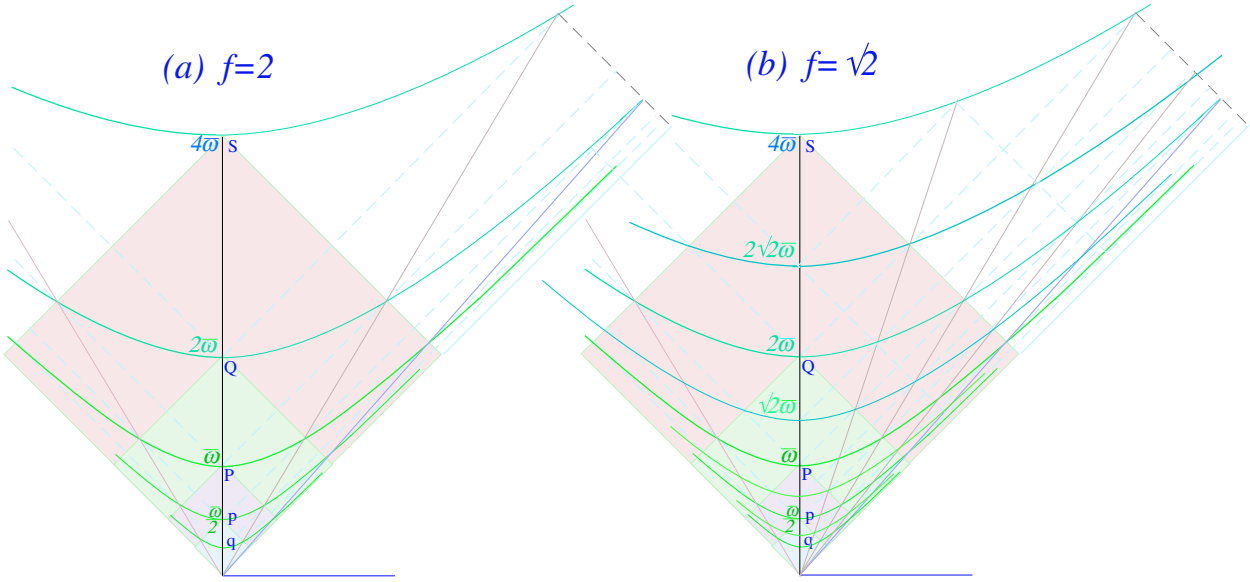

Fig. 26 Compton nets are congruent Compton staircases of transitions. (a) f=2:1 (b) f= √2 :1

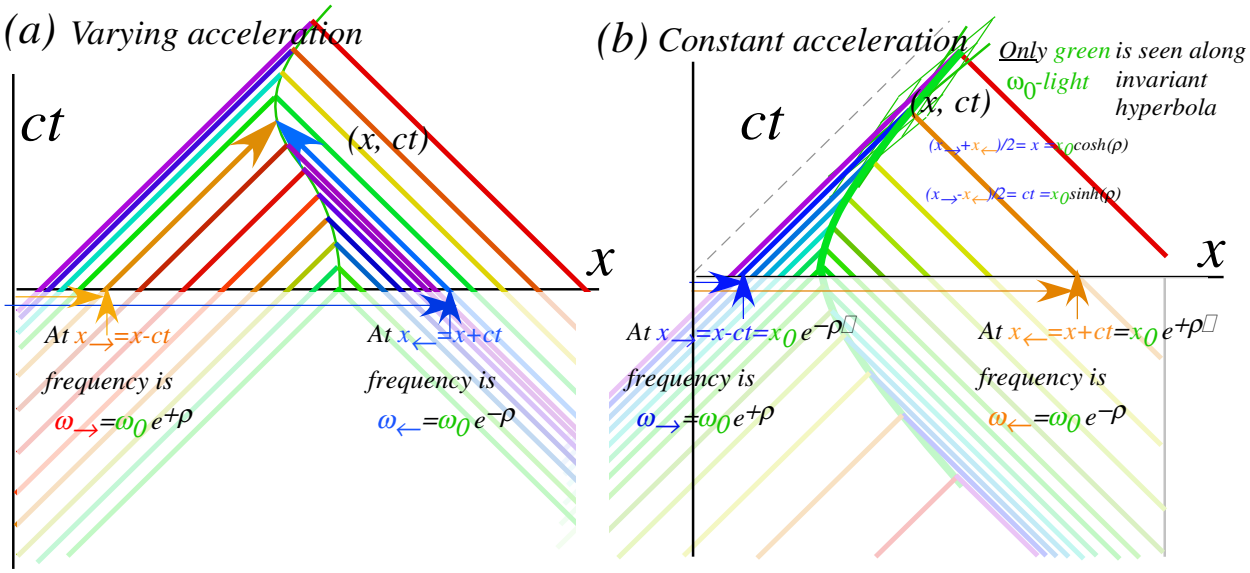

Fig. 27 Optical wave frames by red-and-blue-chirped lasers (a)Varying acceleration (b)Constant g

Chirping and Einstein elevators

A spacetime version of Compton nets are curved coordinates for accelerated Einstein elevators and this helps to visualize equivalence principles for general relativity.[30] Plots in Fig. 27 and Fig. 28 show waves from chirping tunable lasers forming colorful renderings of hyper-net coordinates.

A previous Fig. 7c plotted an atom (x',ct')-view of it running head-on at rapidity ρ into a green ϖ -beam that is blue ($\varpi\, e^{+\rho}$) shifted while the receding laser appears red ($\varpi\, e^{-\rho}$) shifted. The laser (x, ct)-grid then appears as a ρ-tipped Minkowski grid. If instead the lasers had been tuned to frequencies $\varpi\, e^{-\rho}$ and $\varpi\, e^{+\rho}$, respectively, the $(u=c\tanh\rho)$-moving atom could see both beams to be green ϖ –light waves interfering to make a *square* $(\rho=0)$ *Cartesian* (x, ct)-grid like Fig. 6c. (Amplitude would have to be tuned along with frequency to squelch the wave galloping described after Fig. 19 and Fig. 20.)

Varying tuning parameter ρ of the lasers changes local grid rapidity ρ at the beams' spacetime intersection as sketched in Fig. 27a-b. This produces a curved space-time coordinate system of paths with rapidity changing just so *both* beams end up always the *same* color on any given trajectory.

Each trajectory plotted in Fig. 28 has its own constant proper acceleration g and local color ϖ . A mass M following such a $x(t)$-path has a **K** that follows its M-hyperbola in Fig. 26. The lasers each send waves that meet at each trajectory point $x(t)$ and paint a local interference grid of varying rapidity ρ on a trajectory $x(t)$ of varying velocity $u(t)$ given by (6a) and sketched in Fig. 27a.

$$u = \frac{dx}{dt} = c\tanh\rho \qquad (7.9)$$

Setting $x'=0$ and $t'=\tau$ in (2.21) relates proper time interval $d\tau$ to lab dt . This gives $x(t)$ by τ-integrals.

$$\frac{dt}{d\tau} = \cosh\rho \qquad (7.10a) \qquad \frac{dx}{d\tau} = \frac{dx}{dt}\frac{dt}{d\tau} = c\,\tanh\rho\cosh\rho = c\sinh\rho \qquad (7.10b)$$

$$ct = c\int\cosh\rho\ d\tau \qquad (7.10c) \qquad x = c\int\sinh\rho\ d\tau \qquad (7.10d)$$

Path $x(t)$ depends on $\rho(\tau)$ variation in proper τ. Linear rate $u\sim g\tau$ or $\rho=g\tau/c$ gives a hyperbolic path in Fig. 27b of fixed proper acceleration g and a family of concentric paths of different g in Fig. 28.

$$ct = c\int\cosh\left(\frac{g\tau}{c}\right)d\tau = \frac{c^2}{g}\sinh\left(\frac{g\tau}{c}\right) \quad (41a) \qquad x = c\int\sinh\left(\frac{g\tau}{c}\right)d\tau = \frac{c^2}{g}\cosh\left(\frac{g\tau}{c}\right) \qquad (7.11b)$$

Paths closer to the left hand blue-chirping laser have a higher g than flatter ones nearer the red-chirping right hand source. ρ-skewed baseball diamonds of PW and CW paths in lower Fig. 28 are spaced geometrically along the x-axis of a spaceship at a moment when its lab-relative rapidity is $\rho=0.2$.

Geometric $e^{\pm\rho}$-variation (7.11) of wave and coordinate spacing is due to a left-hand laser's right-moving wave of frequency $\omega_{\rightarrow}=\omega_0 e^{+\rho}$ on light cone $x_{\rightarrow}=x-ct=x_0 e^{-\rho}$ and a right-hand laser's left-moving wave of frequency $\omega_{\leftarrow}=\omega_0 e^{-\rho}$ on light cone $x_{\leftarrow}=x+ct=x_0 e^{+\rho}$. Wave interference does the rest.

Initial $(\rho=0)$ position of hyperbola ω_0 is $\ell_0=x_0=c^2/g_0$. Each hyperbola has different but fixed location ℓ, color ω, and artificial gravity g that, by (7.11), are proper invariants of each path.

$$x^2-(ct)^2 = \ell^2\ , \quad \text{where: } \ell=c^2/g \qquad (7.12)$$

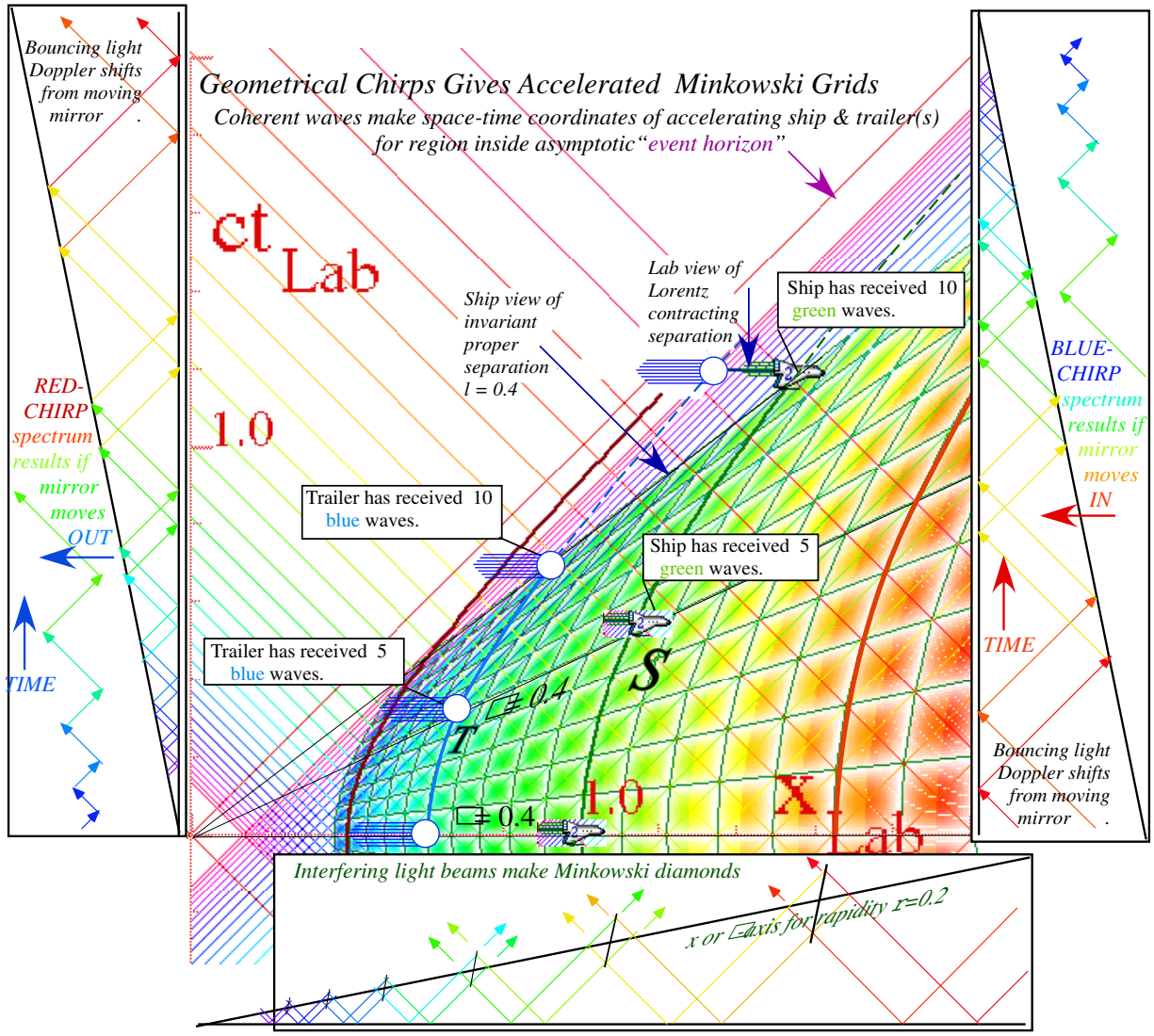

Fig. 28 Accelerated reference frames and their trajectories painted by chirped coherent light

Frequency ω and acceleration g vary inversely with the path's proper location ℓ relative to origin.

$$\omega\,\ell = \omega\, c^2/g = \omega_0\, c^2/g_0 = const. \qquad (7.13)$$

Rapidity $\rho = g\tau/c$ in (7.11) has proper time be a product of hyperbolic radius ℓ in (7.12) and "angle" ρ.

$$c\tau = \rho\, c^2/g = \ell\,\rho \qquad (7.14)$$

This is analogous to a familiar circular arc length formula $s = r\,\phi$. Both have a singular center.

The less familiar hyperbolic center $(x,ct)=(0,0)$ here begins an elementary *event horizon*. The blue-chirp laser would need infinite frequency $\omega_0 e^{+\rho}$ at origin where $ct=e^{-\rho}$ goes to zero, so it gives up *before* $t=0$. After $t=0$, light from the laser to any path S or T given by (7.11) never arrives. Fig. 28 shows paths of a spaceship S and a "trailer" T trailing by invariant length $\ell_{ST}=\ell(S)-\ell(T)$ on an x-axis of rapidity ρ through origin $(x,ct)=(0,0)$. S and T always have the *same velocity* (7.9) relative to the lab, maintain proper interval ℓ_{ST}, but trailer T *feels greater* g. Lower parts of a rigid rod accelerate more, and this gives the lab-observed Lorentz length-contraction indicated at the top of Fig. 28.

In a Newtonian paradigm, asymmetric acceleration seems paradoxical, but if waves make a coordinate frame, asymmetry is a consequence of the DeBroglie relation (3.5b) between *k*-vector and momentum. Accelerating frames require shortening wavelength and this crowds waves.

Wave properties also manifest the accelerated frames' upstairs-downstairs disparity in proper time τ ("later" upstairs by (7.14)) and shift in frequency ω (lower or "red shifted" upstairs by (7.13)). Along nodal (white) lines that are the ship-trailer *x*-axis for a momentary rapidity ρ, wave phase is seen to be some constant $k\ell-\omega\tau=N\pi/2$. The Einstein equivalence of gravity to an accelerated elevator is manifested by a gravitational red shift and an increase of clock rates in the upstairs regions of a field.

A quantized version of Fig. 28 would be an atom with a transition at ω_I, undergoing a sequential *resonant* Compton scattering of exponentially chirped photons ω_I, $e^{\pm\rho}\omega_I$, $e^{\pm2\rho}\omega_I$, $e^{\pm3\rho}\omega_I$,… between the *same* pair of hyperbolas in Fig. 28. The atom sees the *same* color and feels the *same* recoil rapidity at each step in the quantum version of constant acceleration.

Constant velocity gives constant acceleration

This leads one to ask if chirped light might be used for atomic or molecular acceleration. Logarithmic dependence $\rho=\ln b$ of rapidity on Doppler *b* favors ultra-precise *low* energy acceleration, more appropriate for nanotechnology than high energy acceleration with its extreme bandwidth.

The flip symmetry between two sides of a lightcone suggests optical cavities with a geometric chirp. If you flip the diamond sequence in lower Fig. 28 across the light cone to the sides of Fig. 28 you get spacetime light paths bouncing between mirrors moving relative to each other. If mirrors close, trapped light blue-chirps exponentially as on the right side in Fig. 28. It red-chirps if the two mirrors separate as they do on the left side of Fig. 28. Together, a desired $e^{\pm n\rho}$ spectrum is made simply by translating one etalon cavity at constant velocity relative to another stationary cavity that is enclosed by the translating one.

In this way, light generated by mirrors of constant *velocity* provides the spectrum needed to make an interference net of constant *acceleration*. Coherent acceleration like Fig. 28 (but slower) might be done with great precision. Length metrology involves waves, too!

Wave geometry ought to make us more skeptical of the coordinate boxes and manifolds that have been a paradigm for centuries. A common image is the Newton-Descartes empty-box at some absolute time existing whether or not it contains any "particles." Some learn to picture spacetime coordinates as a giant metal frame of clocks like *Fig. 9* in Taylor and Wheeler's[31] relativity text. That figure is more like a parody of common views of spacetime manifolds that remain with us to this day. Such a monstrosity of a framework is decidedly nonexistent and non-operational.

In contrast, a wave frame like Fig. 6, 7, and 22 is *physical* metrological coordinate system whose geometry and logic is both revealing and real. The things being coordinated (waves) come with

their own coordinates and theorems built in. Einstein general theory of relativity trumped Newton's box by showing how it is affected (curved) by any energy or mass it holds. Quantum theory seems to go a step further by indicating that this box and its contents may be one and the same thing.

Pair creation and quantum frames.

Dirac, before others, realized that per-spacetime has the symmetry of spacetime. Past and future (time-reversal) symmetry demands *negative* frequency as well as positive. In order to visualize Dirac's pair-creation process he extends the playing field to back-to-back baseball-diamonds with *four* nets of invariant hyperbolas. Examples of pair-creation are sketched in Fig. 29 as seen from two different reference frames. Pair creation-destruction is then seen a strange sort of Compton process.

The Feynman graph of Compton scattering in Fig. 25c-d is turned on its side in Fig. 29 so it may start and end on different branches of the m-hyperbola corresponding to mass $\pm m$. Two photons, whose energy sum equals the energy gap $2mc^2$, appear to bounce off intermediate hyperbolas in Fig. 29 that are conjugate hyperbolas defining group wavevectors $\mathbf{K_g}$ in Fig. 6 or 7. Such dispersion is said to belong to *instanton* or *tachyon* waves of imaginary frequency $\pm i\,\mu$ that entails a huge damping factor $e^{-mc^2\tau/\hbar}$ that proscribes their direct observation. They are said to be in the virtual or intermediate realm.

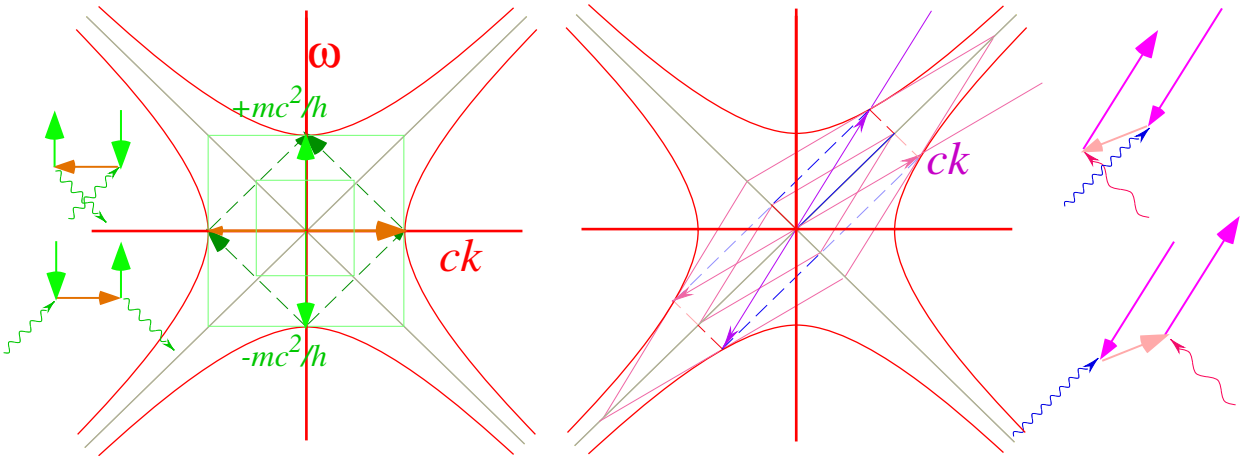

Fig. 29 Dirac matter-antimatter dispersion relations and pair-creation-destruction processes.

Dirac's is the first quantum theory to fully incorporate relativity. It introduces dual anti-worlds, in which all three mass definitions (3.6), (3.7), and (3.9) have negative values, but leaves many questions about their physical meaning. Analogies between the $(2\gamma \rightarrow e + \bar{e})$ process in Fig. 29 and exciton formation in the band theory of solids, shed some light on the physics. However, the exciton process is a straight-up 1-photon process whose momentum is tiny compared to the energy jump, and it lacks the world-anti-world symmetry of the Dirac exciton in which both the electron and an anti-electron have the same group velocity but opposite momentum. The Dirac model has duality of reversed energy (frequency), momentum (k-vector), space, and time that is quite extraordinary.

A number of implications of Dirac's theory have been mostly ignored. Many are unwilling to abandon vestigial concepts associated with absolute classical frames or "boxes." However, quantum frames are like all things quantum mechanical and have an intrinsic *relativity* associated with their wavelike interference. Quantum frames, as they are used in molecular and nuclear physics, are known to have internal or body-relative parts in addition to the more commonly known external or laboratory-relative parts. This inside-and-out duality is a deep quantum mechanical result arising first in the theory of quantum rotors by Casimir, but it also underlies Lorentz-Poincare symmetry that includes locally rotating frames as well as translating ones.

Indeed, the full quantum theory of angular momentum has a built-in duality that is as fundamental as the left-and-right or bra-and-ket duality of the conjugate parts of Dirac's elegant quantum notation $\langle A|B\rangle$. The Wigner $D^J_{m,n}$ –functions are quantum rotor wavefunctions $D^{J*}_{m,n}(\alpha\beta\gamma)$ that have their external laboratory *m*-quantum numbers on the left and their internal or body *n*-quantum numbers on the right. Their *J*-multiplicity is thus *(2J+1)-squared* and not simply the *(2J+1)* so familiar in elementary Schrodinger quantum theory of atomic angular momentum.

It took many years for classical physics to fully accept Einstein's translational relativity principles. Perhaps, if the wave nature of quantum physics had already been established, the relativistic axioms would have been seen as an immediate consequence of wave interference. Indeed, these two subjects are, perhaps, *too* closely related for that to have happened.

Now quantum theory demands a more general kind of relativity involving rotation and other accelerations that is a step beyond the special relativity of constant velocity. This brings up a quite controversial area first explored by Ernst Mach, the originator of *Mach's Principle*. Mach made the seemingly impossible proposal that centrifugal forces, the kind physicists assign the label *ficticious force*, are somehow due to their relativity to all matter in the universe.

Mach's idea may sound silly, but a kind of quantum Mach's Principle is needed to understand spectra and dynamics of quantum rotor $D^J_{m,n}$ waves even in the non-relativistic limit. We are unaware of any fully relativistic quantum treatment of such systems, and it is not clear what if anything would be the cosmological implication of such a grand relativistic quantum wave mechanics. Nevertheless, it seems that the dual 4-by-4 wave-anti-wave space of Dirac is one of the first to re-examine.

Physics is still at a stage where large-scale phenomena use Newton-Einstein particle-in-manifold theory while small-scale phenomena employ Planck-DeBroglie-Schrodinger wave theory. However, both employ some form of space and time coordinates. In this they share an enigma whose existence is largely unquestioned. Supposed invariance to reference frame definition is taken to mean that underlying frames don't matter.

That leaves our fundamental metrology in a dysfunctional dysphoria of an ignored spouse, indispensable, but having only marginal identity. If Evenson and Einstein have taught us anything, it is that this has to be a mistake. Frames *do* matter! The results of Dirac and many others have shown they *make* matter and indeed *are* our matter.

References

[1] K. M. Evenson, J.S. Wells, F.R. Peterson, B.L. Danielson, G.W. Day, R.L. Barger and J.L. Hall, Phys. Rev. Letters 29, 1346(1972).
[2] Guinness Book of Records (1973).
[3] Glauber, Roy J., Hall, John L. and Hansch, Theodor W. *The Nobel Prize in Physics, 2005*. http://nobelprize.org/
[4] J. L. Hall and T. Hensch, Opt. Lett. 9, 502-504 (1984).
[5] N. Ashby, *Physics Today*, 55(5): 41 (May 2002).
[6] J. L. Hall, Laser Spectroscopy VII,(T. W. Hansch and Y. R. Shen, Eds., Springer-Verlag, 1985), pp. 393-394.
[7] William of Occam (1245-1326) *"Pluralitas non est ponenda sine neccesitate"* (Do not assume plurality without necessity.)
[8] A. Cho, Science 306, 1461 (2004).
[9] A. Einstein, Annalen der Physik 17,891(1905). (Translation by W. Perrett and G.B. Jeffery, *The Principle of Relativity*(with notes by A. Sommerfield) (Methuen, London 1923), (republished by Dover, London 1952).
[10] W. G. Harter, J. Mol. Spectrosc. 210, 166(2001).
[11] W. G. Harter, J. Evans, R. Vega, and S. Wilson, Am. J. Phys. 53, 671(1985).
[12] W.G. Harter and T. C. Reimer, //www.uark.edu/ua/pirelli/html/poincare_inv_2.htm
[13] D. E. Herschbach, (unpublished, 2005).
[14] H. Minkowski, *Mathematisch-Physikalische Klasse*, vol. 1, 53 (1908).
[15] H. A. Lorentz Koninklijke Akademie vanWetenschappen te Amsterdam. Section of Science. Proc. 6: 809-831 (1904).
[16] Albert Einstein *"Zur Elektrodynamik bewegter Korper."* Annalen der Physik 18,639 (1905); Annalen der Physik 17,891(1905). (Translation: Perrett and Jeffery, *The Principle of Relativity*, (Methuen, London 1923), (Dover, 1952).
[17] Max Planck "*Zur Theorie des Gesetzes der Energieverteilung im Normal-spectrum.*" Deutsche Physikalische Gesellschaft. Verhandlungen 2: 237-245 (1900).
[18] Louis de Broglie, Nature 112, 540 (1923); Annalen der Physik (10) 2 (1923).
[19] P. A. M. Dirac, "Forms of Relativistic Dynamics" *Rev. Mod. Physics*, 21: 392 (1949).
[20] Albert Einstein "*Uber einen die Erzeugung und Verwandlung des Lichtes betreffenden heuristischen Gesichtspunkt.*" Annalen der Physik 17: 132-148 (1905). (Translation by A.B. Aarons and M.B. Peppard, Am. J. Phys. 33, 367(1965).)
[21] E. Schrodinger, Annalen der Physik (4) 79 361 and 489 (1923); 80, 437 (1926); 81,109 (1926).
[22] Schrodinger's protests about prevailing quantum mechanical interpretations are widely circulated. So far we have been unable to locate more solid references.
[23] N. Bohr, *Zeitschrift fur Physik*, 9, 1-2, (1922).
[24] W. Heisenberg, *The Physical Principles of the Quantum Theory*, (Dover, New York, 1930).
[25] P.A.M. Dirac, *Lectures on quantum mechanics*, (New York, Belfer Graduate School of Science, Yeshiva University, 1964). Dirac's first text in 1931 used α and β to denote bra-ket duality.
[26] A. Einstein, *"I shall never believe that god plays dice with the universe"* Albert Einstein Archives, The Jewish National & University Library, The Hebrew University of Jerusalem (www.albert-einstein.org), Einstein Archives Online, Volume 15, #294, Letter to Cornelius Lanczos, March 21, 1942,http://www.alberteinstein.info/db/ViewDetails.do?DocumentID=30893.
[27] R. Feynman, *The Pleasure of Finding Things Out*, (Perseus Publishing, Cambridge, MA,1999) p. 8.
[28] (unpublished) A huge energy shift is used for sake of geometric clarity. Atoms usually lose less than one part in 10^9 or 10^{10} of their rest mass in optical emission. The atom in the example loses rest mass $1/2\ M_2c^2$ emitting a $3/8\ M_2c^2$ photon.
[29] R. P. Feynman, R. Leighton, and M. Sands, *The Feynman Lectures* (Addison Wesley 1964) Our development owes a lot to Feynman's treatment cavity wave dispersion in Vol. II Ch. 24 and Vol. III Ch. 7.
[30] W. Rindler, *Essential Relativity-Special, General, and Cosmological*, Springer (New York 1977) p. 18. See also ref. 8, p. 111.
[31] E.F.Taylor and J.A. Wheeler, *Spacetime Physics* (W. H. Freeman San Francisco 1966) p. 18.

Acknowledgements

The author would like to thank Ronald F. Fox and Eric J. Heller for careful reading and suggestions regarding early versions of this work and Daniel Kennefick for information from the Einstein Centennial bibliography project. Also, we are grateful to Molly Longstreth and Usha Gupta for help with bibliographic search.

Figure Captions

Fig. 1. Comparison of wave archetypes and related axioms of relativity.

(a) Pulse Wave (PW) peaks locate where a wave is. Their speed is c for all observers.

(b) Continuous Wave (CW) zeros locate where it is not. Their speed is c for all colors (or observers.)

Fig. 2. Pulse Wave (PW) as a sum of 12 Fourier CW's (a) PW parts: real ReΨ, imaginary ImΨ, and magnitude $|\Psi|$.

(b) CW phasor clocks plot real vs. imaginary parts of wave amplitude Ψ.

Fig. 3. Wave addition of counter propagating Fourier components.

(a) 2-PW Sum has binary sum has 4 values (0,0), (0,1), (1,0), (1,1) and diamond grid of peak paths on a plane of zeros.

(b) 2-CW Sum and interference has value continuum and square grid of zeros.

Fig. 4. "Ficticious" sources and their wave coordinate lattices in (a) Spacetime and (b) Per-spacetime.

CW lattices of phase-zero and group-node paths intermesh with PW lattices of "particle" or pulse wave paths.

Fig. 5. Co-propagating laser beams produce a collapsed wave lattice since all parts have same speed c.

Fig. 6. Laser lab view of 600Thz CW and PW light waves in per-space-time (a-b) and space-time (c-d).

Fig.7. Atom view of 600Thz CW and PW light waves in per-spacetime (a-b) and space-time (c-d) boosted to u=3c/5.

Fig. 8. Wave phasor addition. (a) Each phasor in a wave array is a sum (b) of two component phasors.

(c) In phasor-relative views either A or else B is fixed. An evolving sum-and-difference rectangle is inscribed in the (dashed) circle of the phasor moving relative to the fixed one.

Fig. 9. Doppler shift b-matrix for a linear array of variously moving receiver-sources.

Fig. 10. (a) Euclidian mean geometry for counter-moving waves of frequency 1 and 4. (300THz units).

Fig. 10. (b) Geometry for the CW wave coordinate axes in Fig. 7.

Fig. 11. (a) Horizontal G-hyperbolas for proper frequency B=v and 2B and vertical P-hyperbolas for proper wavevector k.

(b) Tangents for G-curves are loci for P-curves, and vice-versa.

Fig. 12. Dispersion hyperbolas for 2-CW interference (a) Laser lab view. (b)Atom frame view.

Fig. 13. Geometry of contact transformation between relativistic (a) Hamiltonian (b) Lagrangian.

Fig. 14. "True" paths carry extreme phase and fastest phase clocks. Light-cone has only stopped clocks.

Fig. 15. Quantum waves interfere constructively on "True" path but mostly cancel elsewhere.

Fig. 16. Trigonometric geometry (a) Unit circular area ϕ=0.86. (b) Unit hyperbolic area ρ=0.99.

Fig. 17. Relativistic wave mechanics geometry. (a) Overview. (b) Details of contact transform tangents.

Fig. 18. Monochromatic (1-frequency) 2-CW wave space-time patterns.

Fig. 19. Dichromatic (2-frequency) 2-CW wave space-time patterns.

Fig. 20. (a-g) Elliptic polarization ellipses relate to galloping waves in Fig. 18. (h-i) Kepler anomalies.

Fig. 21. Cavity 2-CW modes. (a) Invariant "mass" hyperbolas. (b) COM frame. (c) ISOC frame.

Fig. 22. Optical cavity energy hyperbolas for mode number n=1-3 and photon number Nn=0, 1, 2,....

Fig. 23. Simulated spacetime photon counts for coherent (a-c) and photon-number states (d).

Fig. 24. Optical cavity model of (a) Emission, (b) Absorption, and (c) Compton scattering

Fig. 25. Compton scattering. (a) Vector sums on mass hyperbolas of low ω_ℓ, medium ω_m, and high ω_h.

(b-c) Feynman graphs. (d) Center of Momentum (COM) vector sums. (e-f) COM Feynman graphs.

Fig. 26. Compton nets are congruent Compton staircases of transitions. (a) f=2:1 (b) f=$\sqrt{2}$:1.

Fig. 27. Optical wave frames by red-and-blue-chirped lasers (a)Varying acceleration (b)Constant g.

Fig. 28. Accelerated reference frames and their trajectories painted by $e^{\pm\rho}$-chirped coherent light.

Fig. 29. Dirac matter-antimatter dispersion relations and diagrams of pair-creation-destruction processes.

-- The Purest Light and a Resonance Hero – Ken Evenson (1932-2002) --

When travelers punch up their GPS coordinates they owe a debt of gratitude to an under sung hero who, alongside his colleagues and students, often toiled 18 hour days deep inside a laser laboratory lit only by the purest light in the universe.

Ken was an "Indiana Jones" of modern physics. While he may never have been called "Montana Ken," such a name would describe a real life hero from Bozeman, Montana, whose extraordinary accomplishments in many ways surpass the fictional characters in cinematic thrillers like *Raiders of the Lost Arc*.

Indeed, there were some exciting real life moments shared by his wife Vera, one together with Ken in a canoe literally inches from the hundred-foot drop-off of Brazil's largest waterfall. But, such outdoor exploits, of which Ken had many, pale in the light of an in-the-lab brilliance and courage that profoundly enriched the world.

Ken is one of few researchers and perhaps the only physicist to be twice listed in the *Guinness Book of Records*. The listings are not for jungle exploits but for his lab's highest frequency measurement and for a speed of light determination that made *c* many times more precise due to his lab's pioneering work with John Hall in laser resonance and metrology†.

The meter-kilogram-second (mks) system of units underwent a redefinition largely because of these efforts. Thereafter, the speed of light *c* was set to $299,792,458 ms^{-1}$. The meter was defined in terms of *c*, instead of the other way around since his time precision had so far trumped that for distance. Without such resonance precision, the Global Positioning System (GPS), the first large-scale wave space-time coordinate system, would not be possible.

Ken's courage and persistence at the Time and Frequency Division of the Boulder Laboratories in the National Bureau of Standards (now the National Institute of Standards and Technology or NIST) are legendary as are his railings against boneheaded administrators who seemed bent on thwarting his best efforts. Undaunted, Ken's lab painstakingly exploited the resonance properties of metal-insulator diodes, and succeeded in literally counting the waves of near-infrared radiation and eventually visible light itself.

Those who knew Ken miss him terribly. But, his indelible legacy resonates today as ultra-precise atomic and molecular wave and pulse quantum optics continue to advance and provide heretofore unimaginable capability. Our quality of life depends on their metrology through the Quality and Finesse of the resonant oscillators that are the heartbeats of our technology.

Before being taken by Lou Gehrig's disease, Ken began ultra-precise laser spectroscopy of unusual molecules such as HO_2, the radical cousin of the more common H_2O. Like Ken, such radical molecules affect us as much or more than better known ones. But also like Ken, they toil in obscurity, illuminated only by the purest light in the universe.

In 2005 the Nobel Prize in physics was awarded to Glauber, Hall, and Hensch†† for laser optics and metrology.

† K. M. Evenson, J.S. Wells, F.R. Peterson, B.L. Danielson, G.W. Day, R.L. Barger and J.L. Hall, Phys. Rev. Letters 29, 1346(1972).

†† *The Nobel Prize in Physics, 2005*. http://nobelprize.org/

hysics, 2005. http://nobelprize.org/

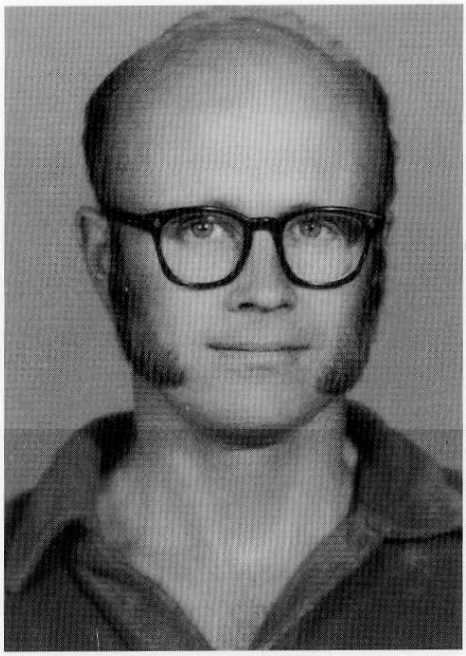

PAULINIA, BRASIL 1976

THE SPEED OF LIGHT IS
299,792,458 METERS PER SECOND!

Kenneth M. Evenson – 1932-2002